Scanning Probe Chemical and Topographical Microanalysis

Thesis by

Dmitri A. Kossakovski

In Partial Fulfillment of the Requirements

for the Degree of

Doctor of Philosophy

California Institute of Technology

Pasadena, California

1999

(Submitted November 5, 1999)

For my wife Olga,

our son Fedor

and

my mother Natalie

ACKNOWLEDGMENTS

The years in graduate school at Caltech have been a wonderful and fascinating experience. During this time my whole perspective on science in general and chemistry in particular has been fundamentally transformed from a dry, scholastic attitude towards the vivid atmosphere of exciting experimental research and advanced instrumentation development. Having Jack Beauchamp as an academic advisor was the major factor in this transformation, for which I am greatly indebted to Jack. His critical evaluation, research intuition and overall guidance of my graduate work were the key elements in completing the Ph.D. program at Caltech.

I would like to thank John Baldeschwieler for being my mentor and patient listener to the most craziest ideas, and for encouragement in my projects. It was extremely exciting to observe and participate over the years in the variety of high tech developments that percolated from John's lab into the applied field. And John, I tried not to split infinitives in the Thesis!

I was lucky to meet Ron Gamble when working in Baldeschwieler group on fluoroscanner development. This initial collaboration grew with time into a good friendship and partnership in a number of endeavors. Ron's perspective on life and attitude towards work helped me tremendously to adjust to life in America.

I am very grateful to past and present members of Beauchamp and Baldeschwieler groups for sharing ups and downs of work and life in graduate school. Steve O'Connor was crucial for recruiting me in the lab, showing the ropes in the SPM field and interfacing me with all kinds of people on campus. Marc Unger was a superb collaborator on the IR-NSOM project as well as on a number of other endeavors. Sangwon Lee possesses terrific chemical intuition, something I totally lack. His constant

willingness to help is greatly appreciated. Hakno Lee and Jim Smith have also helped me a lot in the first years in the lab.

I was fortunate to overlap with Daniel Austin who spearheaded the Dustbuster project. He simply gets the things done. I am also very thankful to new members of Beauchamp lab – Heather Cox, Ron Grimm and Ryan Julian. Thanks for support, care and genuine interest.

The staff members at Chemistry machine shop, Mike Roy, Guy Duremberg and Ray Garcia were terrific tutors. Their stock of practical knowledge and common sense helped me in all hands-on developments, ranging from precision mechanics to building a toy race car for my son.

The multidisciplinary and collaborative atmosphere of Caltech allowed me to meet a number of people from different departments on campus. I am grateful to Tom Ahrens and members of his group Ingrid Mann and Patricia Persaud for education in space dust science and for putting together the effort in new instrumentation development. Glen Cass and his Ph.D. student Lara Hughes helped us in understanding the properties of aerosols and provided the samples for instrument performance evaluation. George Rossman was always willing to share his vast knowledge of mineral properties, which helped us a lot in IR-NSOM and TOPOLIBS projects. I would like to thank my Thesis committee members Mitchio Okumura, Geoff Blake and Doug Rees for attention and help with moving through the graduate school.

Finally, I want to thank my wife Olga for endless support and encouragement during the years at Caltech. Our son has made his first steps on campus alleys and is still considering Caltech to be a large playground. And I agree with him – it really is a terrific playground for grown-ups!

ABSTRACT

The last decade has seen a rapid rise of Scanning Probe Microscopy, SPM, as a prominent and versatile approach for surface studies. SPM instruments are differentiated from the beam-based ones by the fact that they use solid proximal probes for localized analysis. The most commonly used SPM methodology is Atomic Force Microscopy, AFM. In its basic implementation, AFM provides topographical information with nanometer resolution. The most common modifications allow the magnetic, electrostatic, and specific chemical environment to be examined. However, there is no direct way today to perform general chemical analysis with AFM probes.

Near-field Scanning Optical Microscopy, NSOM, is another variation of SPM where sharp tapered optical fibers serve dual purposes, being proximal probes of sample topography, and providing the means for localized light delivery for optical studies with sub-wavelength spatial resolution. Again, NSOM itself does not have a general chemical contrast capability. However, the capability to deliver light to localized area opens the way to a multitude of experiments that can be devised using different aspects of light interaction with the sample.

This thesis demonstrates several approaches for combined topographical and chemical investigations. Infrared spectroscopy is a sensitive molecular analysis tool. Without scanning proximal probe, IR microscopy has very poor spatial resolution. Enabling methodology for probe fabrication for Near-field Scanning Infrared Microscopy, NSIM, is presented.

The efforts in combining NSOM with mass spectrometry, which is probably the most general chemical analysis tool, are outlined. We have demonstrated the possibility of simultaneous topographical and molecular imaging.

Another variation of chemical imaging is the combination of SPM and Laser Induced Breakdown Spectroscopy, LIBS. In this method the elemental composition of samples is obtained by analyzing optical emissions from transient plasma plumes formed by intense laser pulses delivered through fiber probes. We have demonstrated the feasibility of this approach. The instrument that we have developed is an attractive complementary tool for established methods of spatial elemental analysis, such as X-ray Fluorescence. Among its attractive features are operation in ambient conditions, minimal requirements for sample preparation, and ease of use.

TABLE OF CONTENTS

ACKNOWLEDGMENTS iii
ABSTRACT v
CHAPTER 1. CHEMICAL IMAGING TECHNIQUES 1
REFERENCES 4
CHAPTER 2. PROBE FABRICATION FOR NEAR-FIELD SCANNING INFRARED MICROSCOPY 5
INTRODUCTION 5
EXPERIMENTAL 8
RESULTS AND DISCUSSION 9
A. POLYAMIDE COATING REMOVAL 9
B. CLADDING REMOVAL 10
C. CHALCOGENIDE CORE ETCHING 10
D. CHALCOGENIDE CORE ETCHING MECHANISM 15
E. IR RADIATION THROUGHPUT MEASUREMENTS 23
CONCLUSION 29
REFERENCES 30
CHAPTER 3. TOPO-MS: SCANNED PROBE COMBINED WITH MASS SPECTROMETRY 33
INTRODUCTION 33
EXPERIMENTAL 34
RESULTS 36
DISCUSSION 42
CONCLUSION 43
ACKNOWLEDGMENTS 44
REFERENCES 45
CHAPTER 4. TOPOLIBS: SCANNED PROBE COMBINED WITH LASER INDUCED BREAKDOWN SPECTROSCOPY 47
INTRODUCTION 47
LIBS BACKGROUND 48
TOPOLIBS 50
EXPERIMENTAL SECTION 52
RESULTS AND DISCUSSION 54
FOCUSED BEAM: TRADITIONAL LIBS 54
FOCUSED BEAM AND FIBER PROBE: LIBS SIGNAL COMPARISON 61
STUDIES OF MURCHISON METEORITE 61
STUDIES OF BASALT SAMPLE 65
PARTICLE ANALYSIS 74
TECHNICAL ISSUES TO BE ADDRESSED 79
CONCLUSIONS 82
ACKNOWLEDGMENTS 83
REFERENCES 83
APPENDIX A. PROBE FABRICATION BY CHEMICAL ETCHING OPTICAL FIBERS 85
REFERENCES 89
APPENDIX B. SHEAR-FORCE POSITION FEEDBACK USING PIEZOELECTRIC TUNING FORKS 91
SHEAR FORCE BASICS 91
PREPARING A FORK 97
MOUNTING FIBERS ON THE FORKS 100
HARDWARE/ELECTRICAL DESIGN 101
REFERENCES 103
APPENDIX C. DESIGN DETAILS OF TOPO-MS II 104
INSTRUMENT DESIGN 104
SCANNER: CURRENT DESIGN AND CONSIDERATIONS FOR FUTURE 107
PROBE ASSEMBLY 109
PROBE TRANSFER 110
TOF MASS SPECTROMETER 110

Chapter 1. Chemical Imaging Techniques

Imaging of chemically inhomogeneous surfaces is a common analytical task. Depending on the nature of the sample, characteristic size of analyzed features, and type of information required, various methods are employed. The majority of currently available commercial instrumentation utilizes particle beams originating from a remote source to probe local chemical environment on the sample. Particles in the beam can be electrons (Electron Microscopy, Auger Microprobes), ions (Secondary Ion Mass Spectrometry), X-ray photons (X-ray Fluorescence) and other sources. A good review of these well established techniques is a recent book by Vickerman[1]. Laser microanalysis methods are thoroughly reviewed in the book by Moenke-Blankenburg[2].

The last decade has seen a rapid rise of Scanning Probe Microscopy, SPM, as a prominent and versatile approach for surface studies. SPM instruments are differentiated from the beam-based ones by the fact that they use solid proximal probes for localized analysis. The most commonly used SPM methodology is Atomic Force Microscopy, AFM. In its basic implementation, AFM provides topographical information with nanometer resolution. The most common modifications allow the magnetic, electrostatic, and specific chemical environment to be examined[3]. However, there is no direct way today to perform general chemical analysis with AFM probes. This is reflected in Figure 1 which represents a comparative chart of most common chemical analytical techniques and their spatial resolution. AFM is off the chart because it does not have a direct means for chemical contrast.

Near-field Scanning Optical Microscopy, NSOM, is another variation of SPM where sharp tapered optical fibers serve dual purposes, being proximal probes of sample topography, and providing the means for localized light delivery for optical studies with sub-wavelength spatial resolution. Again, NSOM itself does not have a general chemical

contrast capability. However, the capability to deliver light to localized area opens the way to a multitude of experiments that can be devised using different aspects of light interaction with the sample.

This thesis demonstrates several approaches for combined topographical and chemical investigations, which allows addition of SPM to the chart in Figure 1.1. Chapter 2 deals with aspects of Near-field Scanning Infrared Microscopy, NSIM, namely the probe fabrication methodology. NSIM derives chemical contrast from IR spectroscopy of thin samples. Chapter 3 describes our efforts in combining NSOM with mass spectrometry, which is probably the most general chemical analysis tool. In Chapter 4 we present the combination of SPM and Laser Induced Breakdown Spectroscopy, LIBS. In this method the elemental composition of samples is obtained by analyzing optical emissions from transient plasma plumes formed by intense laser pulses delivered through fiber probes.

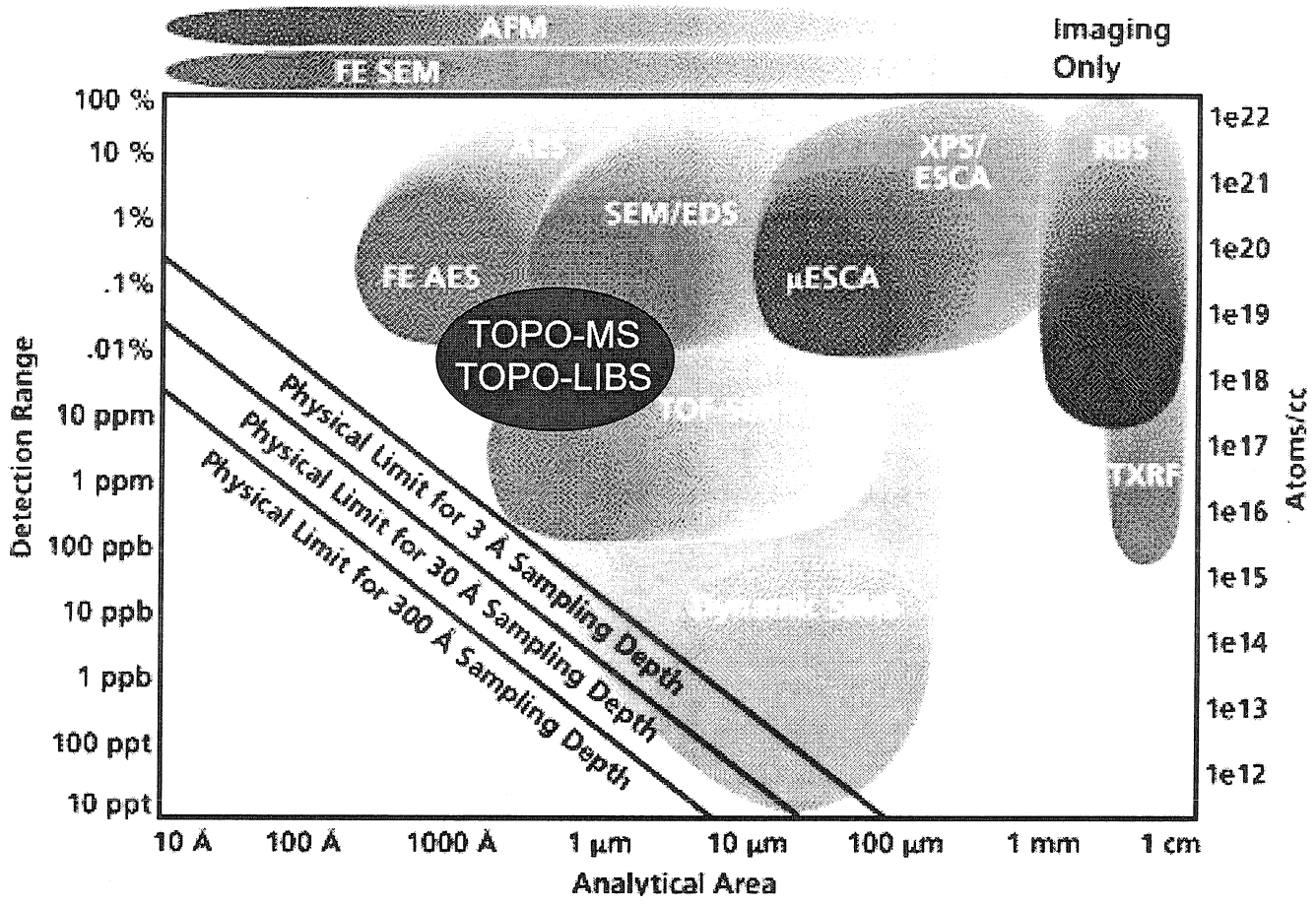

Figure 1.1. Comparative chart of most common chemical imaging techniques. With addition of chemical contrast mechanisms, Scanning Probe Microscopy can be placed on the chart complementing other, more established methods. Adapted from the web site of Charles Evans and Associates, www.cea.com.

REFERENCES

[1] J.C. Vickerman (ed.), Surface analysis : the principal techniques, Chichester; New York : John Wiley, 1997.

[2] L. Moenke-Blankenburg, Laser microanalysis, New York : Wiley, 1989.

[3] H. Takano, J.R. Kenseth, S.S. Wong, J.C. O'Brien and M.D. Porter, Chemical And Biochemical Analysis Using Scanning Force Microscopy, *Chemical Reviews* **99** (1999) 2845-2890.

Chapter 2. Probe Fabrication for Near-Field Scanning Infrared Microscopy

This chapter is adapted with permission from the article "Etched Chalcogenide Fibers for Near-Field IR Scanning Microscopy" by M.A.Unger, D.A. Kossakovski, R.Kongovi, J.L.Beauchamp and D.V.Palanker, published in Review of Scientific Instruments 69 (1998) 2988-2993, Copyright 1998, American Institute of Physics.

INTRODUCTION

Near-field Scanning Optical Microscopy (NSOM) allows optical microscopy[1,2,3,4,5] and spectroscopy[4,5,6] with resolution on the order of 10-100 nm, which is far smaller than the far-field diffraction limit ($\lambda/2$). Part of the price for achieving this resolution is the necessity of constructing a probe with an aperture of the size of the desired resolution. As with all scanned probe techniques, the power of the technique depends in large part on the quality of the probe.

Typical NSOM instruments use a pulled optical fiber, coated with metal except for an aperture at the apex, for a probe. They are therefore limited to the wavelength range transmitted by the fiber. With glass (SiO_2) fibers, this is typically[7] 375-850 nm. The throughput (measured in the far field) is typically[8] 10^{-5} - 10^{-6}.

Near-field Scanning Infrared Microscopy (NSIM) is an obvious extrapolation of the NSOM technique. In principle, NSIM has a definite advantage over NSOM: in contrast to the visible region, almost every molecule has an absorption in the IR region. Furthermore, IR absorption bands give direct information about the presence and nature of molecular bonds in the observed region.

High spatial resolution Raman microscopy is another way to extract molecular specific information from a sample. It is known that Raman and IR absorption

spectroscopy provide somewhat complementary information due to the nature of IR radiation interaction with the matter. However, NSIM with a tapered fiber probe provides an advantage over Raman imaging: the probe is maintained at constant distance from the sample while scanning which provides topographical information in addition to IR absorption data. As in NSOM, this provides a means to correlate topographical information with spectroscopic data.

Several near-field IR microscope designs have been published[9,10,11,12,13]. To date, however, only two of them[12,13] have made use of IR-transmitting fibers. This is probably because making NSIM probes from IR fibers has been very difficult.

The primary source of difficulty in making NSIM probes from IR fibers is the physical properties of the fiber material. Perhaps the most tractable set of compounds from which IR-transmitting fibers are made are the chalcogenides. Chalcogenide fibers have good chemical stability and are less brittle than the other families of compounds from which IR fibers have been made. Like optical fibers, they are also glasses, so they can be heat-pulled with a capillary puller in a fashion similar to optical fibers. However, heat-pulling chalcogenide fibers is significantly more difficult than heat-pulling glass (SiO_2) fibers. It has been accomplished, to our knowledge, only by Hong[13] *et al.* Pulled IR fibers also have relatively low light throughput (on the order of 10^{-6}, measured in the far field[14]). They also have a very long taper length (several mm - See Figure 2.1).

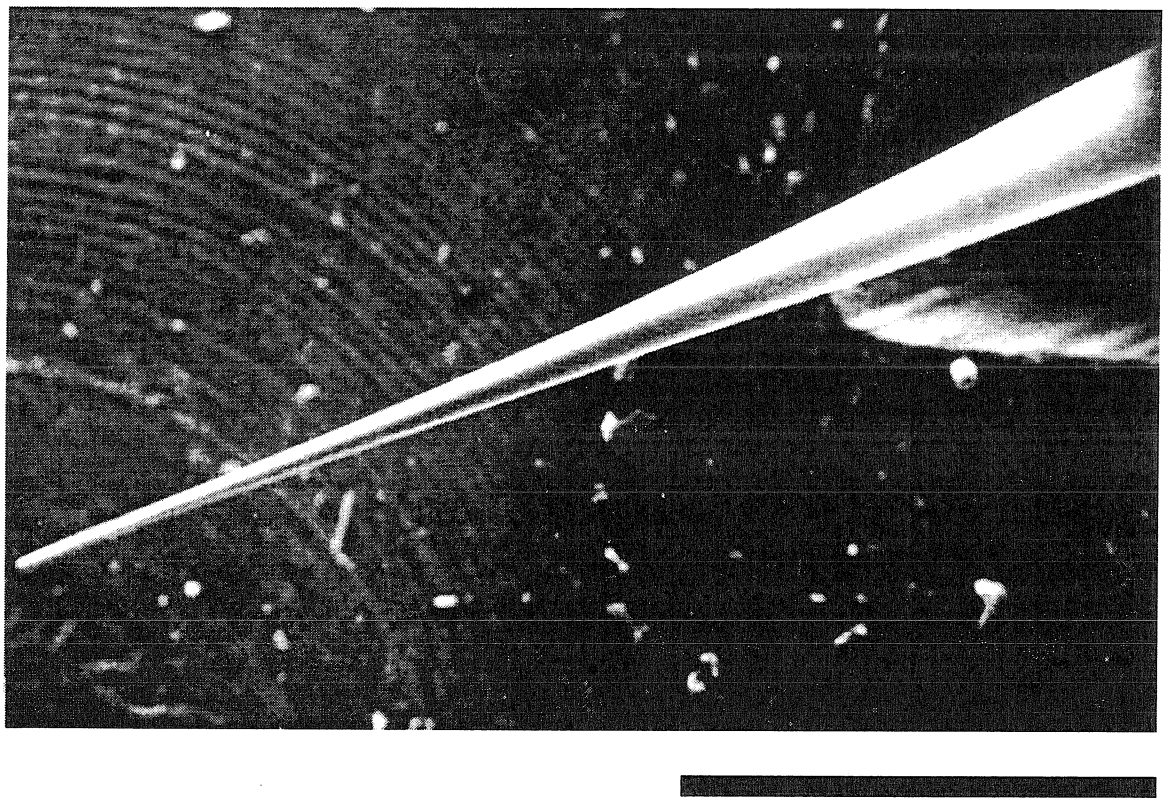

Figure 2.1. SEM micrograph of heat-pulled chalcogenide fiber. Scale bar = 1 mm. Note the long taper length.

Zeisel *et al.* have reported[15] that chemically etched optical fiber probes have far-field light throughput that is 100 - 1000 times greater than pulled fiber probes, probably because the taper region is much shorter. The longer the taper region, the longer the region where radiation must propagate in a waveguide narrower than its wavelength. A shorter taper region is thus expected to deliver light more efficiently to the aperture, resulting in higher intensity in both the propagating (far field) and non-propagating (near-field) components. It is thus a reasonable assumption that the increase in far-field throughput mirrors a proportional increase in near-field intensity.

In the present work we describe the application of a simple chemical etching technique to IR-transmitting chalcogenide fibers. The fiber probes etched this way taper to a sharp point (≤ 150 nm end-radius-of-curvature) in approximately one fiber diameter (~ 100 μm). Such sharp probes when scanned in position feedback will easily give spatial topographical resolution of 150nm. One should distinguish topographical resolution from the spatial resolution of IR imaging, which will be determined by the size of the aperture used.

Simple chemical methods are also described for the removal of the polyamide plastic coating and sulfur-selenide cladding used on these chalcogenide fibers. We also present a preliminary data about the IR radiation throughput measured with etched fibers.

EXPERIMENTAL

Chalcogenide fibers were obtained from Amorphous Materials, Inc., 3130 Benton, Garland, TX 75042. Both thin (unclad, but plastic coated) and thick (clad and plastic coated) fibers were used in this study. In both cases the chalcogenide core is an

As-Se-Te glass. The cladding is primarily S-Se. Both types of fiber are Plate # 94-131-8, Run # 71395.

Thin fibers have a core diameter of .0058 inch (145 μm) and a polyamide coating .0009 inch (22.5 μm) thick (for a total fiber diameter of .0076 inch (190 μm)).

Thick fibers have a core diameter of .010 inch (250 μm), S-Se cladding .004 inch (100 μm) thick, and a polyamide coating .003 inch (75 μm) thick (for a total fiber diameter of .024 inch (600 μm)).

In the process of creating the fiber probes it was useful to use an optical microscope with an epi-fluorescence/reflectance microscopy attachment. The polyamide coating is slightly fluorescent (under both blue and green light) making it easy to tell if it has been completely removed. Microscopy of the probes under both backlighting and reflected light makes it much easier to determine the shape of the fiber.

The best method for examination of the probe tip is scanning electron microscopy. Chalcogenides are semiconductors, so sputtering the tips with gold is not strictly necessary, although it does improve image clarity at very high magnifications.

RESULTS AND DISCUSSION

A. POLYAMIDE COATING REMOVAL

The polyamide coating can be easily removed by repeatedly immersing the coated fiber in stirred room-temperature solvent for 1-2 minutes and wiping with a laboratory tissue. Several solvents work for this purpose, including 4-chloro-1-butanol, methanol,

and acetone. Properly stripped fibers feel very smooth when wiped with a laboratory tissue. If not all the polymer has been removed, higher friction can be noticed.

B. CLADDING REMOVAL

If the fiber is clad, the cladding must be removed before etching. This can be done by soaking the polyamide-stripped fiber in room-temperature 0.1 M NaOH for approximately 18 hours. At the end of this time, the portion of the fiber that was in the NaOH solution generally has lost its reflective sheen. Upon wiping gently with a laboratory tissue, the treated portion of the cladding will come off the core.

If the fiber is removed from the NaOH solution too soon, wiping will not remove the cladding, but the fiber may be safely put back in the solution. We hypothesize that the NaOH must diffuse completely through the cladding before the cladding will come off. If the fiber is left too long in the NaOH solution (> 24 hours), the NaOH will very slowly start to etch the chalcogenide core.

If the polyamide comes into contact with the NaOH solution, the core may become extremely brittle, especially at the point of contact.

C. CHALCOGENIDE CORE ETCHING

Once the core has been exposed, etching the core is straightforward. A container is prepared with a two-phase etching system. The lower phase is the etchant solution, while the upper phase is a protective solvent. (see Figure 2.2.)

The etchant solution is piranha solution, a 7:3 mixture of concentrated sulfuric acid and 30% hydrogen peroxide. *Caution! Piranha solution may react violently with organic compounds and should not be stored in sealed containers.* Many different organic compounds may serve as the protective solvent. The authors have had the most success with tetramethylpentadecane (TMPD), polydimethylsiloxane (PDMS) and CCl_4, with TMPD having the best long-term stability against piranha solution.

The fiber is immersed in the etching system. At room temperature and without stirring, the fiber will "neck in" approximately one diameter down from the solvent-piranha meniscus. Ultimately, the "neck" will be completely etched through, and the lower piece will fall off. (See Figures 2.3 and 2.4.)

This is referred to as the "falloff" point. The time it takes to reach "falloff" depends on the age of the piranha solution, its temperature, and the thickness of the chalcogenide core. As a guideline, with freshly made piranha at room temperature, and a 145 μm core, etching takes ~15 minutes. With 2-month old piranha (stored at 5°C), starting slightly below room temperature, and a 250 μm core, etching takes ~50 minutes. Etching times are relatively consistent, but variations of a few minutes must be allowed for.

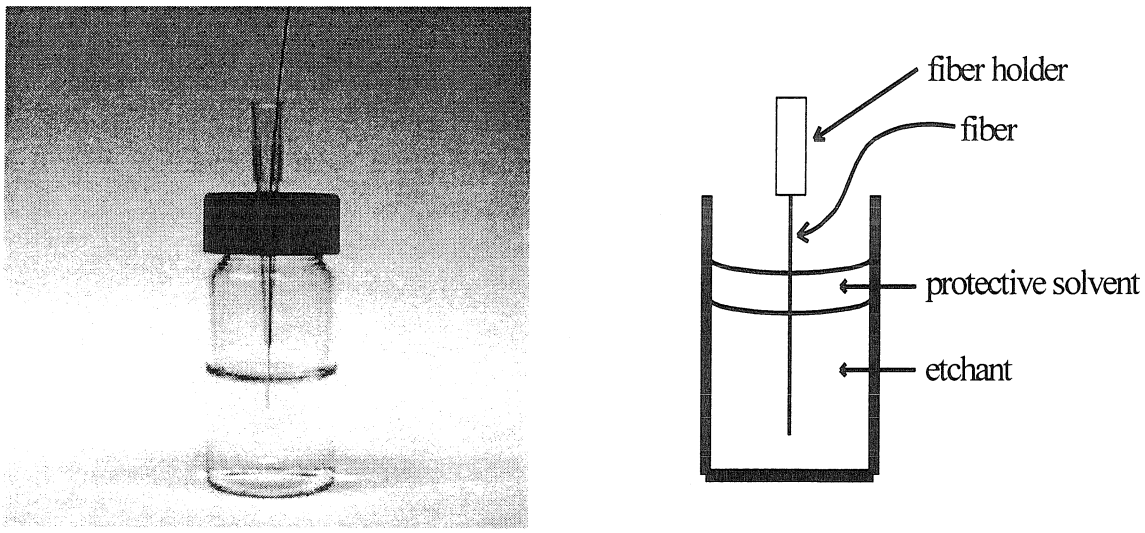

Figure 2.2. Schematic and photo of the two-phase etching apparatus. Only 1-2 mm of protective solvent are required. The protective solvent serves to keep the meniscus flat at the fiber-etchant interface.

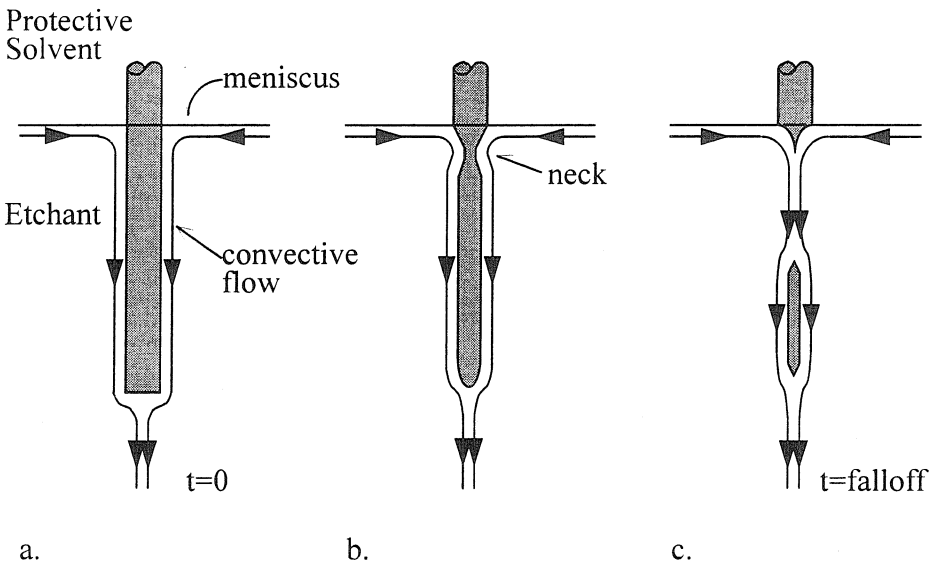

Figure 2.3. Two-phase etching mechanism Schematic of etching mechanism under normal conditions (convective control). (a) The system at the beginning of etching, (b) after etching has progressed approximately halfway to completion, and (c) at the falloff point.

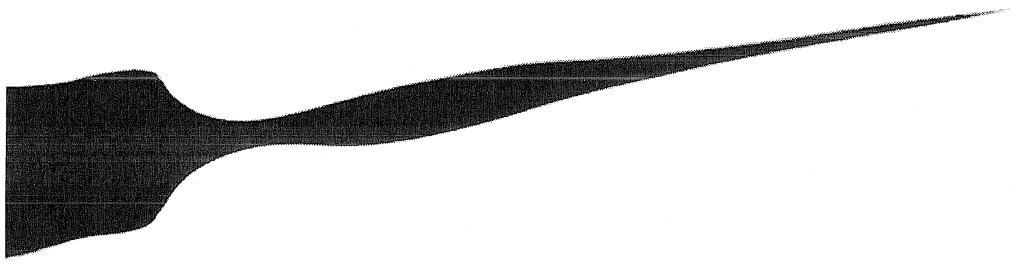

Figure 2.4. Fiber removed from etching solution before falloff point. Optical micrograph. Scale bar = 150 μm. Note the pronounced "neck."

Approximately 30 seconds after the "falloff," the fiber is withdrawn from the etchant, washed in gently stirred room-temperature methanol, and gently blown dry with N_2 (blowing on-axis onto the tip, rather than from the side).

Figures 2.5 and 2.6 show an etched unclad 145 μm fiber. Figures 2.7, 2.8, and 2.9 show an etched, clad fiber with a 250 μm core.

D. CHALCOGENIDE CORE ETCHING MECHANISM

The mechanism of tip formation is believed to be convective control of chemical etching. This etching is hypothesized to occur as follows:

As the etching agent dissolves the fiber, the solution density increases next to the fiber surface. Since it is more dense than the rest of the solution, it flows down the fiber; under these conditions the flow is laminar. As it flows down the fiber, more etchant solution must move to take its place. Since there is a fluid layer moving parallel to the surface of the fiber everywhere but close to the meniscus (the "top" of where the etchant touches the fiber), new etchant solution enters the convection pattern primarily at the meniscus, as shown in Figure 2.3. Since the etchant solution contacting the fiber is more reactive (i.e., contains more H_2O_2 and less dissolved chalcogenide) at the meniscus, it etches faster there. This results in a "necking" effect. Eventually the "neck" will be dissolved completely away, and the fiber below the neck will fall.

The protective solvent overlayer serves to make tip shape more smooth and reproducible. Fibers etched without solvent overlayers are typically asymmetric and lack the smooth concave conical shape of fibers etched with solvent overlayers. See Figure 2.10.

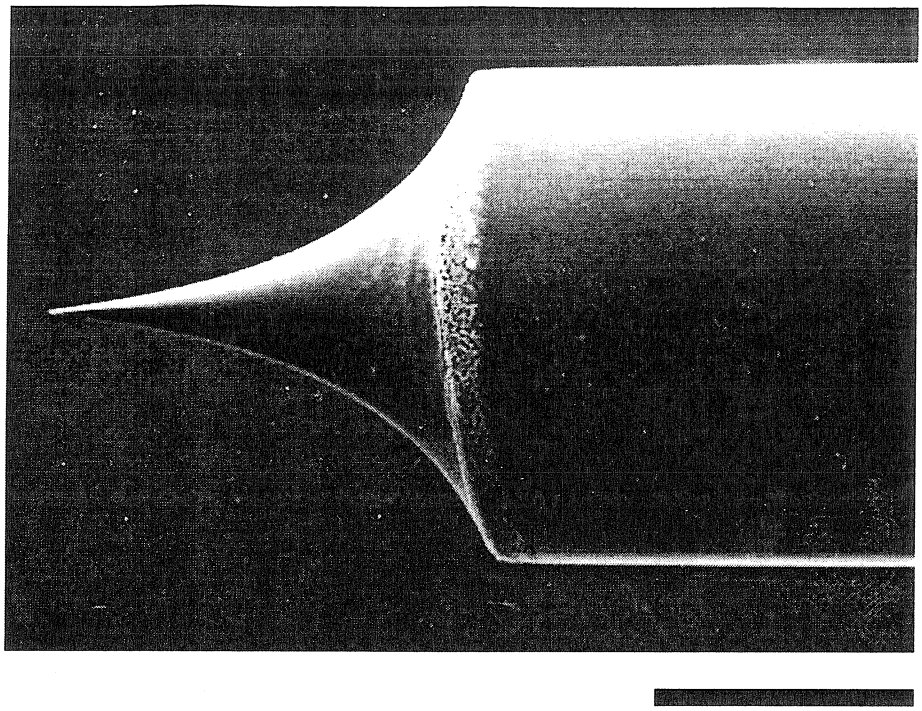

Figure 2.5. Scale bar = 100μm. SEM micrograph of a 145 μm diameter core chalcogenide fiber etched by the described method.

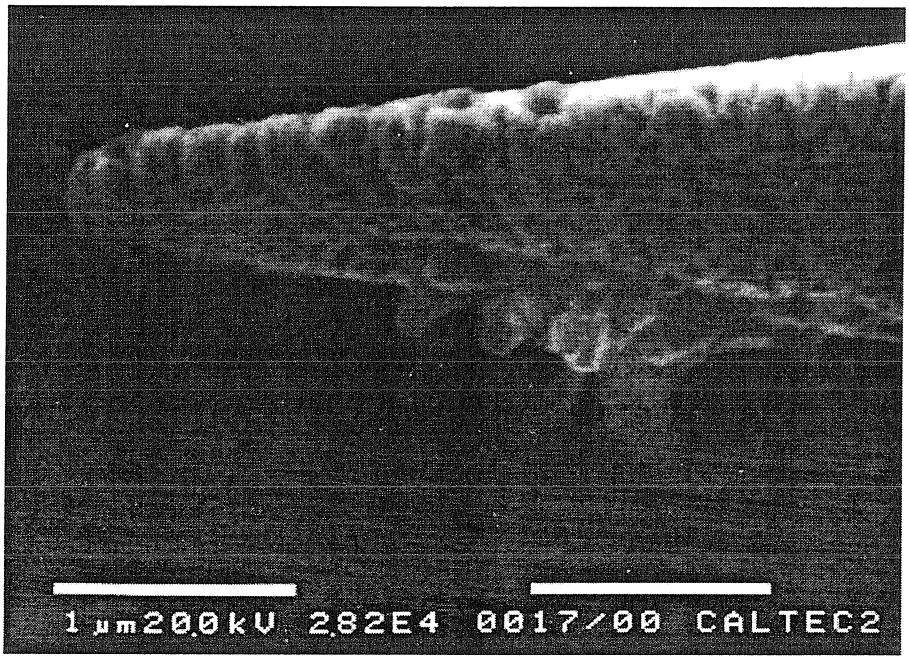

Figure 2.6. Scale bar = 1μm. Zoom onto the apex of the tip shown in Figure 2.5. The corrugations and the structure on the underside of the tip are believed to be due to the thin layer of gold applied for SEM imaging.

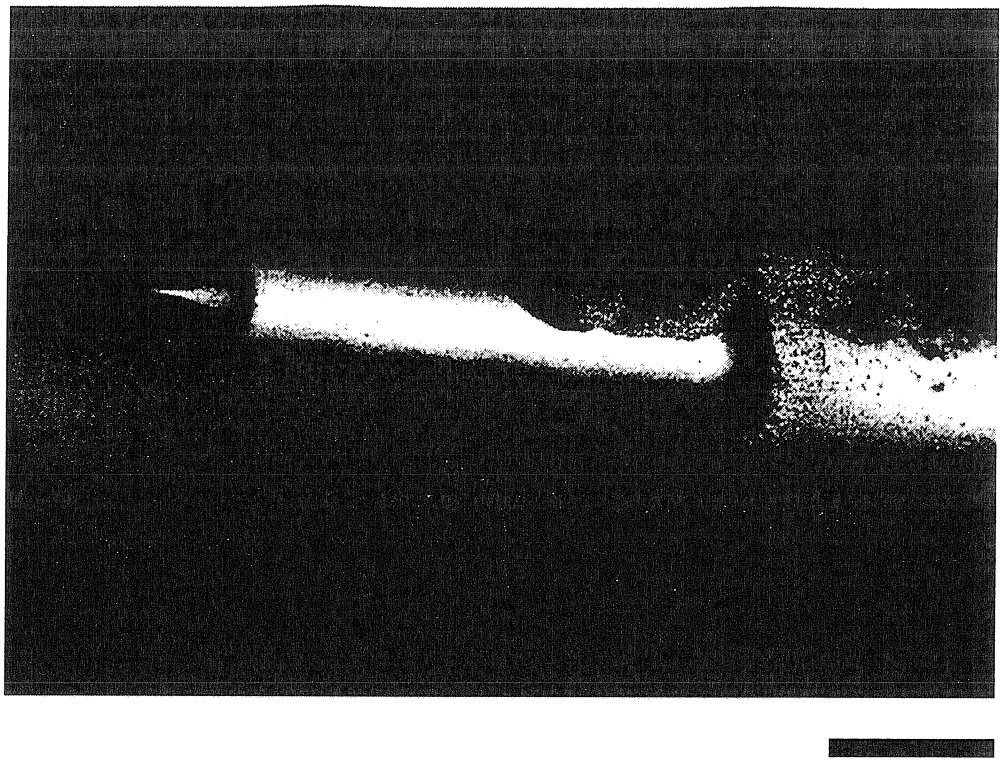

Figure 2.7. Scale bar = 500 μm. SEM micrograph of a clad 250 μm diameter core chalcogenide fiber etched by the described method. Removal of the clad and etching of the core are visible. The "blob" at the top is silver paint applied to provide a conductive path to ground for SEM imaging.

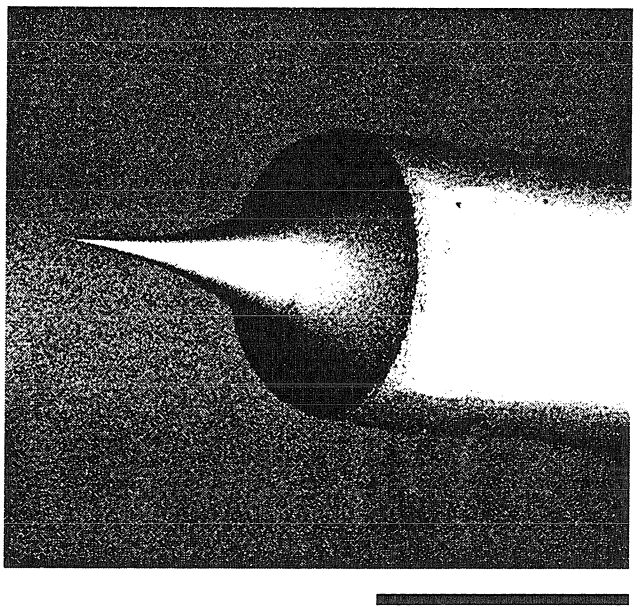

Figure 2.8. Scale bar = 250 μm. Zoom onto the tip shown in Figure 2.7.

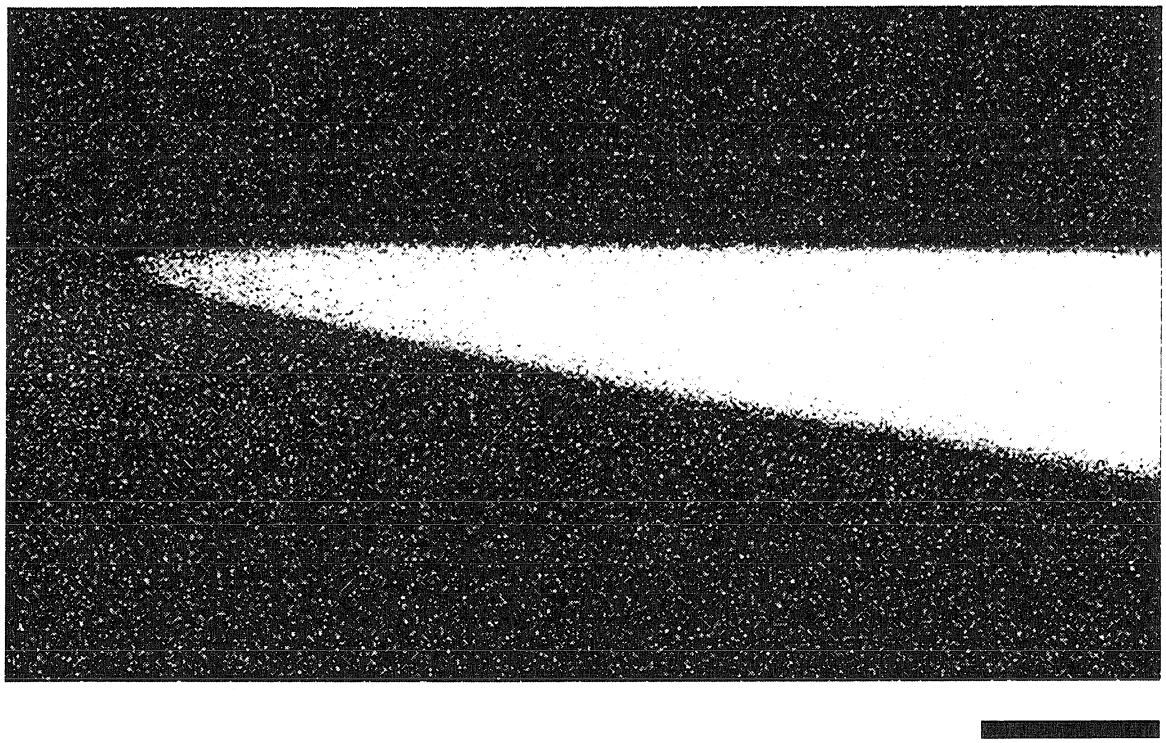

Figure 2.9. Scale bar = 1μm. Zoom onto the tip apex of the tip shown in Figure 2.7.

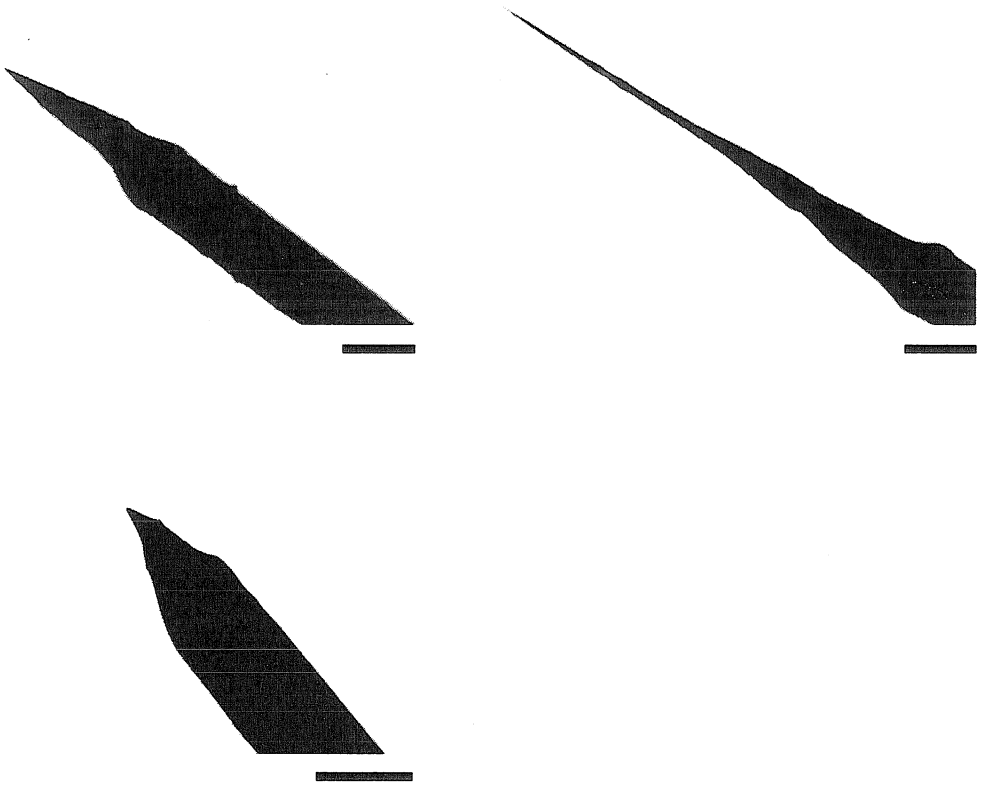

Figure 2.10. Scale bars = 150 μm. Optical micrographs of tips etched without protective solvent overlayers. Note the asymmetry and large-scale corrugation.

Experimentally, it is observed that without a solvent overlayer, the meniscus of piranha solution at an inserted fiber curves up, whereas with a solvent overlayer the meniscus of the piranha solution at the fiber is flat. This meniscus curvature is believed to disrupt the convection pattern responsible for producing smooth, concave-conical tips.

According to the convective control hypothesis, if the effects of convection are reduced relative to diffusion and reaction, more isotropic etching would be expected. See Figure 2.11.

Three different experiments were performed to test this prediction. In the first experiment, etching was performed in the normal apparatus, but at reduced temperature (5 °C - see Figure 2.12).

Reduced temperatures increase the viscosity of the piranha solution, thus making convection slower. In the second experiment, etching was performed in the normal apparatus, but with fairly rapid stirring of the piranha solution. Stirring essentially equalizes the concentration of H_2O_2 and dissolved chalcogenide throughout the piranha solution (see Figure 2.13).

In the third experiment, a glass capillary (i.d. ~ 1.5 mm) was used instead of a glass vial (i.d. ~ 2.5 cm). Since the fiber itself took up a substantial portion of the interior space in the capillary, convection was seriously impeded (results not shown). In all three cases, long, high aspect-ratio fiber tips without evidence of "necking" were produced. It is more difficult to judge "completion" with these fibers, since there is no "falloff" event.

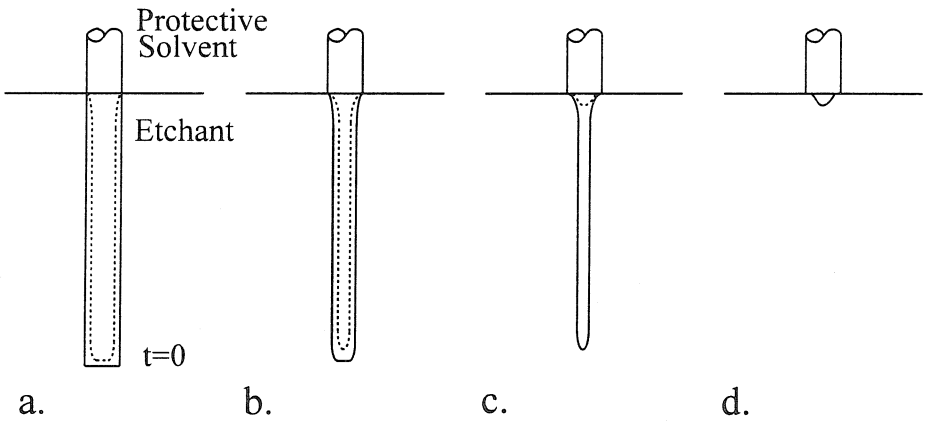

Figure 2.11. Schematic of the two-phase etching mechanism under conditions of isotropic etching. The dotted lines qualitatively indicate rates of etching, or the new profile of the tip after a discrete time-interval. No "necking" or falloff is expected.

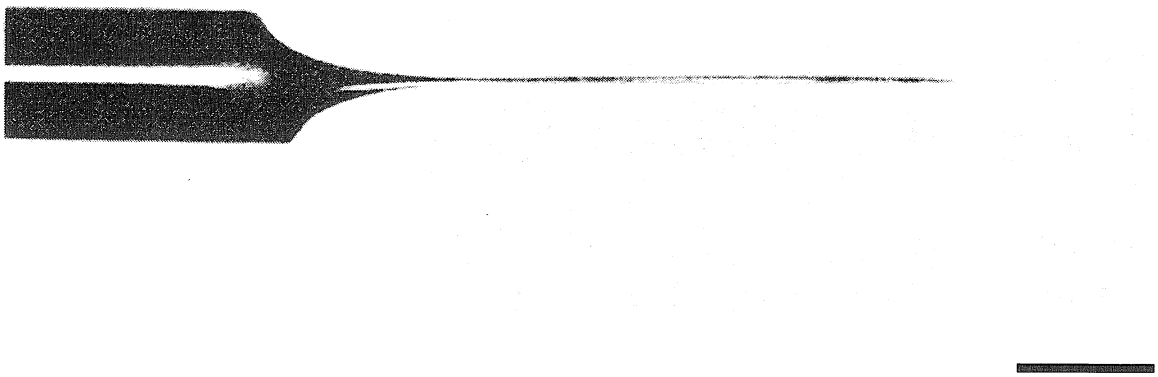

Figure 2.12. Scale bar = 150 μm. Optical micrograph of a 145 μm core chalcogenide fiber etched at reduced temperature (5°C).

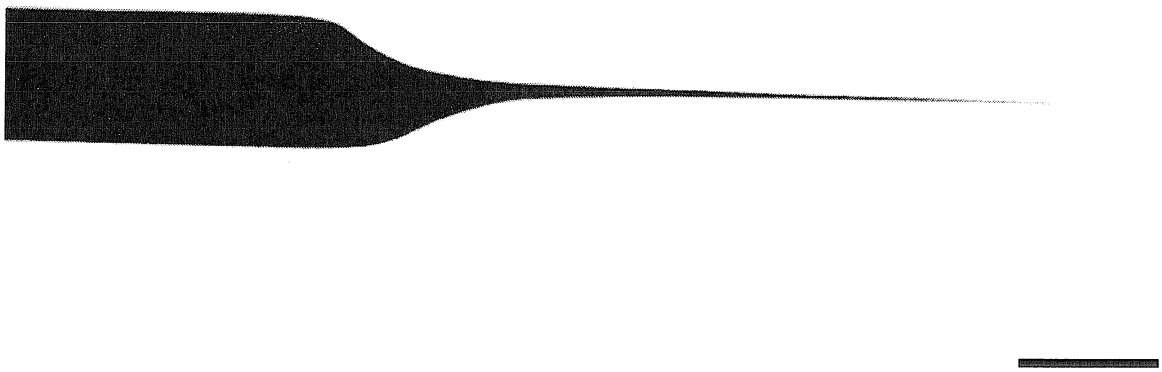

Figure 2.13. Scale bar = 150 μm. Optical micrograph of a 145 μm core chalcogenide fiber etched in stirred pihrana solution.

From our hypothesis, we would also expect that the neck should always point straight down from the meniscus. To test this prediction, etching was performed in the normal apparatus, but with the glass vial tilted at ~60°. As predicted, the tip thus produced pointed off-axis by approximately 60° (results not shown). The tip was, however, asymmetric and not very sharp.

E. IR RADIATION THROUGHPUT MEASUREMENTS

For transmission measurements chalcogenide glass fibers with a 250μm core were used. A two step etching procedure has been used to ensure the straight taper and sharp taper angle. At the first step, the long (about 1 mm) concave taper has been achieved during about 30 min. of etching, then the fiber was inserted an additional 0.5 mm into the etching solution and etched another 1-2 min. until the straight taper of about 20° (half angle) has been achieved. The resulting shape of the etched tip is shown in Figure 2.14 with optical original magnification x200.

The thickest portion of the fiber in this picture corresponds to initial core diameter of 250 microns. The second step of etching is clearly seen on this photograph at about 0.6 mm from the tip.

The etched fiber was coated with a 190 nm layer of gold. During the gold deposition the fiber was rotated around its axis oriented at about 45° to the direction towards the source, with the tip pointing towards the evaporation boat. Such a coating geometry should result in complete opacity of the tapered tip.

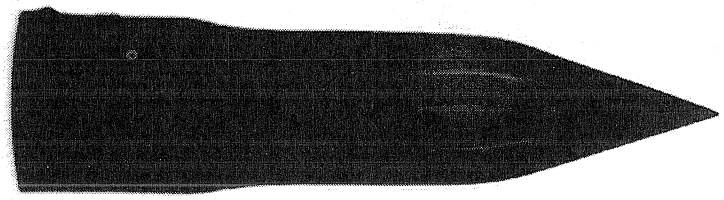

Figure 2.14. Optical micrograph of a 250 μm core chalcogenide fiber etched in piranha solution utilizing two-step procedure (described in text). The thickest portion of the fiber in this picture corresponds to initial core diameter.

The coated fiber was fixed in a micromanipulator on an inverted microscope (Zeiss, Axiovert 35) with a tip looking down, towards the objective. For detection of the IR radiation a Cassegrain objective was used (N.A. 0.65, Ealing Electrooptics Inc., Holliston, MA). The collimator lens was removed to ensure transmission of the IR radiation. A MCT detector (Kolmar Technologies Inc., Conyers, GA) was used for detection of the IR radiation collected by the objective and reflected towards the epi-illumination port. The reflector slider contained two reflector slides - one with gold coating for full reflection of the measured IR light, and the other - an uncoated glass slide - for observation of the fiber tip with epi-illumination. A T-shaped adapter was used at the rear port of the microscope to accommodate both, the illumination lamp and the MCT detector.

The radiation of the Free Electron Laser (FEL) was focused on the input end of a ~1m long fiber. Macropulses of about 3 ms duration and repetition rate of 10 Hz were applied at the wavelength of 6.01 μm with the average power of 2.5 mW. A small portion of the FEL beam has been reflected to the reference detector for monitoring the input beam intensity, and the signal received through the fiber was ratioed to the reference signal to ensure the signal stability at various input energies.

The fiber tip was positioned in focus of the objective (the tip was observed through the microscope with x20, x40, and x100 refractive objectives under epi-illumination) and the IR signal has been detected using the reflective objective. The non-zero signal at this point indicated a leak of the radiation through the holes in coating. Such holes may result from the dust particles occasionally stack to the fiber prior to coating or from the small droplets of gold ejected from the evaporation boat. After the

measurement of the background signal, a 0.1 mm thick glass slide was positioned under the fiber tip. A thin polishing film with a particle size of 0.05 μm was attached to the slide. The microscope objective was focused on the film, and the fiber was carefully brought into contact with the film. Contact was detected by slight movement of the film out of focus resulting from deflection of the film and/or the glass slide supporting the film. To ensure the flexibility of the system, the slide was held only at one side providing a long cantilever under the polishing film and the film was attached to the slide at one end providing some free space between the film and the glass under the tip. The film was scanned in x and y directions over a few microns, then the tip was withdrawn from contact, and the slide with polishing film was moved aside.

The resulting flat aperture was observed through the x100 objective and its dimensions measured with resolution of about 0.5 μm. Then the IR signal transmitted through the tip was measured using the reflective objective. The polishing procedure and corresponding transmission measurements were repeated until the taper was completely removed. The background was subtracted and the data normalized to 1.0 for an aperture equal in width to the fiber (i.e., no taper). The curve of throughput as a function of the aperture area is shown in Figure 2.15.

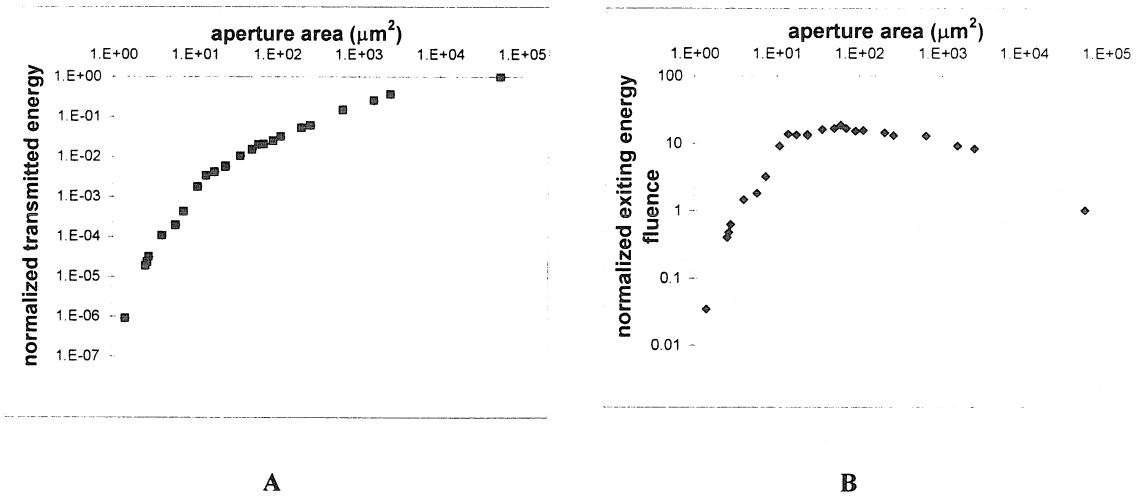

A B

Figure 2.15. IR radiation transmission at D=6.01μm through an etched gold coated fiber as a function of exit aperture area: (a) normalized transmission, (b) normalized transmitted power fluence at the surface of exit aperture.

We used the aperture area instead of diameter due to the fact that the aperture was not round and the elliptical axis ratio varied with the distance from the tip. In Figure 2.15b the power fluence (i.e., power per unit area) at the tip exit is depicted as a function of the tip size (this curve is a result of division of transmitted power (shown in Figure 2.15a) by corresponding aperture area). As can be seen on this graph, the power fluence grows at the beginning of the taper up to about 15 times the input fluence due to the light concentration, and remains constant up to the aperture size of about 10 μm^2, which correspond to about $(\lambda/2)^2$; this behavior is typical for macroscopic tapered fibers. At smaller apertures the power fluence drops due to exponential attenuation of the light intensity in the waveguide below the cut-off diameter[16]. The throughput becomes lower than 10^{-4} at the aperture size below about 4 μm^2, which corresponds to the round aperture diameter of about $\lambda/3$. By comparison, pulled fiber probes with a $\lambda/3$ aperture typically[17] have a throughput of $< 10^{-6}$.

The described results indicate higher throughput of etched fiber probes as compared to pulled probes. Demonstrated characteristics of etched probes make it possible to substitute an Optical Parametric Oscillator (OPO) laser as a light source. As OPO lasers are far more common and much less costly than FELs (~250k$ vs 1M$ + shielded facility cost), this would make NSIM a vastly more accessible technique.

Another potential use of etched IR fiber probes is for high-spatial-resolution temperature measurements, such as those required in semiconductor device diagnostics. Tapered IR-transparent fibers are also used as attenuated total reflectance (ATR) "cells"

in FTIR spectroscopy[18]. Chemical etching, as opposed to hot-filament-pulling, may also be a useful way to fabricate probes for this application.

CONCLUSION

We have demonstrated methods to remove the coating and cladding from chalcogenide infrared transmitting fibers, as well as a simple chemical method to etch the fibers to a point with submicron radius of curvature. Chemical etching is simpler and more reproducible than heat pulling infrared fibers. The tips produced also have a much shorter taper length; this makes them more robust and also improves throughput by minimizing the distance that light must travel in a subwavelength aperture.

The chemical etching mechanism has been shown to be convective control of tip etching. Laminar flow down the fiber causes the least saturated (most reactive) etching solution to enter the flow stream primarily just below the meniscus. The presence of a protective solvent overlayer serves to keep the meniscus flat, regularizing the laminar flow down the fiber. Reducing the effects of convection (by reducing temperature or stirring) produces isotropic etching and reduces tip sharpness dramatically.

REFERENCES

[1] A. Harootunian, E. Betzig, M. Isaacson, and A. Lewis, Superresolution Fluorescence Near-Field Scanning Optical Microscopy. *Appl. Phys. Lett.* **49** (1986) 674.

[2] E. Betzig, J. Trautman, T. Harris, J. Weiner and R. Kostelak, Breaking the Diffraction Barrier – Optical Microscopy on a Nanometric Scale, *Science* **251** (1991) 1468.

[3] D. Courjon and C. Baineier, Near-field Microscopy and Near-field Optics, *Reports on Progress in Physics* **57** (1994) 989.

[4] R. Kopelman and W. H. Tan, Near-field Microscopy, Spectroscopy, and Chemical Sensors, *Applied Spectroscopy Reviews* **29** (1994) 39.

[5] E. Betzig and J. K. Trautman, Near-field Optics – Microscopy, Spectroscopy, and Surface Modification Beyond the Diffraction Limit, *Science* **257** (1992) 189.

[6] J. K. Trautman, J. J. Macklin, L. E. Brus, and E. Betzig, Near-field Spectroscopy of Single Molecules at Room Temperature, *Nature* **369** (1994) 40.

[7] Assuming cutoff at 50 dB/km, or 20 dB/m.

[8] G.A. Valaskovic, M. Holton, and G.H. Morrison, Parameter Control, Characterization, and Optimization in the Fabrication of Optical Fiber Near-field Probes, *Appl. Opt.* **34** (1995) 1215.

[9] G. A. Massey, J. A. Davis, S. M. Katnik, and E. Omon, Subwavelength Resolution Far-Infrared Microscopy, *Applied Optics* **24** (1985) 1498.

[10] T. Nakano and S. Kawata, (1993). Infrared Evanescent-field Microscope using CO_2 Laser for Reflectance Measurement, *Optik* **94** (1993) 159.

[11] A. Lahrech, R. Bachelot, P. Gleyzes, and A. C. Boccara, Infrared Reflection-mode Near-field Microscopy Using an Aperatureless Probe with a Resolution of Lambda/600, *Optics Letters* **21** (1996), 1315.

[12] A. Piednoir, C. Licoppe, and F. Creuzet, Imaging and Local Infrared Spectroscopy with a Near-field Optical Microscope, *Optics Communications* **129** (1996) 414.

[13] M. K. Hong, S. Erramilli, P. Huie, G. James, and A. Jeung, *SPIE* **2863** (1996) 54.

[14] S. Erramilli and M. Hong, personal communication.

[15] D. Zeisel, B. Dutoit, V. Deckert, T. Roth, and R. Zenobi, Optical Spectroscopy and Laser Desorption on a Nanometer Scale. *Anal. Chem.* **69** (1997) 749.

[16] For example: page 207 in T.R. Corle, G.S. Kino. Confocal Scanning Optical Microscopy and Related Imaging Systems, Academic Press, San Diego 1996.

[17] Personal communication, Daniel Palanker, Stanford Free Electron Laser Facility.

[18] M. C. Ertan-lamontagne, S. R. Lowry, W. R. Seitz, and S. A. Tomellini, Polymer-coated Tapered Cylindrical ATR Elements for Sensitive Detection of Organic Solutes in Water, *Applied Spectroscopy* **49** (1995) 1170.

Chapter 3. TOPO-MS: Scanned Probe Combined with Mass Spectrometry

This chapter is partially adapted from the article "Spatially Resolved Chemical Analysis with an NSOM-based Laser Desorption Microprobe" by D.A. Kossakovski, S.D.O'Connor, M.Widmer, J.D. Baldeschwieler, and J.L. Beauchamp, published in Ultramicroscopy 71 (1998) 111-115, Copyright 1998, with permission from Elsevier Science.

INTRODUCTION

Chemical imaging with high spatial resolution is needed in a variety of different fields, including biology, geology, materials science, and microelectronics. At present there are a number of methods which provide chemical information relating to surface species, mainly utilizing different contrast mechanisms (see review reference[1] for a comparative review of the performance of different methods). A common problem in surface analysis involves observation of an interesting topographical feature, followed by an attempt to identify the chemical nature of the feature, e.g., investigation of impurities on semiconductor surface or meteorite inclusions. No single technique today can provide simultaneous topographical and chemical analysis of surface structures. Scanning probe microscopy (SPM) methods, which excel in topographical studies, generally lack chemical contrast capabilities.

The instrument developed in our laboratory combines the attractive features of two techniques: surface profiling with high resolution by means of scanning probe microscopy and chemical analysis by mass spectrometry. We use an NSOM apparatus[2] to deliver UV radiation from a pulsed nitrogen laser (337 nm) through a UV fiber to a feature of interest on the sample. Species desorbed and ionized by the pulsed laser are analyzed using a TOF mass spectrometer. The method is similar in some respects to desorption with a focused laser that can be scanned over the surface (LAMMA or

LAMMS)[3] and secondary ion mass spectrometry (SIMS)[4]. There are some significant differences to be noted in comparing these experimental methodologies to our experiment: (1) with NSOM-TOF the spatial resolution is not diffraction limited as it is in the case of LAMMA, and (2) since the probe is maintained at a constant distance from the sample by NSOM feedback, we are simultaneously acquiring topographical information (i.e., height of surface features) to correlate with chemical information.

EXPERIMENTAL

To demonstrate the feasibility of combining NSOM with TOF-MS, we assembled the simple instrument illustrated schematically in Figure 3.1. A scanning head of a near-field microscope is located inside a vacuum chamber (at pressure 10^{-7} Torr or lower). A UV transparent quartz multimode fiber (HFS-50 from Radiant Communications) is coupled (fiber coupler from Oz Optics) to a pulsed nitrogen laser (3 ns pulses at 20 Hz repetition rate, 250 μJ per pulse, VSL33ND from LSI Inc.) outside the chamber. The coupling efficiency is about 50% which is in part related to the peculiarities of the beam profile of nitrogen laser.

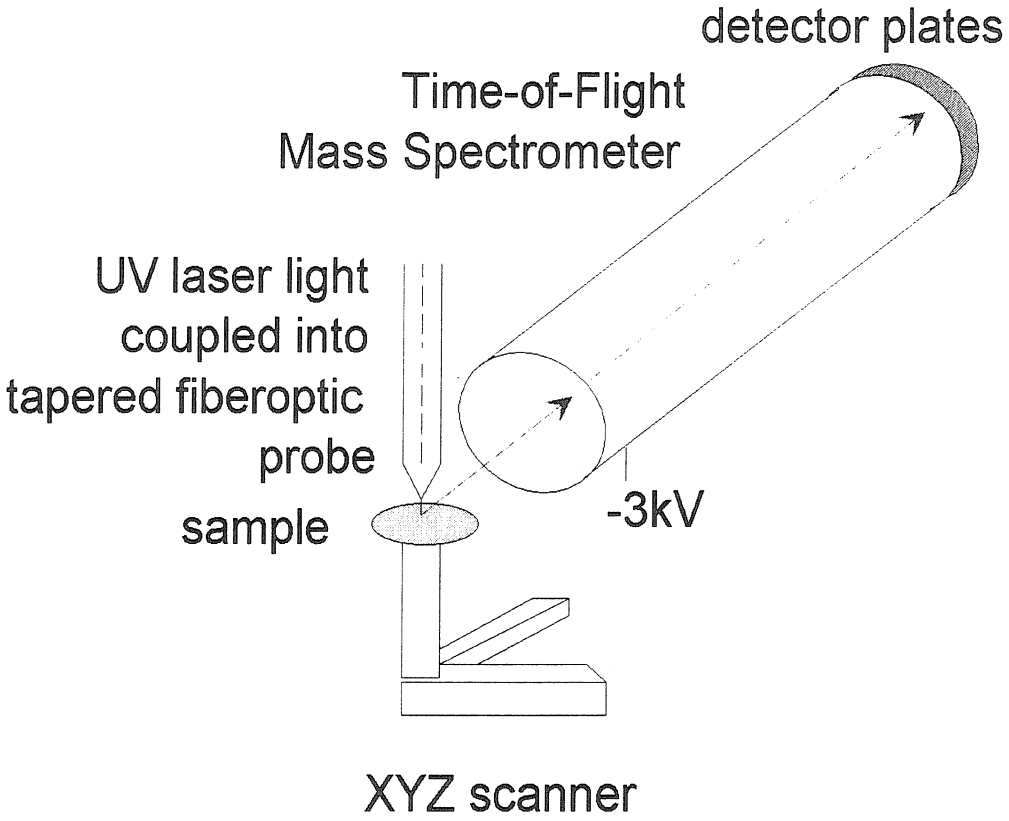

Figure 3.1. Schematic of an instrument for spatially resolved chemical analysis. The UV fiberoptic probe is scanned over the surface to generate an image of spatially resolved laser desorbed ions, with simultaneous recording of sample topography.

An etched uncoated probe is brought to the sample utilizing a shear force feedback and tuning fork detection scheme[5]. The end radius of curvature of the probe is less than 200nm. The power delivered to the sample can be varied by using an iris between the laser and fiber coupler. At small openings of the iris no ions are observed. When the size of iris opening is continuously increased, the threshold fluence is reached and ion production is observed. At present time we do not have a quantitative value for the power density delivered to the sample surface. The threshold fluence is known to be around 10^6 W/cm^2, so the fact that we observe ion production proves that the power at the sample exceeds this value. Increasing laser power usually results in higher degree of ion fragmentation, so our expectation is that in future studies we will be able to perform both elemental and molecular analysis by varying the laser power.

The ions are analyzed with a custom built mass spectrometer. A compact TOF mass spectrometer (30 cm flight tube) is focused onto the sample. The sample is maintained at ground potential and the flight tube is biased at –3 kV to accelerate positive ions toward a dual channel plate detector. The arrival time distribution of laser desorbed ions is measured with a LeCroy model 9450 digital oscilloscope and analyzed after transfer to a 486 computer with TOFWARE (Ilys Software) to provide a mass spectrum.

RESULTS

Our first goal was to demonstrate that laser desorption and mass spectrometry analysis is achievable with NSOM probes and with engaged feedback. For this purpose a sample was prepared by drying a solution of acetylcholine (ACh) and dihydroxybenzoic acid (DHB), on a copper plate. DHB is commonly employed as a matrix to enhance

yields of laser desorbed ions[6]. ACh is a small neurotransmitter with a quaternary nitrogen center (an "organic salt") to facilitate desorption as an ionic species. The probe was brought into feedback and the laser was fired. Figure 3.2 demonstrates a mass spectrum of this sample, which was obtained by integrating 100 consecutive pulses at the same probe position. The feedback was engaged at all times during the desorption sequence. The spectrum shows clearly resolved peaks for different components in the sample, including a prominent feature corresponding to the mass of the molecular ion of Ach. The sample/probe separation in this experiment was about 10 nm, the end radius of the uncoated probe tip was approximately 200 nm.

Having demonstrated capability for chemical analysis in a single location the next goal was to perform simultaneous topographical scanning and chemical mapping. To accomplish this a substrate with a well defined topography, a copper TEM grid with 25 μ pitch (G1000HS from Ted Pella Inc., square pattern) was chosen. The same sample solution used to obtain the data in Figure 3.2 was applied to this grid.

Figure 3.3 shows a topographical scan of the grid. It is known that when DHB solution is dried on a solid substrate, it forms crystals the size distribution of which depends strongly on drying conditions, initial solution concentrations and other factors[7]. Also, a non-crystallized film of DHB can be formed in some sample areas. We observed DHB crystals on our TEM grid by using a medium power optical microscope.

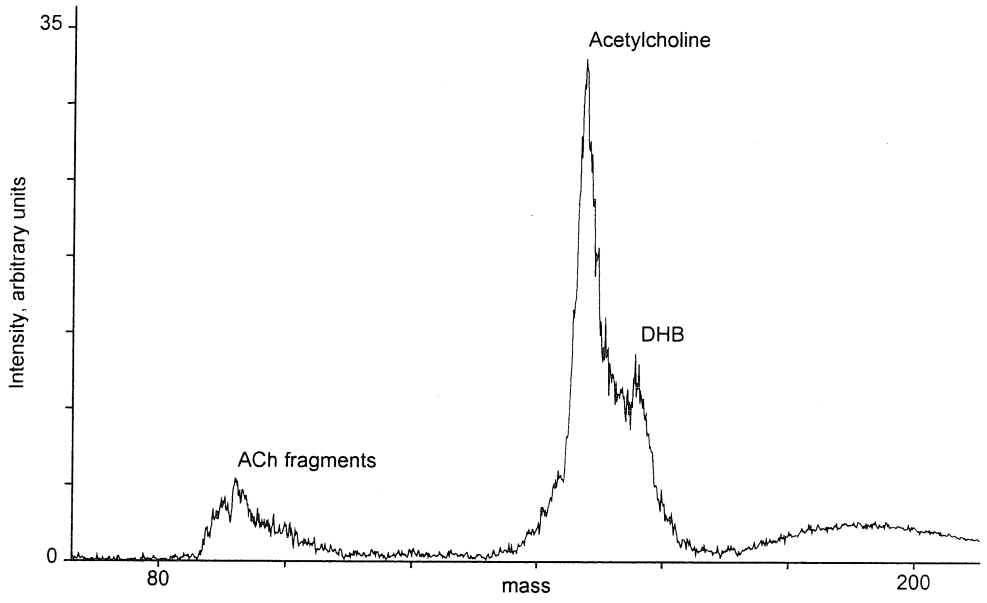

Figure 3.2. Mass spectrum of laser desorbed ions using the instrument in Figure 1, with a sample comprising acetylcholine in the MALDI matrix dihydroxybenzoic acid.

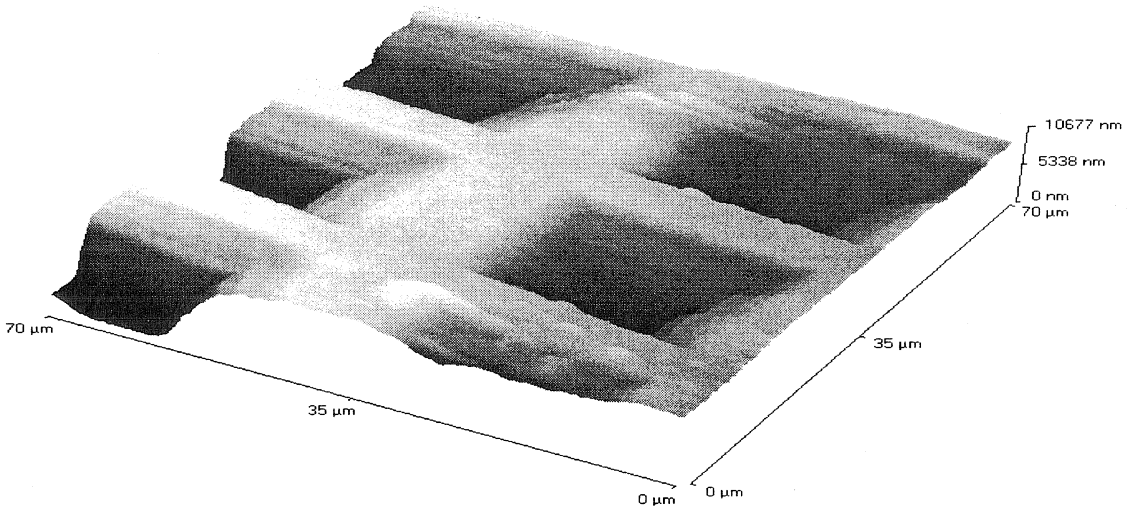

Figure 3.3. Topography of a TEM grid (25 µ pitch) with DHB/Ach deposited on it. Scan area 50 x 50 µ.

The goal of the experiment was to demonstrate a correlation between substrate topography (TEM grid in this case) and chemical composition, so when the sample was mounted on our NSOM scanner, the survey of the grid was performed and a portion of the grid without large crystals was chosen for the experiment. One can see small particles in Figure 3.3; most probably those are small DHB crystals.

The distribution of acetylcholine was mapped in a line across the grid, using 20 laser shots for each pixel of the topographical line scan. The pixel size of the topographical scan was 1μ. For each laser shot a signal corresponding to the ACh peak was acquired and integrated. Figure 4 shows the ACh distribution along this line scan. The pattern clearly repeats the topography of the grid with the correct pitch value. The continuous slope on Figure 3.4 in the parts of the line scan corresponding to TEM grid bars may result from non-uniform sample deposition, or be related to the scan direction, which is from left to right for the data shown in Figure 3.4. We do not have a precise control of laser power and beam shape emanating from the probe. As a result, the light which leaks sideways from the uncoated taper of the probe may deliver over-the-threshold fluence to the sample. This means that the matter is being desorbed not only right underneath the probe but also in some finite area exceeding the tip apex size, which leads to the broadening of the desorption spot. This may in part explain the apparent spatial variation of ACh signal along the line.

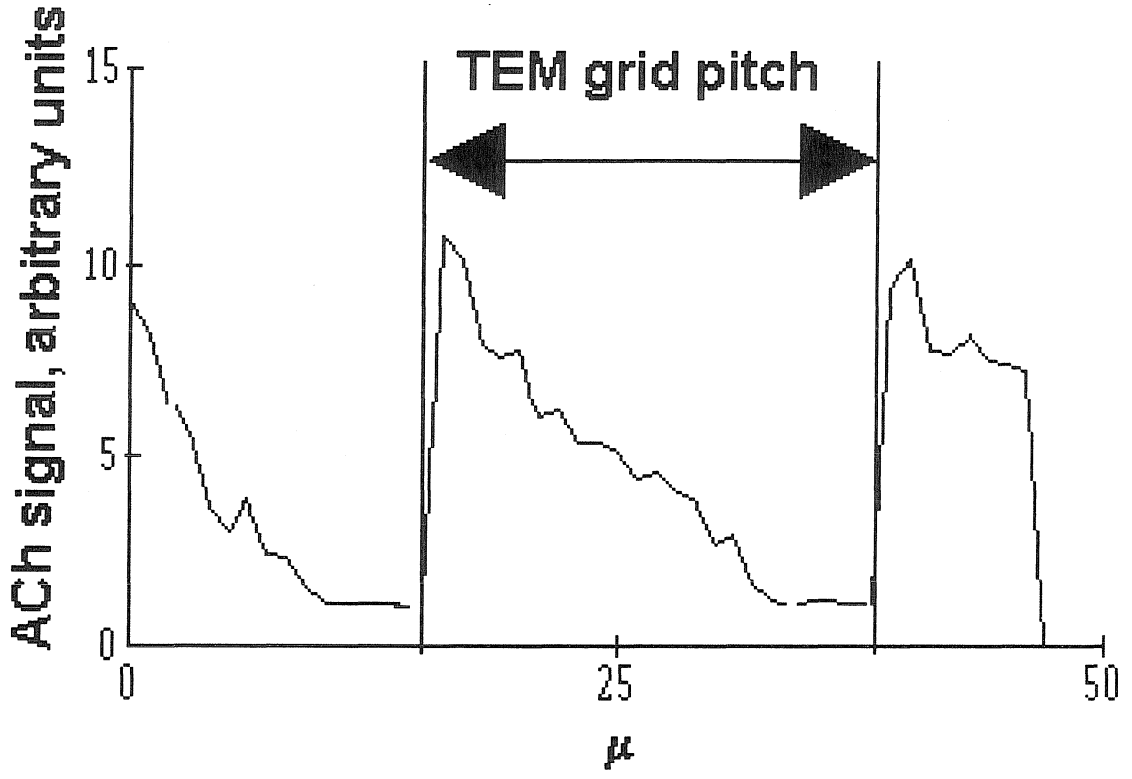

Figure 3.4. Line scan of acetylcholine ions from a TEM grid with 25 μm pitch. The probe is scanned from left to right.

DISCUSSION

The mass resolution of the spectrum in Figure 3.2 is low compared with that of state of the art TOF mass spectrometers. The resolution will be significantly improved in the next generation of our instrument. The instrument was calibrated on a different sample which contained sodium and potassium chloride which are known to be easily ionized. This calibration was applied to the spectrum shown in Figure 3.2. DHB is known to form a fragment ion at mass 137 a.m.u. We do not observe a clear peak corresponding to this mass in Figure 3.2, although it may be obscured by the left shoulder of ACh peak. We also do not observe a sodiated DHB ion ($DHB+Na^+$) which can be commonly seen when working with DHB preparations. One of the reasons of low performance of our TOF mass spectrometer is that the dielectric probe is brought into the region of ion formation. Charging of the probe may disturb the flight path of the ions.

The spatial resolution of the line scan in Figure 3.4 is about 1μ judging from the slope corresponding to the edge of a grid aperture. We believe that it will be possible to bring the spatial resolution into the sub-micron range, with our final goal being 100 nm. This requires both optimization of our probes and improvement of TOF–MS sensitivity. The former will be achieved by careful control of the probe shape and laser power delivered to the sample and the latter can be realized by using more efficient ion collection optics and ion counting techniques. Several authors have used uncoated probes for lithography applications, for which the process on surface is also threshold fluence controlled, as in our experiment, and it was shown that the spot size with surface power density exceeding some critical value can be constrained to about 100nm[8]. We

hope that we will be able to achieve similar performance with our setup, although one important difference is that in the reported studies singlemode fibers were used. We are using multimode fibers, the only type currently available for the UV radiation emitted by nitrogen laser.

We have not experimented yet with larger molecules (i.e., peptides), for analysis of which the TOF mass spectrometry is widely used. We anticipate the mapping of spatial distribution of such compounds over the substrates as one of the areas of application of the instrument.

Currently we are studying the limitations of the technique, which may result from desorption crater formation and displacement of material. The desorption damage is expected to be highly dependent on the nature of the sample. "Soft" or compliant samples, like biological specimens, are more vulnerable than "hard" samples, such as geochemical preparations.

We want to emphasize that the data presented is the result of our initial effort to demonstrate the feasibility of the technique. We are in the process of construction of an improved instrument, TOPO-MS II, which incorporates features to facilitate changing samples and probes. After the completion of this new instrument we will be in a position to do a thorough investigation of the method capabilities.

Appendix C of this thesis contains information on design of TOPO-MS II.

CONCLUSION

We have developed an instrument for simultaneous surface topographical and chemical analysis. Laser desorption and TOF-MS analysis has been demonstrated with

uncoated fiber probes. Spatially resolved chemical analysis has been performed on test samples. We anticipate that this instrument, which provides chemical imaging with high spatial resolution, will have widespread applications in many fields of science.

ACKNOWLEDGMENTS

We would like to thank ONR/ARPA (N00014-92-J-1901) and the Beckman Institute of the California Institute of Technology for partial support of this project.

REFERENCES

[1] R.K.Wild, *Adv. Mat. Opt. Electr.* **5** (1995) 53. Also, a good review of surface analysis techniques is presented on the website of Charles Evans & Associates: http://www.cea.com.

[2] E. Betzig, J. Trautman, T.D. Harris, J.S.Weiner, and R.L. Kostelak, *Science* **251** (1991) 1468.

[3] L.Vanvaeck, H. Struyf, W.Vanroy, and F. Adams, *Mass. Spectr.***13** (1994) 209.

[4] J.M.Chabala, K.K.Soni, J.Li, K.L.Gavrilov, and R.Levi-Setti, *Int. J. Mass Spec. Ion Proc.* **143** (1995) 191.

[5] K. Karrai, R.D. Grober, *Appl. Phys. Lett.* **66** (1995) 1842.

[6] B. Spengler, D. Kirsch, R. Kaufmann, M. Karas, and F. Hillenkamp et al., *Rap. Comm. Mass* **4** (1990) 301.

[7] S.L.Cohen and B.T.Chait, *Anal. Chem.* **68** (1996) 31.

[8] G. Krausch, S.Wegscheider, A. Kirsch, H. Bielefeldt, J.C. Meiners and J. Mlynek, *Opt. Comm.* **119** (1995) 283; S. Madsen, M. Mullenborn, K. Birkelund, and F.Grey, *Appl. Phys. Lett.* **69** (1996) 544.

Chapter 4. TOPOLIBS: Scanned Probe Combined with Laser Induced Breakdown Spectroscopy

INTRODUCTION

This chapter describes the development of a new instrument for chemical imaging of surfaces that combines a fiber-based scanning probe microscope with laser induced breakdown spectroscopy, LIBS. The information derived from these studies is similar to that provided by spark-gap atomic emission microscopy experiments with STM probes[1]. LIBS is widely used to study elemental composition of samples by analyzing optical emissions from pulsed plasmas created by a focused laser beam. It was pioneered by Radziemski in the early eighties[2]. Other names which are sometimes used to describe essentially the same technique are Laser Induced Plasma Spectroscopy (LIPS) and LAser Spark Spectroscopy (LASS). Today, with broad availability of pulsed lasers the applications of LIBS grow every year. Song and co-authors have recently published an extensive review of LIBS applications[3]. This analytical method is very attractive because of its simplicity, speed, affordability and virtually no requirements for sample preparation if the study is conducted under ambient conditions.

Near-field scanning optical microscopy (NSOM) on the other hand derives advantage of its capability to combine local topography studies with optical probing of samples. Sharp optical fiber is used as a proximal topography probe and as a light delivery means. Common varieties of optical studies, such as transmission, reflection and fluorescence, can be carried out with superb spatial resolution defying the diffraction limit.

Fiber probe can be also used for delivery of pulsed laser radiation for localized LIBS analysis. Combination of LIBS and scanning probe microscopy delivers a simple and elegant way to achieve chemical contrast to complement topographical studies performed by SPM. This chapter describes our efforts in the development of such combined analytical approach.

LIBS BACKGROUND

Mechanisms and theory of LIBS are treated in detail in the book edited by Radziemski[4]. The following are several key concepts and experimental parameters which are pertinent to the present studies.

LIBS has associated with it a distinct threshold behavior. Once the surface power density from laser radiation rises above a certain value, a pulsed plasma is formed. The threshold value depends on the sample, being roughly ~10^9 W/cm^2.

Two processes act in concert to produce the pulsed plasma, Multi-Photon Ionization (MPI) and Laser-Induced Breakdown (LIB). MPI involves simultaneous absorption of several photons to ionize the species:

$$M + mh\nu \rightarrow M^+ + e^- \qquad \text{(Eqn.1.)}$$

LIB is a cascade event similar to dielectric breakdown of solids, liquids and gases. The cascade reaction is started by producing free electrons in the focal volume with energy exceeding the ionization potential (or band gap) of the sample. Ionization of the sample results in production of free electrons

$$M + e^- \rightarrow M^+ + 2e^- \qquad \text{(Eqn.2.)}$$

The cascade grows as long as the energy of generated electrons exceeds ionization potential of neutrals.

Both mechanisms or only one may be operative in a particular case. Comparing equations (1) and (2), one can see that the output of MPI can feed the early stages of LIB by producing the required free electrons.

MPI depends on the laser wavelength while LIB does not. A wide variety of lasers have been used for LIBS studies. The most commonly used one is Nd:YAG operated at the fundamental wavelength of 1,064 nm.

The plasma which is produced by the laser pulse is very hot, with a temperature reaching several thousand degrees. This high temperature generates a substantial thermal background in the emission spectrum. Another source of background emission is *bremsstrahlung* radiation.

Optical emission from transient plasma has a lifetime of several microseconds. In the early stages, the major components of the spectrum are wide band background and emissions from excited ions. Later, about 1-2 μs after the pulse, those signals vanish and emissions from neutral species are observed. This means that it is extremely important in LIBS experiment to have the capability of starting spectrum acquisition *after* the laser pulse. It is a common practice in LIBS experiments to trigger the optical analyzer off the laser pulse with adjustable delay. It is also beneficial to gate the acquisition if equipment allows for it.

If experiments are conducted in air or a controlled environment, there is a possibility that plasma components will react with the gases present. This will lead to formation of new molecular species, which may be observed in the emission spectrum.

Sometimes these secondary signals are comparable or even stronger than weak primary LIBS emissions. This facilitates the study of samples which have intrinsically weak LIBS spectra in the absence of reactive gases. For example, this is the case with graphite in air. Elemental carbon has very weak atomic emissions however, when LIBS is conducted in air, molecular emission bands from C_2, CO and CN are observed. Those molecules are formed in the ablation process and during plasma interaction with ambient gases[5].

TOPOLIBS

In order to achieve spatially resolved chemical imaging, we have combined LIBS with a shear-force fiber probe SPM in a single instrument which we refer to as TOPOLIBS. A diagram and photograph of the instrument are shown in Figure 4.1. This instrument was assembled to demonstrate the feasibility of the method. The experimental approach embodies the following steps.

1. Topographical analysis: Sharp optical fiber probe is brought into shear force feedback to maintain probe-sample separation and scanned at constant distance from the surface to examine the sample topography. No laser radiation is used in this analysis.
2. Chemical analysis: After features of interest are located in the topographical image, the probe is positioned and LIBS data recorded to provide chemical information to further characterize the sample. When specific chemical signatures are observed, they can be monitored during a rescan of the surface to generate a spatially resolved image of the identified species.

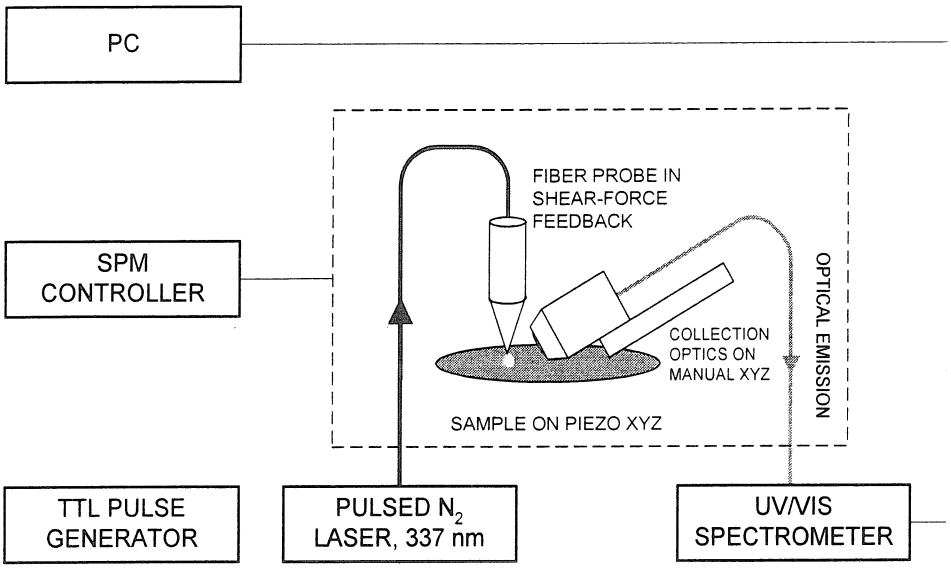

A

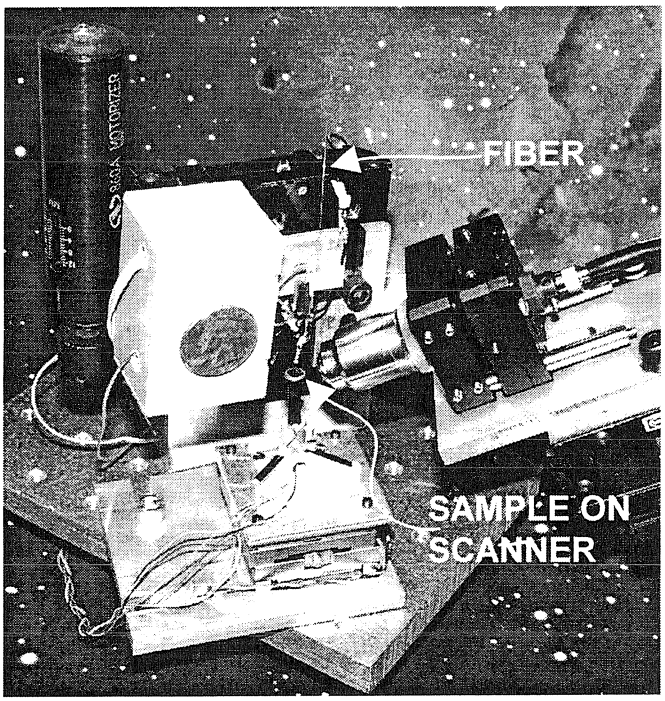

B

Figure 4.1. Details of TOPOLIBS instrument. (a) Schematic diagram showing major components of the system. (b) Photograph of the proof-of-concept setup showing the scanner, optical fiber and microscope objective for LIBS signal collection. A quarter coin is attached to demonstrate the miniature size of the system.

EXPERIMENTAL SECTION

SPM. The home-built scanning probe microscope uses uncoated etched fiber optics probes[6] and tuning fork position feedback[7]. We have utilized multimode UV transparent fiber HFS-50 from Radiant Communications (South Plainfield, NJ). The operation of the scanner is controlled by PScan2 SPM electronics from Pacific Scanning (Pasadena, CA). The Signal Access Console of PScan2 is used to feed the output of the tuning fork circuit into controller and also to provide master TTL pulses for LIBS system.

LIBS. A pulsed nitrogen laser from Laser Science (Franklin, MA), model VSL-337ND (337 nm emission wavelength with a 3 ns of 250 μJ l pulse, maximum repetition rate of 20 Hz) was used to perform both traditional LIBS experiments and TOPOLIBS. The non-Gaussian beam is square shaped with ~35 mm^2 beam cross-section. In LIBS experiments the beam was focused on the sample by a quartz lens with 100 mm focal distance. In TOPOLIBS the beam was coupled into the fiber with HPUC-337 coupler by OZ Optics (Canada).

Optical emission from the plasma plume was collected with a standard ×20 microscope objective, coupled into a 400 μm fiber and delivered to the 25 μm entrance slit of a miniature spectrometer, S2000 from Ocean Optics (Dunedin, FL). The CCD detector of the spectrometer was operated in external trigger mode to synchronize data acquisition with laser pulse. The recommended timing arrangement for LIBS experiments is to start data acquisition *after* the laser pulse, the delay being dependent on the laser wavelength but generally in the microsecond region. The delayed acquisition usually provides dramatically improved signal-to-noise ratios for individual emission lines in the spectrum. Unfortunately, the hardware of the S2000 spectrometer does not allow for

careful timing of the measurement. The delay between incoming trigger pulse and start of the acquisition is ~20 μs with a variation of at least 1μs. This makes delayed acquisition impossible for LIBS purposes with the S2000. In order to capture LIBS emission, the S2000 spectrometer had to be triggered before the laser. As a result the spectra contain contributions from the laser line (including second order of diffraction in the spectrometer) and a broadband background. It is expected that with delayed acquisition the quality of spectra will be significantly improved.

The timing scheme of our experiment was as follows: A TTL pulse from the PScan2 controller was delivered to an arbitrary waveform generator model 75A from Wavetek (Research Triangle Park, NC). On arrival of the trigger pulse the waveform generator produced either a single pulse or a burst of TTL pulses at 10Hz. Each pulse had a duration of 10 ms. The spectrometer was triggered off the rising edge of the pulse while the laser was triggered off the falling edge. Spectrometer integration time was 27 ms. This timing scheme allowed the spectrometer to capture the spectrum before the next trigger pulse arrived.

Spectral data were exported from Ocean Optics software in ASCII format and analyzed off-line with SigmaPlot by SPSS (Chicago, IL) package. Tables of spectral line intensities by W.F.Megger et al.[8] were used to assign the spectral features arising from elemental contributions, while the classic text of Pearse and Gaydon[9] was used to analyze molecular emissions. Another extremely useful tool for peak assignment is the NIST database available through the Internet[10].

No automatic peak recognition/assignment software was used in our studies. A variety of such packages are available from different manufacturers. Galactic Industries

(www.galactic.com) sells the package GRAMS/32 which is widely used in spectroscopic community. GRAMS can perform automatic peak labeling, but not assignment. A promising tool for peak assignment is the FindEM module for GRAMS sold by Multichannel (Sweden, www.multichannel.se). The database used by FindEM contains the well-known atomic lines (200 - 1100 nm) of the air emission wavelengths for neutral atoms and their first four ionisation stages. It also contains band heads of more than 230 molecules. FindEM identifies and displays the atomic and molecular structures in spectra viewed with the GRAMS/32. At the time of writing this thesis we have not yet evaluated this package.

RESULTS AND DISCUSSION

FOCUSED BEAM: TRADITIONAL LIBS

In order to gain experience with the LIBS experiment, initial studies were conducted using a traditional LIBS arrangement, without an optical fiber. The nitrogen laser beam was focused with a 10 cm quartz lens on a sample mounted on a manual X-Y translator. A variety of samples were used to explore the capabilities of the system. Several spectra obtained from different samples are shown in Figure 4.2. Table 4.1 summarizes the experiments performed and species observed. All experiments were conducted in air.

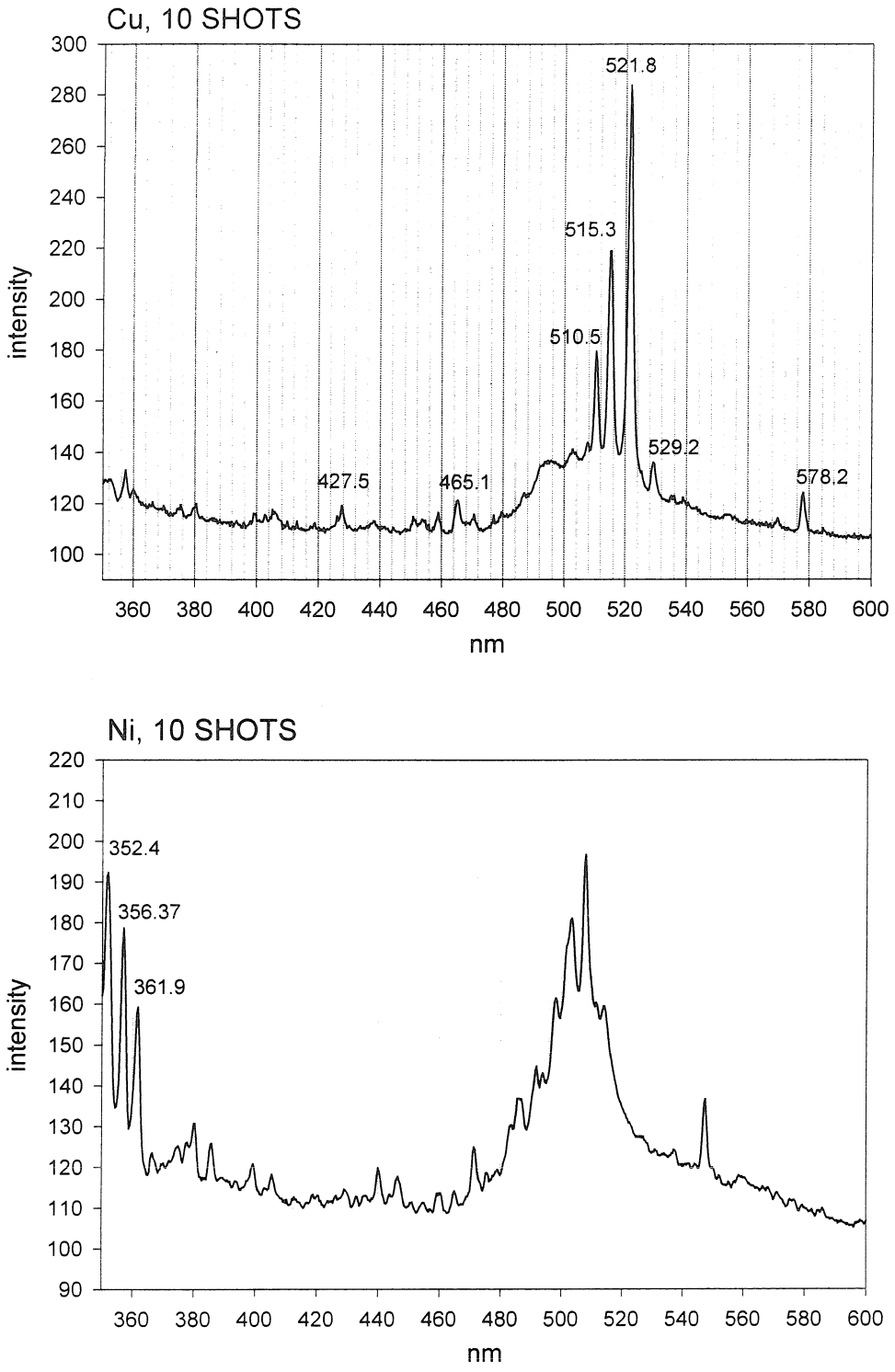

Figure 4.2. LIBS spectra acquired in traditional arrangement – without fiber probe: (a) copper foil, (b) nickel foil. Continued on the next page.

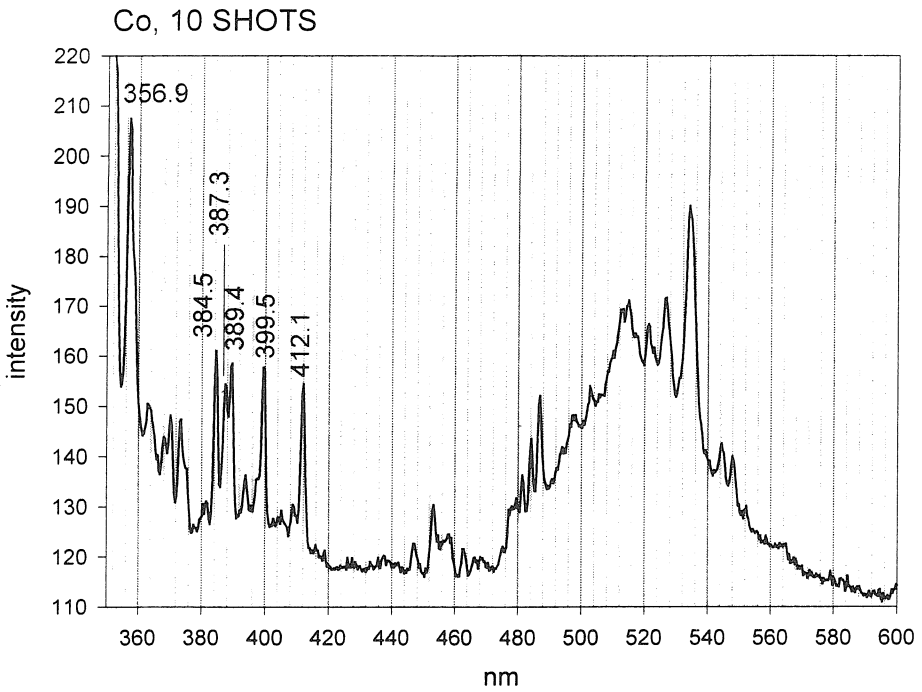

C

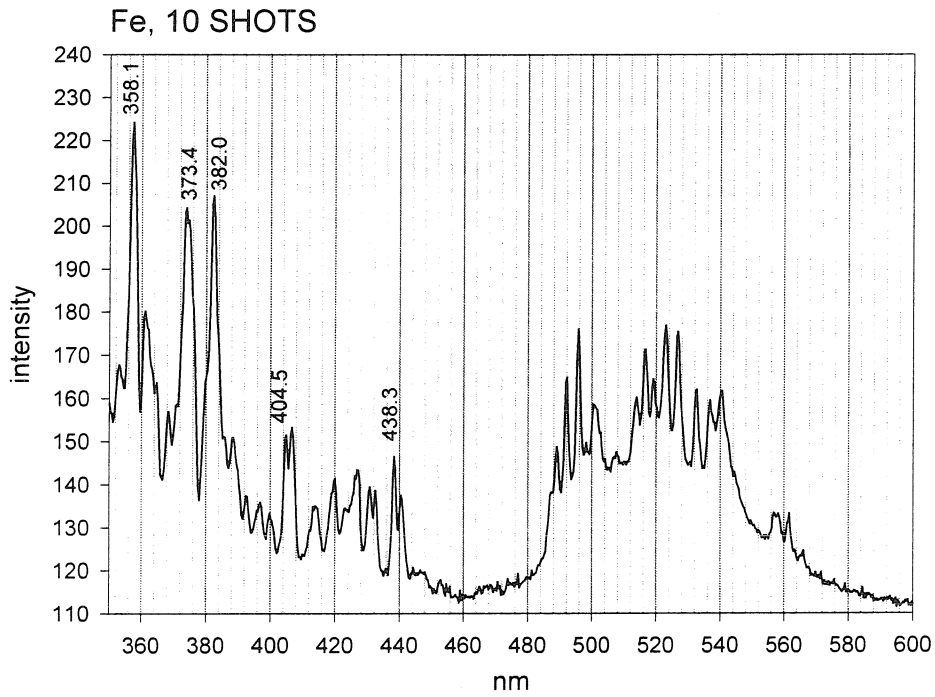

D

Figure 4.2. LIBS spectra continued: (c) cobalt foil, (d) iron foil.

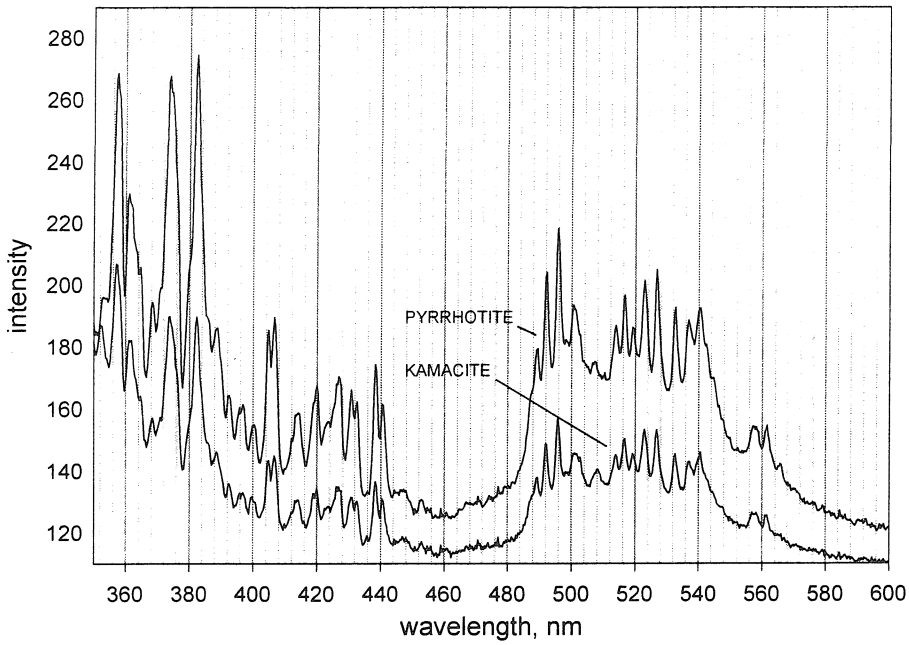

E

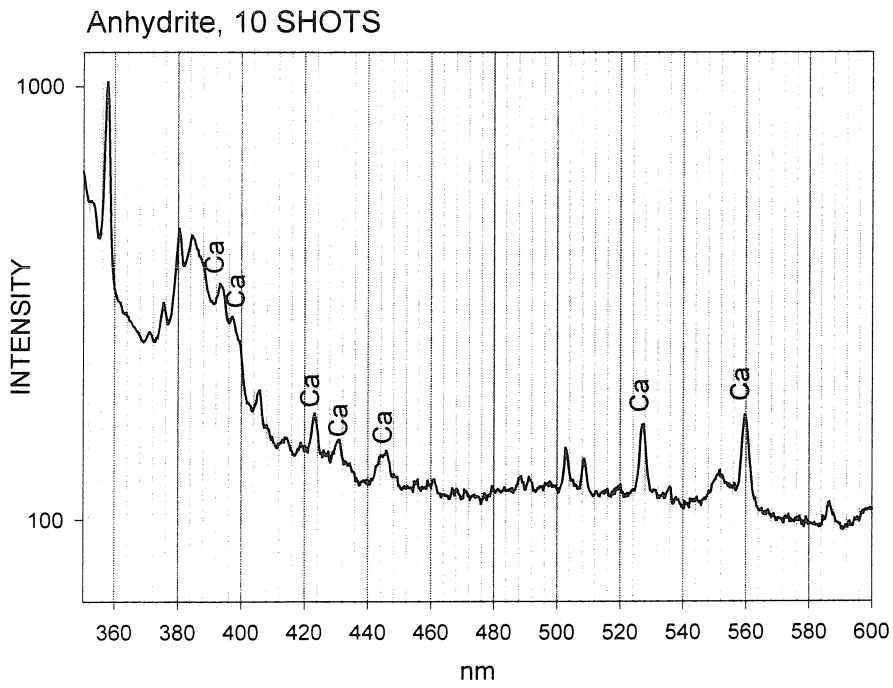

F

Figure 4.2. LIBS spectra continued: minerals (e) kamacite and pyrrhotite, (f) anhydrite.

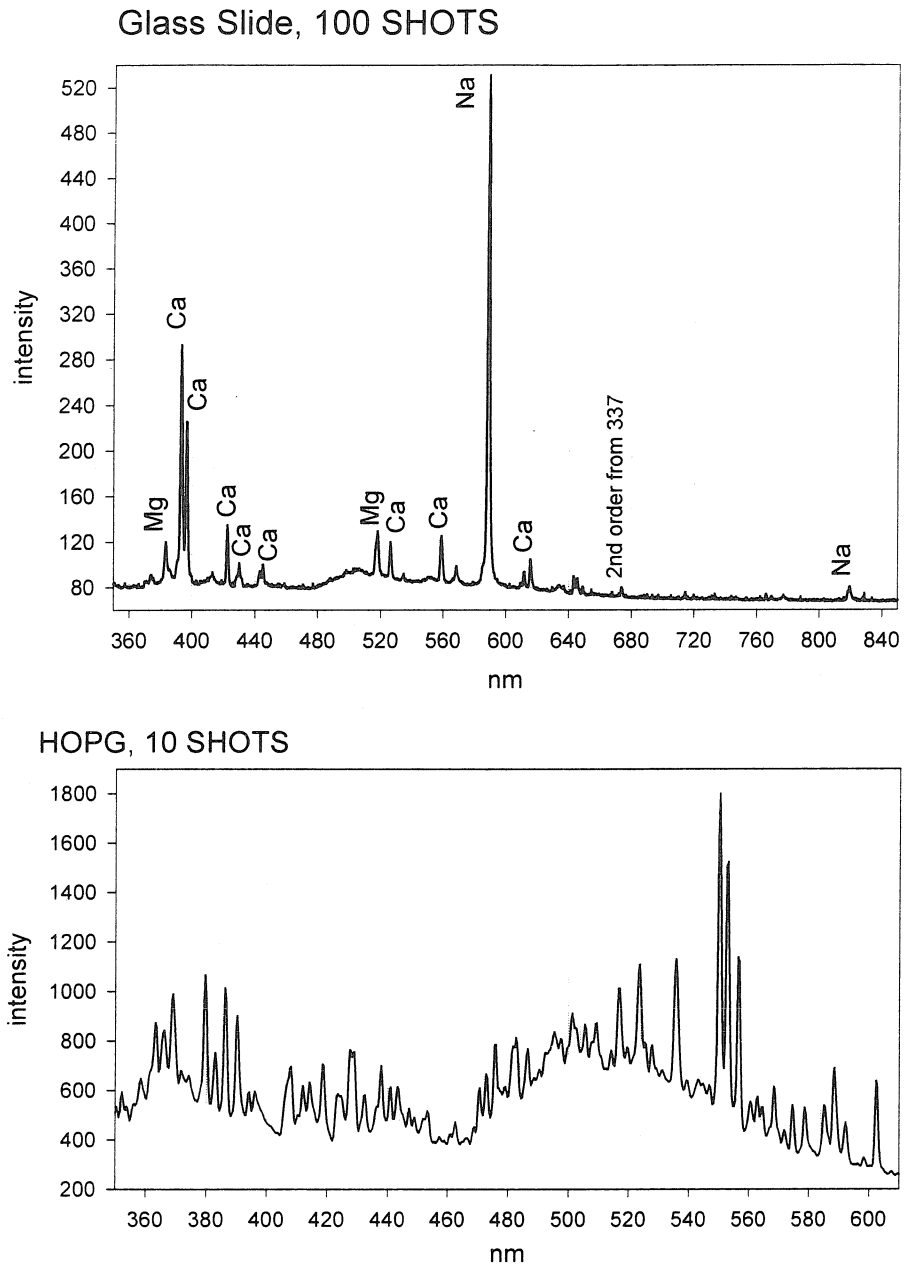

G

H

Figure 4.2. LIBS spectra continued: (g) glass (h) graphite, HOPG.

Table 4.1.

SAMPLE	SIGNAL OBSERVED	COMMENTS
Metals		
Copper foil	Cu	
Nickel foil	Ni	
Cobalt foil	Co	
Iron foil	Fe	
Aluminum foil	Al	
Minerals		
Kamacite	Fe, Ni	
Pyrrhotite	Fe, Ni	Fe1-xS, no sulfur lines observed
Anhydrite	Ca	$CaSO_4$
Other materials		
Glass	Na, K, Ca	
Silicon	Si	Only lines from singly ionized Si
Graphite	C_2, CH, CN	No atomic carbon lines observed

In general, conducting traditional LIBS in air is straightforward. Optical emissions were collected with a 20x microscope objective mounted on a XYZ-tilt stage. Signal from the laser at 337 nm is within the spectrometer measuring range. This makes it easy to adjust collection optics to maximize the amount of signal. However, having a major interference exceeding useful signal by several orders of magnitude around 337 nm renders the spectrum unusable in the range ~329-345 nm. This is unfortunate because many elements have characteristic emissions in this range. Also, second order diffraction

from the strong 337 nm line appears as a sharp spectral feature at 674 nm. Such problems could be eliminated if delayed triggering of the spectrometer were possible.

Experiments with graphite demonstrate an interesting variation of LIBS signal generation. While no atomic signal from carbon is observed, the spectrum is rich with emission from molecules formed in interaction between the pulsed plasma and ambient air. This effect indicates the possibility of detecting elements which are weak emitters themselves but can produce strong emitters in reactions with atmospheric gases. In addition it may be possible to develop special environments to target analysis of specific weak emitters, like sulfur or phosphorus.

There are indications in the literature that using specific atmospheres may enhance signal intensity for certain species[11]. However, the effects discussed in this paper by Wisbrun and co-workers are different from what we observed in case of graphite. They have experimented with a series of gases with different atomic/molecular sizes and different ionization potentials (IP). The basic trend is that the LIBS signal from a given sample intensifies with the increase of atomic radius of background gas and the decrease of its IP. The explanation involves two effects. A low IP simplifies plasma formation in the multiphoton ionization cascade scenario (see Eqn.1 in the beginning of this chapter) while increased sizes of background gas atoms result in less effective collisional energy transfer from plasma components to background gases. This leads to longer living plasmas and prolonged optical emissions. The best background gas in terms of LIBS signal increase appeared to be argon. LIBS intensity increased approximately 1.8 times in its presence. Xe, Ne, N_2 and He were also tried.

FOCUSED BEAM AND FIBER PROBE: LIBS SIGNAL COMPARISON

The critical test of the TOPOLIBS concept was to prove that laser pulses delivered to the sample through etched fiber optic probe in position feedback can produce enough signal without damaging the probe. To compare LIBS and TOPOLIBS we have used a specimen of Murchison meteorite as a test specimen. This meteorite is widely studied and its composition is well known.

Figure 4.3 shows a comparison of LIBS signals excited by a single laser pulse delivered to the sample by focusing the laser beam and by feeding the beam through a fiber probe on position feedback. The most notable and exciting feature of the spectrum with probe is that it is not much different from that with focused beam in terms of signal intensity and signal-to-noise ratio. The two spectra were acquired in different locations of meteorite sample, which explains the variability in presence or absence of specific spectral features in particular spectrum.

STUDIES OF MURCHISON METEORITE

Peak Assignment.

LIBS spectra from Murchison meteorite carry a lot of information about local chemical composition of the sample. Figure 4.4 shows two spectra generated by single laser pulses in different locations on the sample. A lot of known components of the meteorite are observed in the spectra including iron, magnesium, calcium and sodium. Aluminum and silicon (which are present in form of oxides) are not observed. This is probably because aluminum oxide is a minor component of the meteorite composition. Silicon is hard to detect in general.

The analysis of spectral features shows similar metal content in both locations. However, one location is clearly enriched in calcium relative to another. This study is a good example of localized chemical analysis with TOPOLIBS.

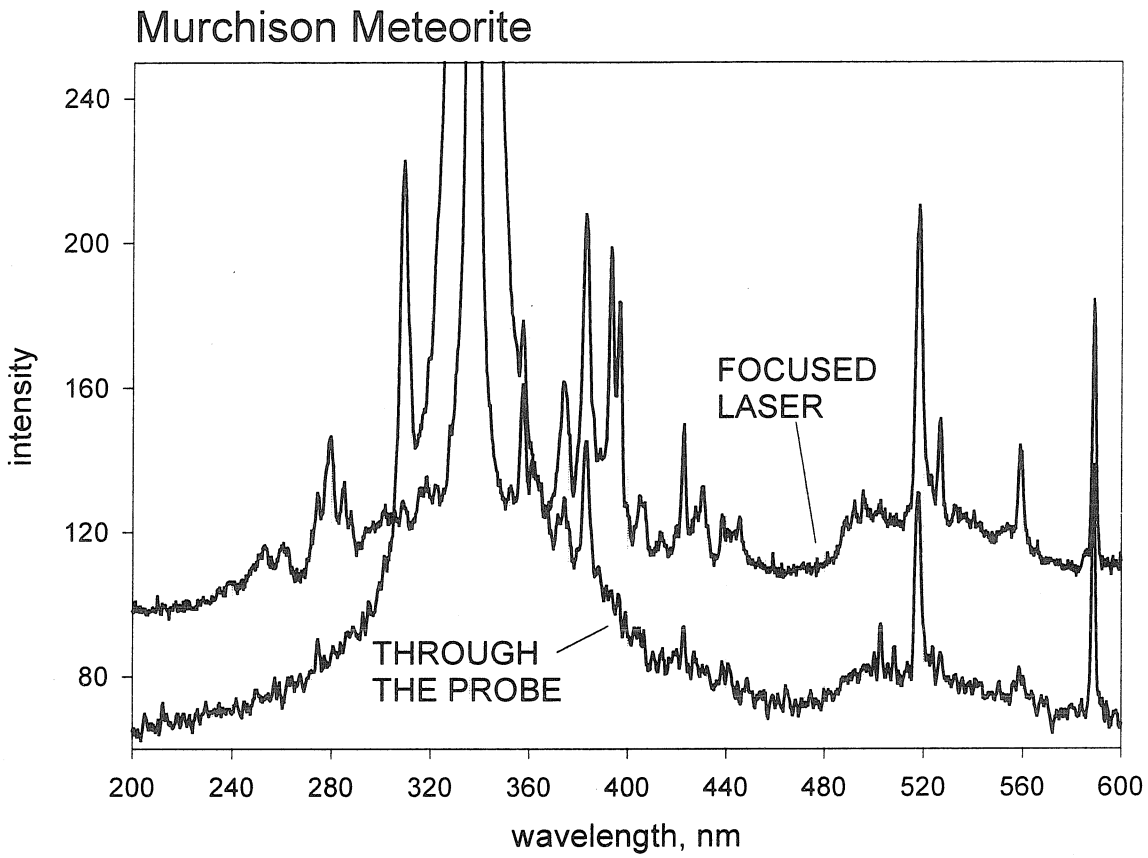

Figure 4.3. Comparison of LIBS spectra from plasmas produced in different locations of the sample by a single pulse with a focused laser beam and laser radiation delivered through etched fiber probe. Dominating feature around 337 nm is the laser line.

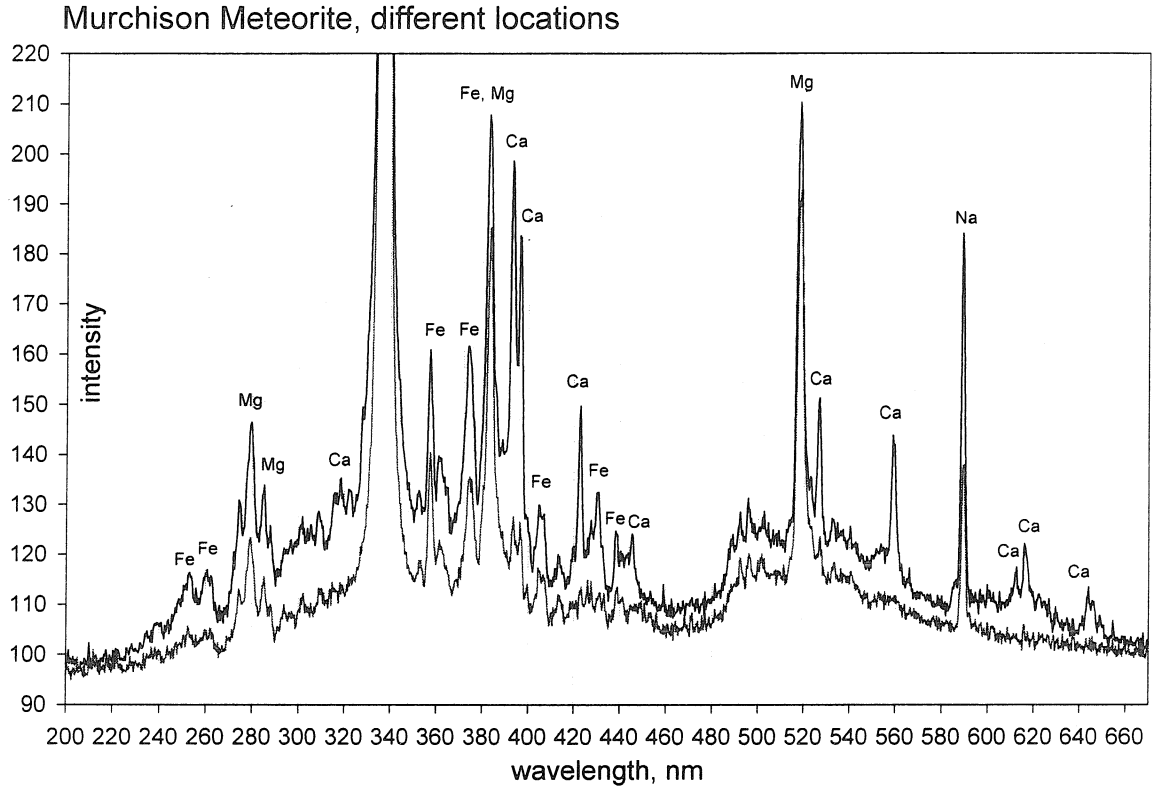

Figure 4.4. Inhomogeneous nature of Murchison meteorite. Two spectra taken in different locations show local calcium enrichment for one of them.

Localized Analysis.

Correlated studies of sample topography and chemical composition is the essence which makes TOPOLIBS concept attractive for surface analysis. Figure 4.5a shows topographical analysis of the Murchison sample with chemical study in two locations corresponding to two different grains in the sample. Once again, one location is clearly enriched in calcium compared to another.

Elemental Mapping.

Local chemical analysis provides insight into chemical composition of the sample. Once the presence of particular substance is detected in a single location, it can be mapped across an area. Figure 4.6 shows the distribution of three different species - magnesium, sodium and iron - over an area of 50 μm^2. Sodium and magnesium have very similar spatial distribution while for iron it is totally different. This once again illustrates the inhomogeneous nature of the sample and TOPOLIBS capabilities for spatially resolved chemical mapping.

STUDIES OF BASALT SAMPLE

In order to investigate a material with known chemical composition and different chemical phases, a sample of basaltic rock was prepared in the Mineralogy lab with the help of Prof. Rossman. This metamorphic rock is highly inhomogeneous with feature size ranging from tens of microns down to fractional micron. Major phases and their chemical composition are listed in the table below.

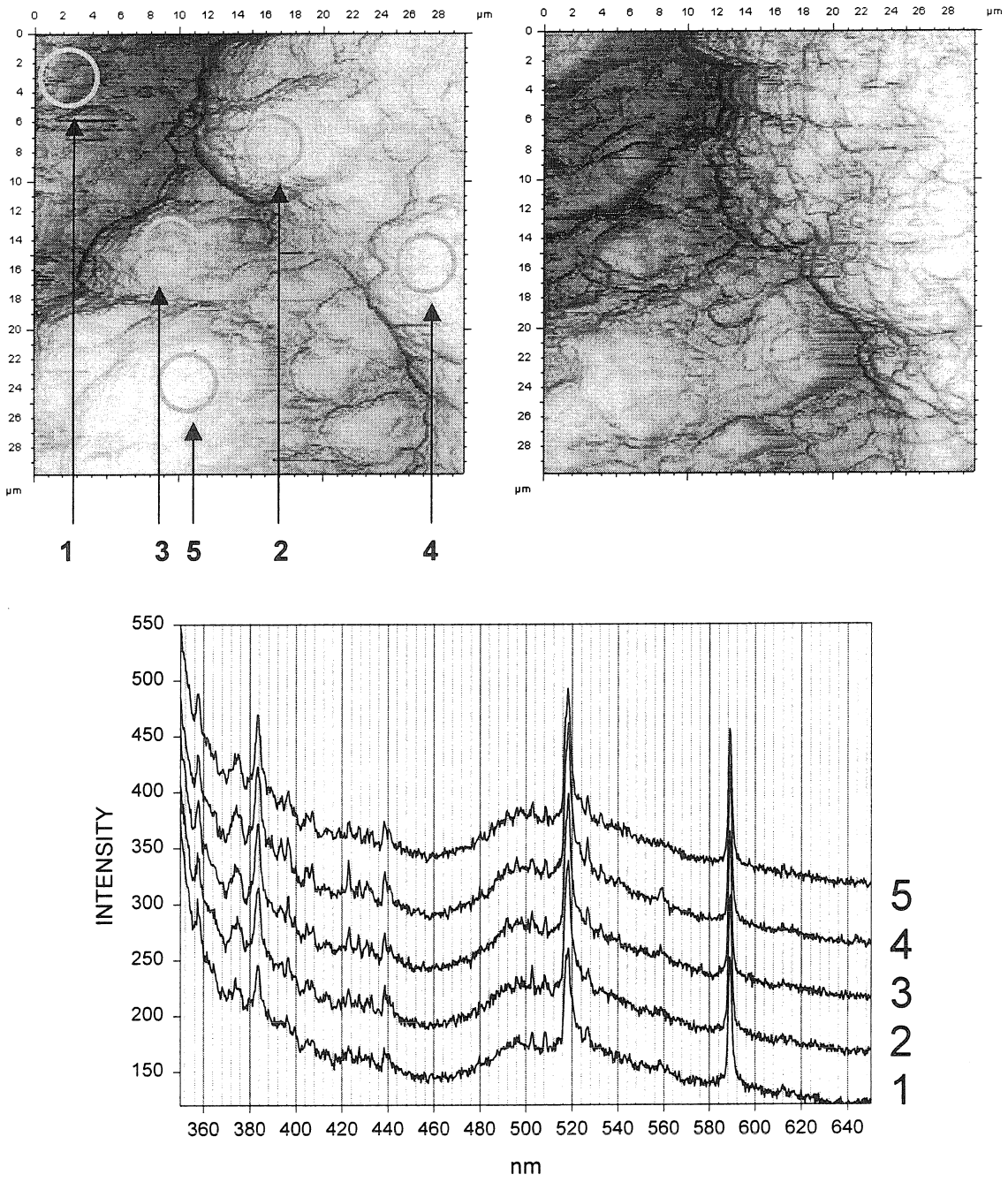

Figure 4.5. Localized analysis of Murchison meteorite – topography correlated with chemistry. Five locations were probed with a single laser pulse each. LIBS spectra are normalized on the overall spectral intensity in the range 350-650 nm and shifted vertically for clear view. All spectra are similar except for increased calcium intensity in spectrum (and location) #4, while for location #5 calcium content is minimal.

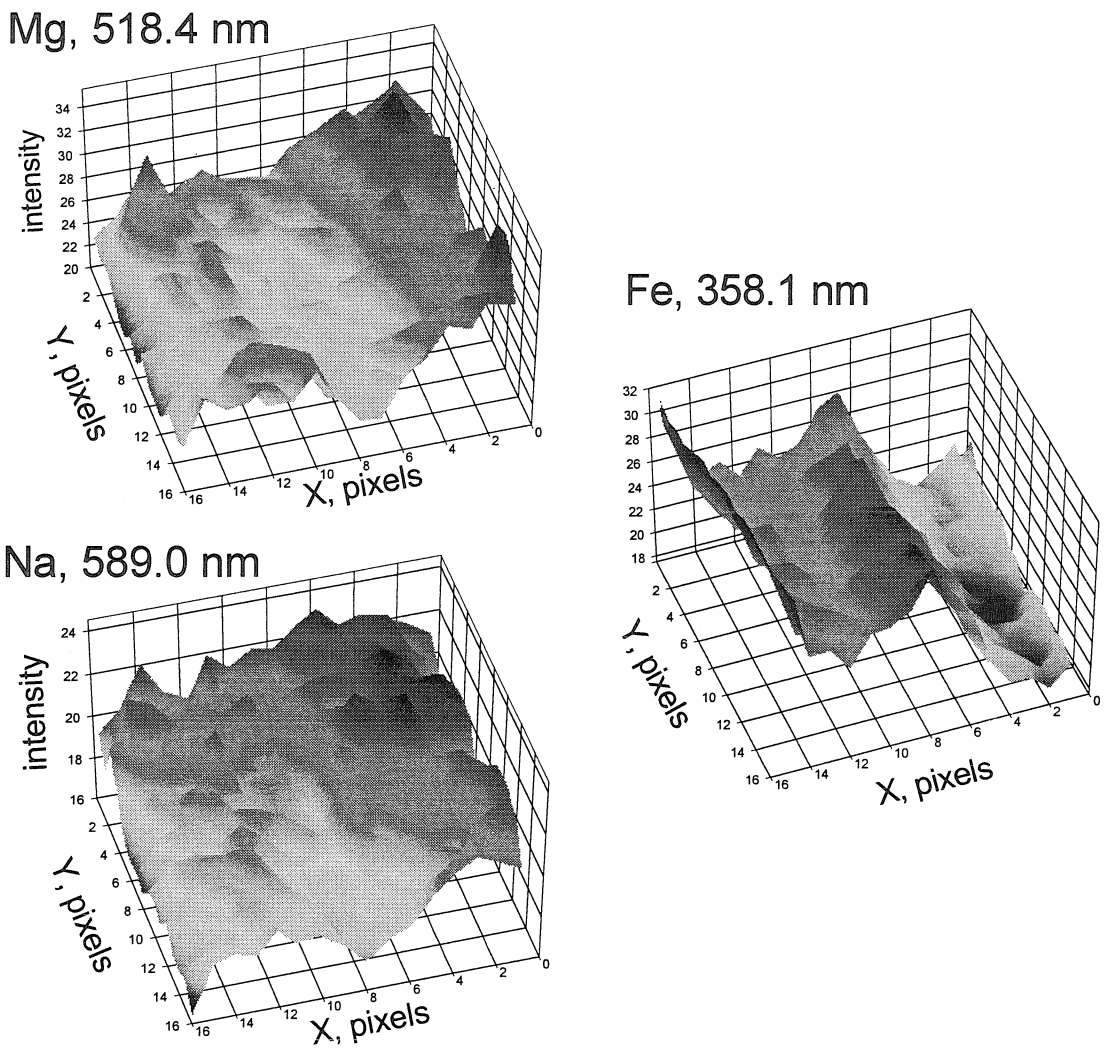

Figure 4.6. Elemental mapping: distribution of three elements across the same area of Murchison meteorite sample. 50x50 μm scan, 16x16 pixels, one laser shot per pixel. Magnesium and sodium maps are similar while the one for iron is totally different.

Phase	Chemical Composition
Olivine	$(Mg_{0.9}^{++}Fe_{0.1}^{++})_2SiO_4$
Plagioclase Feldspar	$(Ca_{1-x}Na_x)\ Al_{2+x}Si_{2+x}O_8$
Magnetite	Fe_3O_4
Pyroxene	$Ca(Mg,Fe)Si_2O_6$
Glass	60-70% Silica with MgO, FeO and other
Titanium containing phase	TiO

A chip was broken off the bulk rock and polished with a progression of abrasive materials down to 1 micron finish. At this roughness the surface has a mirror look. When observed in a reflective light microscope, a variety of regions with different grayscale shades are observed. Reflective microscopy is commonly used in mineralogy, and it is known that each grayscale shade corresponds to chemically different phase.

After polishing, the chip was glued on a magnetic steel washer and placed on the TOPOLIBS scanner. Examples of typical topography scans are shown in Figure 4.7. Relatively flat area shown in Figure 4.7a is probably a large domain of a single phase. However, Figure 4.7b shows rich landscape with features on various scales. This relief was probably formed by interaction of abrasive material with different phases of the rock. Hardness of a phase depends on its chemical composition, so softer phases exhibit more depression after polishing compared to harder ones.

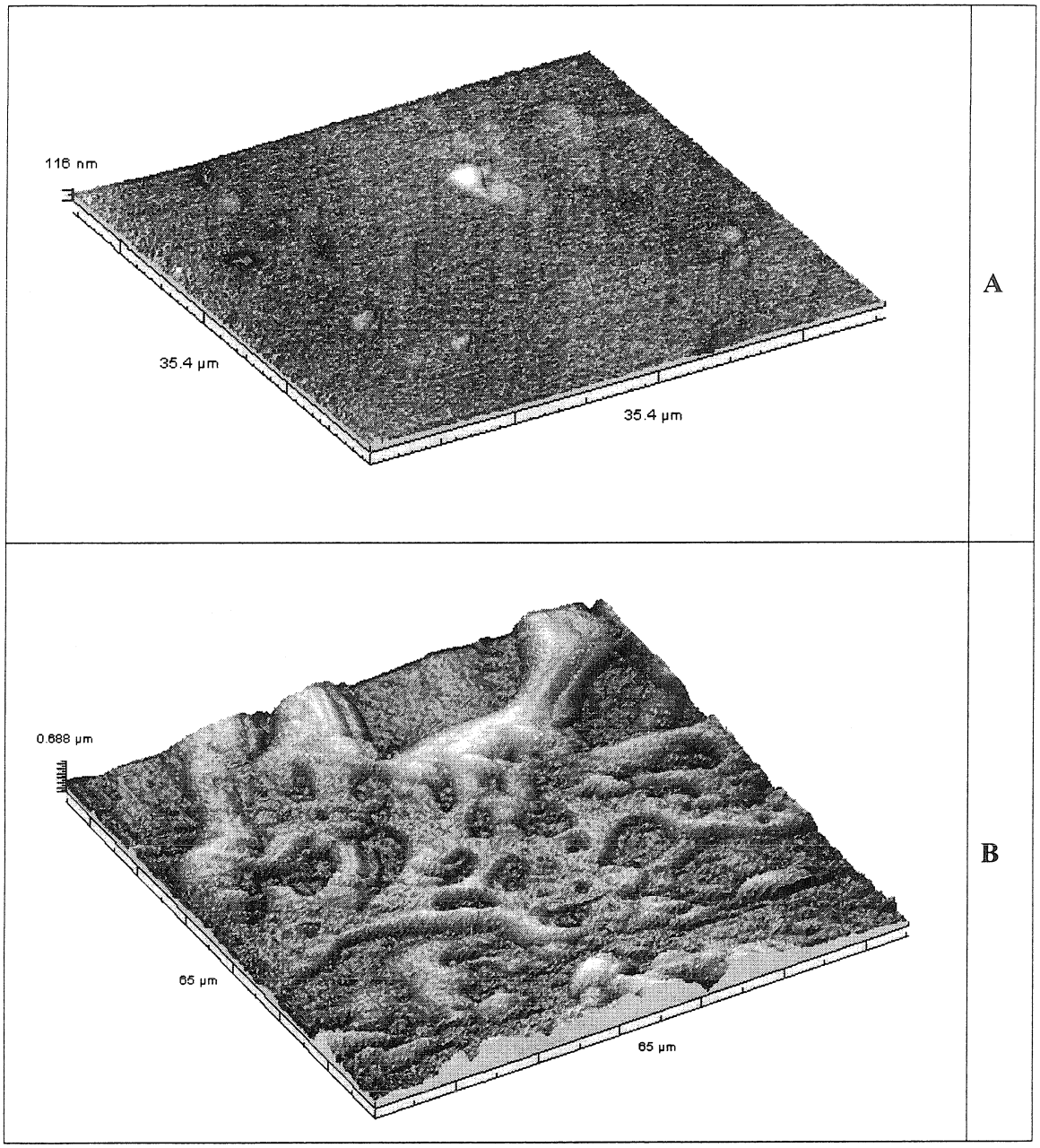

Figure 4.7. Topography of polished basalt sample. (a) Very flat region with a few features and polishing grooves. (b) Rich topography region. Submicron relief is probably formed during polishing – different phases have different hardness, so the abrasive removes softer phase more aggressively.

After topography analysis, chemical analysis has been performed. Figure 4.8 shows four LIBS spectra acquired in different locations on the sample. Each sample was generated with a single laser pulse with no attenuation of laser beam. Spectra are noticeably different. In particular, spectrum #3 shows iron enrichment and calcium depletion, which probably corresponds to olivine phase.

Analysis of craters formed on basalt sample by single laser pulses through fiber probe shows large scale sample damage. Figure 4.9 shows two areas of surface deformation caused by laser pulses in each case the damage is on the order of tens of microns. Corresponding LIBS spectra are also shown in Figure 4.9. Again, the spectra are different and probably belong to different phases.

As seen in Figure 4.9 the damage to the sample extends over several tens of micrometers. If the laser power is reduced, crater size decreases as well. This is demonstrated in Figure 4.10. Laser beam was attenuated before entering the fiber optic coupler by neutral density filters. Using lower laser powers crater size is reduced to sub-micron dimensions. The amount of LIBS signal is also reduced. One needs a detection system more sensitive than the S2000 spectrometer in order to be able to detect LIBS spectra from sub-micron sampling spots. Ultimate resolution is limited by the laser wavelength employed for LIBS.

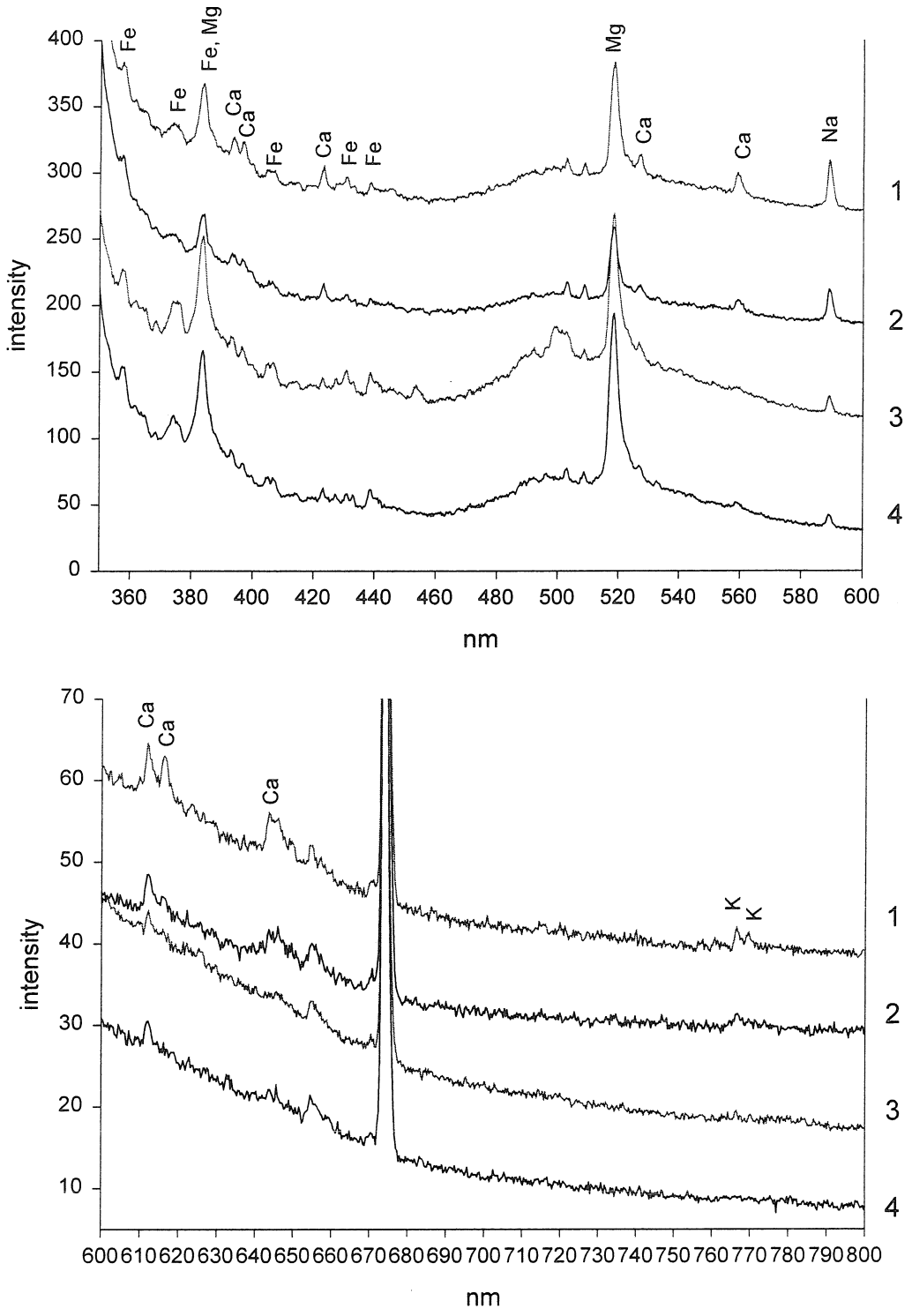

Figure 4.8. LIBS analysis of basalt sample. Four spectra acquired with TOPOLIBS probe in feedback, single laser pulse per spectrum. Spectrum #3 shows iron enrichment and calcium depletion, which probably corresponds to olivine phase.

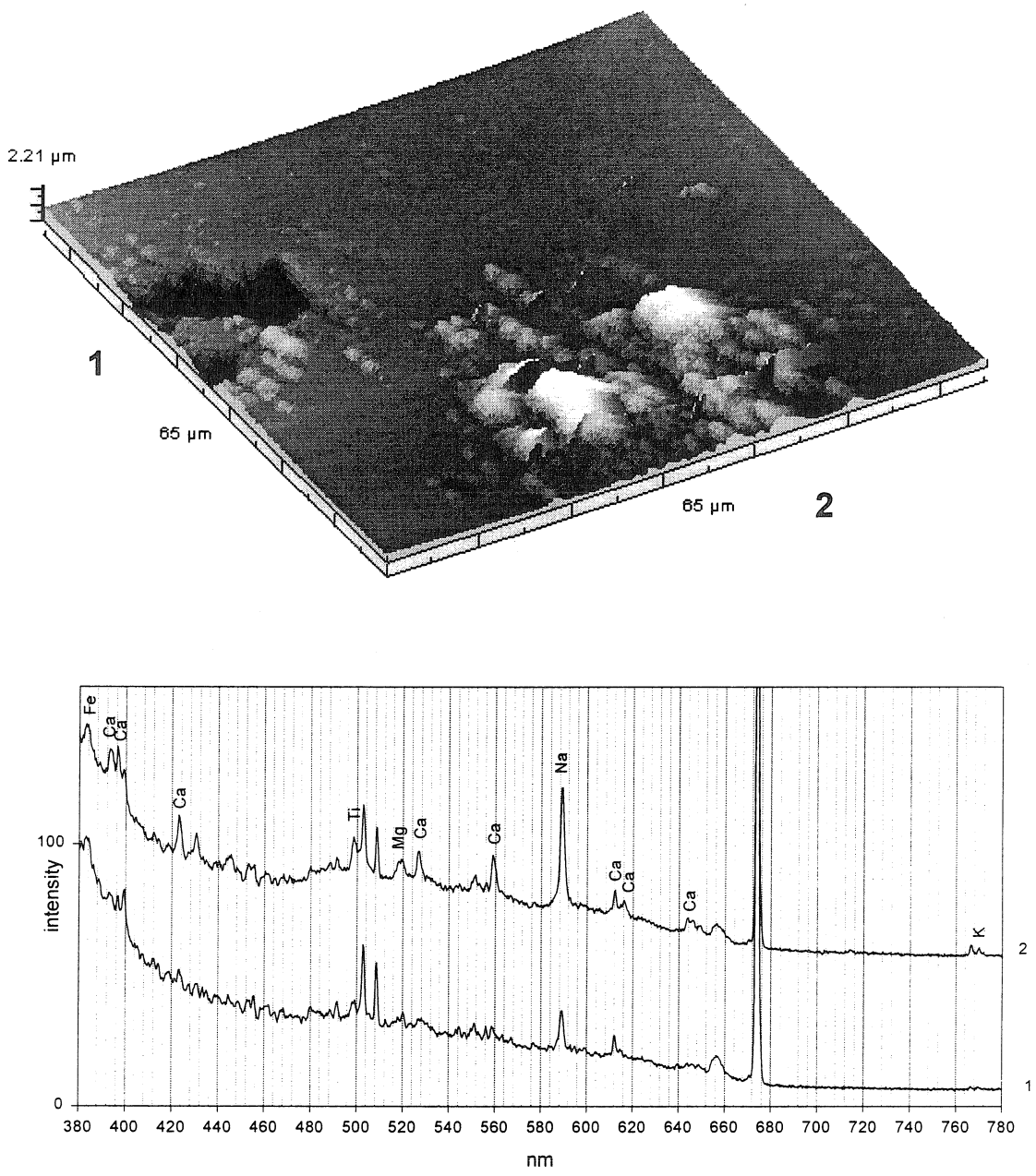

Figure 4.9. Basalt sample damage by laser sampling. LIBS spectra correspond to sampling locations, numbered 1 and 2.

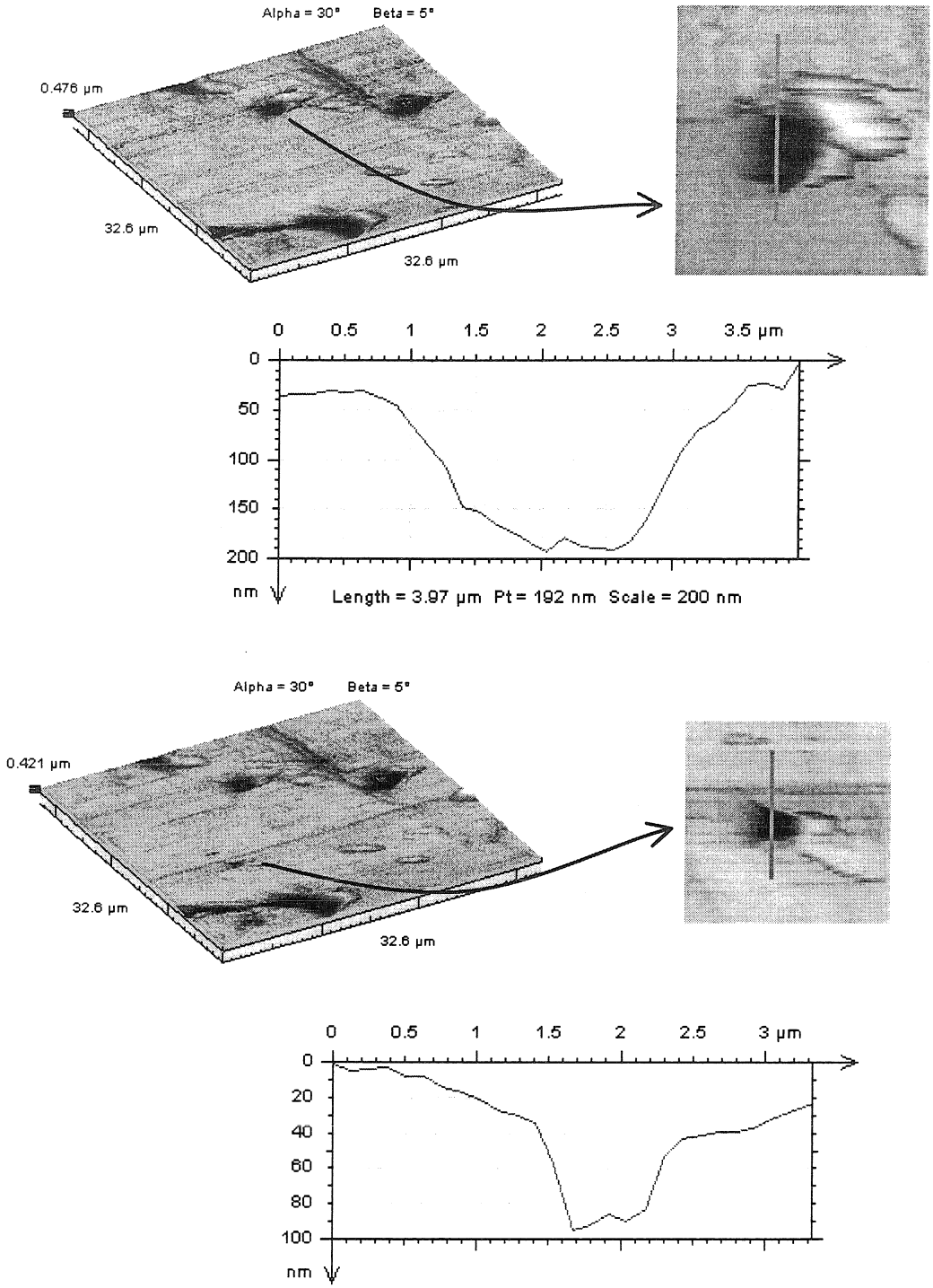

Figure 4.10. Crater size dependence on the applied laser power, basalt sample. An iris was used to attenuate laser beam before entering fiber optic coupler. Crater size can be less than 1 micron however, the LIBS signal intensity is insufficient to be detected with the S2000 spectrometer.

PARTICLE ANALYSIS

BACKGROUND

Aerosol particles are one of the major contributors to air pollution. Knowledge of particle size and chemical composition is essential for air contamination control. Traditionally, off-line studies of aerosols are conducted in two stages: the samples are collected in the test location and then analyzed in the lab. The analysis usually involves weighing the particles and measuring their chemical composition. Particle contamination analysis and control is also important for a number of other applications such as wafer contamination control in semiconductor processing, and soil analysis, and pharmaceutical manufacturing.

Off-line analysis of individual particles is performed either by using an optical microscope for counting and sizing of particles, or by employing a vacuum based chemical analysis method such as Electron Microprobe, X-ray Fluorescence, Laser Microprobe, Secondary Ion Mass Spectrometry or others[12]. Sample preparation for these vacuum techniques is extremely tedious which in most of the cases prohibits such studies. In addition, some aerosol particles are volatile, and they do not survive vacuum conditions long enough for analysis purposes. This complicates all vacuum-based approaches to particle analysis.

Why is it important to know both particle size and chemical composition? This knowledge allows better understanding on how the aerosols produced and what evolution

do they undergo in the atmosphere. The following is the list of pertinent facts and concepts adapted from Seinfeld's text on air pollution[13].

Particle sizes range from tens of nanometers to several microns. Roughly, size distribution of "average" particulate population has two peaks. One is centered around 10μm particle size and another one around 0.1μm. Large particles are mostly of natural (non-anthropogenic) origin containing Fe, Ca, Si, Na, Cl, Al. Smaller particles can have either anthropogenic or secondary natural origin, i.e., they are the products of decomposing larger particles. The smaller particles are composed of sulfates, nitrates, ammonia, lead and carbon.

Particulates include dust, dirt, soot, smoke, and liquid droplets. Particles are emitted directly into the air by sources such as factories, power plants, cars, construction activity, fires, and natural windblown dust. Particles also form in the atmosphere from the condensation or transformation of emitted gases such as sulfur dioxide and volatile organic compounds.

Particles of the same size do not necessarily have the same chemical composition. Same size particles may originate from different sources, and they inherit chemical composition specific to the source. However, bulk methods of chemical analysis like ICP-MS can not distinguish between individual particles. Knowledge of chemical differentiation of similar sized particles is very important for atmospheric studies as it provides information on particle history. One of the approaches to explore chemical composition of individual particles is online mass spectrometry analysis of single particles[14].

Attractive features of TOPOLIBS compared to other methods for individual particle analysis is minimal sample preparation requirements and the fact that the experiment is conducted in the air. This means that volatile particles will stay intact until analyzed. The experiment turnaround time is decreased by eliminating complicated sample preparation procedures.

TOPOLIBS is an appropriate tool for analysis of aerosols. It is essentially an off-line method, which can be applied to samples collected on substrates. By using scanning probe capabilities it will be possible to locate individual particles and measure their sizes. Automated analysis of size distribution of particle populations can be performed routinely by using standard image analysis software algorithms for particle counting and sizing. Size range of particles suitable for topographical analysis is from several microns down to approximately 50 nm. The lower range is determined by the spatial resolution of topographical imaging, which in turn depends on the sharpness of the fiber probe.

After the topographical analysis, chemical analysis of individual particles can be performed. Probe is brought on top of a particle and LIBS study is carried out. Crucial questions are how small a particle can be to produce enough optical emission and what chemical classes of particles can be detected.

The question of lower cut-off of particle size in LIBS experiment remains open. Our studies have just recently begun, and they will be optimized in the future to push the detection limit down.

In regards to the question of possibility to analyze particles of different chemical composition, a preliminary forecast of relative sensitivity of LIBS for different particle types can be made based on literature data and our experience:

SEA SALT METAL DUST SOOT, SMOKE SULFATES, NITRATES

EASY TO DETECT ⟷ HARD TO DETECT

STUDIES OF AEROSOLS FROM MALDIVE ISLANDS

To evaluate TOPOLIBS applicability for aerosol studies, we used an aerosol sample collected on aluminum foil substrate collected by Prof. G.Cass' group (Environmental Engineering, Caltech) at Maldive islands. This sample was chosen for two reasons: the particles were size selected around 1.8μm (good starting range for TOPOLIBS) and their expected composition should be mostly sodium and potassium which are easily detectable in LIBS spectrum.

The sample collection methodology is described in detail elsewhere[15]. The particles were deposited by the cascade impactor on the substrate in several well defined locations, each deposition area being approximately 2mm diameter. Inside the deposition spot the particles are piled up, so it is hard to localize individual particles. This is demonstrated by topographical study performed with a fiber probe shown in Figure 4.11a. Far from the deposition spot, rare individual particles can be seen on the background of aluminum substrate, shown in Figure 4.11b. Finally, just outside the rim of the deposition spot, surface density of the particles is increased, but the majority of the particles are still not agglomerated, shown in Figure 4.11c.

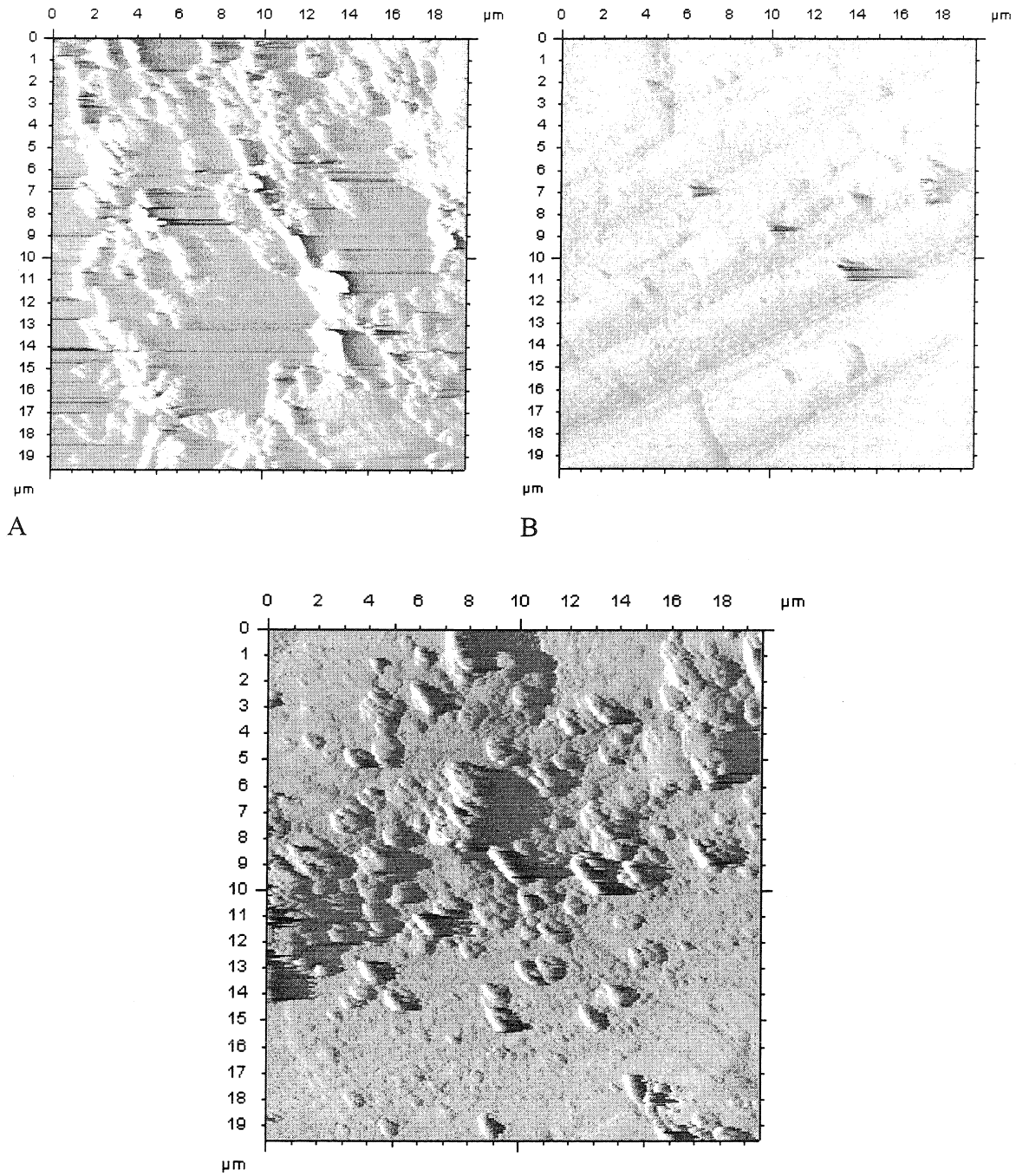

Figure 4.11. Topography of aerosol particles collected in cascade impactor on aluminum foil: (a) on top of the impactor dot – particles aggregated together, (b) far from the impactor dot – sparse particles, (c) along the rim of the dot – lots of particles suitable for individual analysis.

Another topography study of the sample is shown in Figure 4.12a. Individual particles as well as particle agglomerates are easily distinguishable. After performing the topographical study, the probe was placed on top of one of the larger particles (indicated on the figure). Single laser pulse was delivered to this location. LIBS spectrum generated by this laser pulse is shown in Figure 4.12c. Apart from aluminum signal coming from the substrate, the spectrum shows strong sodium emission and weaker potassium signal. Recalling that these aerosols were collected on the islands in the Indian Ocean, the natural conclusion is that those are sea salt particles, which are composed mostly of sodium chloride.

This study is a very first example of how TOPOLIBS can be used in aerosol analysis.

TECHNICAL ISSUES TO BE ADDRESSED

Sample Damage.

When pulsed laser radiation is delivered to the sample, a crater is formed in the sampling area. Some material from the crater is transformed into plasma producing optical emission. There is also ballistic material transfer in the radial direction from crater. Sometimes, a rim is formed by such displaced material. Another reason for material displacement is probably acoustic shock wave that is generated by laser pulse impeding on the sample. This shock wave may dislocate smaller particles weakly bound to the substrate.

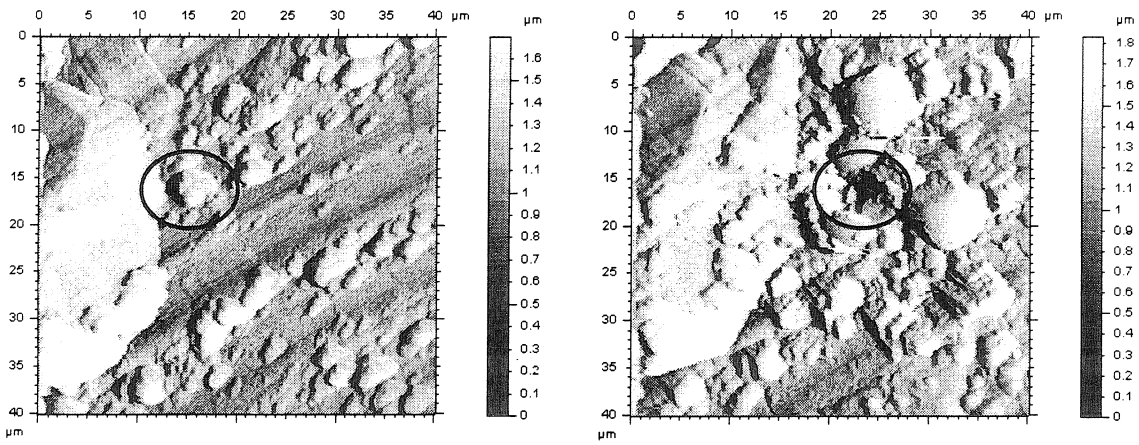

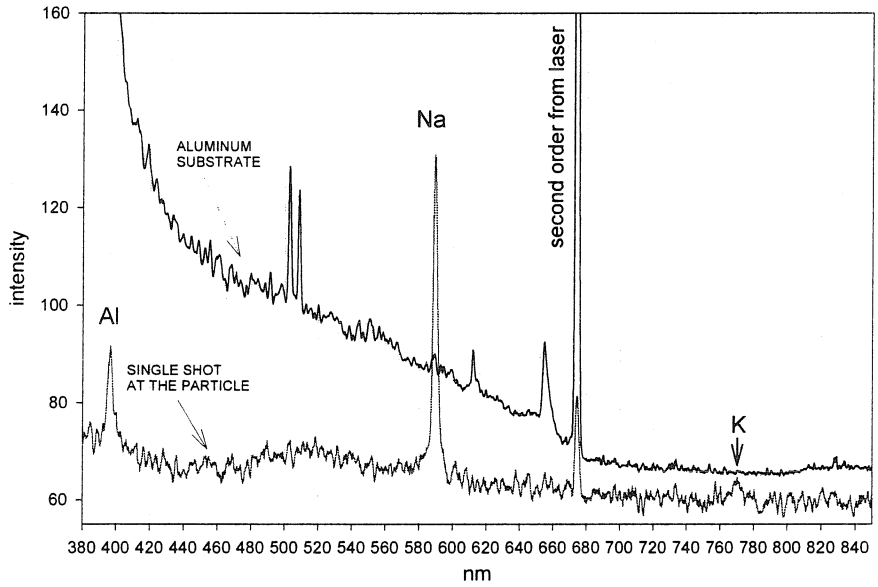

C

Figure 4.12. Aerosol studies, Maldive Islands sample: topography of the sample (a) before and (b) after LIBS analysis, (c) LIBS spectrum generated with a single laser pulse in the indicated location. Crater formation and material redistribution are visible.

An example of sample modification by laser pulse is shown in Figure 4.12b. A distinct crater is formed in the probe location. Additionally, there is significant material redistribution in the area surrounding the sampling location. In this experiment aluminum foil substrate was not treated in any way to enhance the adhesion of aerosol particles, so the particles were weakly bound to the substrate. This is why we believe that material transfer around the sampling area in this case is mostly due to shock wave.

Crater geometry appears to be a strong function of laser wavelength and power, and absorption properties of the sample. A study of crater formation in LIBS experiments at different laser wavelengths was performed by Hemmerlin and Mermet[16], while Zeisel and co-authors[17] investigated material transfer and crater geometry produced by laser pulsed delivered to the sample through etched fiber probes. In general, short wavelength radiation produces more localized sample damage for the same laser spot size in LIBS experiment. This suggests that UV lasers are preferred for TOPOLIBS to minimize sample modification.

While reducing spatial resolution of TOPOLIBS experiment, material removal potentially gives advantage of the access to sub-surface layers of the sample. Depth profiling has been performed with LIBS in the past[18] and can be used in TOPOLIBS to analyze buried features.

Probe Contamination.

In regular LIBS all optical components are located remotely from the plasma plume region. In TOPOLIBS however, the fiber probe is placed in the midst of the

plume. Some vapors and particles from the plume may be deposited onto the probe and later re-desorbed giving rise to spurious LIBS signal. One way to decontaminate the probe between the samples or from shot to shot is to retract the probe from the sample and feed several laser pulses through it, effectively removing deposited species.

Need for Delayed Acquisition.

As was discussed before, regular LIBS employs delayed spectrum acquisition which usually starts 1-2 μs after the laser pulse. In our studies the spectrometer was triggered *before* the laser pulse, so the spectrum included both the laser line and broadband thermal background. It is expected that with incorporation of delayed acquisition, better sensitivity will be achieved allowing detailed studies of aerosol samples. In particular, for Maldive Islands sample we may see metal and carbon contributions due to the industrial pollution and the winds blowing off the coast of India.

CONCLUSIONS

We have demonstrated the feasibility of TOPOLIBS concept for topographical and chemical analysis of samples. Attractive features of this instrument include minimal to no sample preparation, capability to perform studies in ambient environment, and portable design. We believe that a wide variety of applications will benefit from using this type of instrumentation including wafer contamination studies in semiconductor quality control, particle analysis in environmental problems and surface analysis in materials science.

ACKNOWLEDGMENTS

This work was supported by NASA (grant NAG5-7081) and Beckman Institute. We thank Lara Hughes and Glen Cass for providing the aerosol sample, Thomas Ahrens for providing Murchison meteorite sample, and George Rossman for basaltic rock sample.

REFERENCES

[1] P.G.VanPatten et al., *J.Phys.Chem.* **100** (1996) 3646-3651.

[2] L.J. Radziemski et al., *Anal. Chem.*, **55** (1983) 1246-1252.

[3] K. Song, Y-I. Lee and J. Sheddon, *Appl.Spec.Rev.* **32** (1997) 183-235.

[4] Laser-Induced Plasmas And Applications, L.J. Radziemski and D.A.Cremers, Ed., Marcel Dekker, NY 1989.

[5] F.Varga and L.Nemes, *J. Mol. Struct.* **481** (1999): 273-276.

[6] D.R.Turner, US Patent 4,469,554.

[7] K. Karrai and R.D. Grober., *Appl.Phys.Lett.*, **66** (1995) 1842-1844.

[8] W.F. Megger, C.H. Corliss and B.F. Scribner, Tables of Spectral Line Intensities, Part I, National Bureau of Standards, 1975.

[9] R.W.B. Pearse and A.G. Gaydon, The Identification Of Molecular Spectra, John Wiley, NY 1963.

[10] http://physics.nist.gov/PhysRefData/ASD1/nist_atomic_spectra.html

[11] R.Wisbrun et al., *Anal.Chem.* **66** (1994) 2964-2975.

[12] C. Xhoffer et al., in *Environmental Particles* by J. Buffle and H.P. vanLeeuwen., Ed., Lewis Publishers 1992, v.1., pp. 107-144.

[13] J.H. Seinfeld, *Atmospheric Chemistry and Physics of Air Pollution*, John Wiley and Sons, 1986.

[14] D.T. Suess and K.A. Prather *Chem.Rev.* **99** (1999) 3007-3036.

[15] L. Hughes et al., *Environ.Sci.Technol.* **32** (1998) 1153-1161.

[16] M. Hemmerlin and J.M. Mermet, *Spectr.Acta B* **51** (1996) 579-589.

[17] D. Zeisel et al., *Appl.Phys.Lett.* **68** (1996) 2491-2492.

[18] J.M.Vadillo et al., *Fresenius J. Anal. Chem.* **355** (1996) 909-912.

Appendix A. Probe Fabrication by Chemical Etching Optical Fibers

Hydrofluoric acid is the standard agent used for etching silica compounds. However, direct etching of optical fibers in HF produces tapers of poor quality. They are long, corrugated and resemble icicles. The taper length is hard to control, and the shape is irreproducible.

Several attempts have been made in the past to develop HF etching procedures for optical fibers. Most of the approaches involved some type of time and/or temperature control[1]. Although giving acceptable results, the methods were labor intensive and tedious.

On the other hand, researchers at AT&T Bell Labs, the cradle of the fiber optic technology, had been working on the approaches to taper fibers even before these were used for NSOM. Turner and Marchman have developed a simple, reproducible method to taper the fiber by using two-phase etching, described below[2].

The process is illustrated in Figure A.1. A fiber without plastic jacket is inserted in the etch bath. The bath is prepared in a plastic beaker. A layer of organic liquid is placed on top of HF. Typically, in our experiments 20 ml of 48% HF and 5 ml of the organic was used. CAUTION IS ADVISED! HF is a very hazardous substance and all appropriate safety procedures should be followed when working with it.

Different organic compounds can be used for the experiment. The requirements for layer formation are to be lighter than HF (to float on top), inert to HF, and involatile. We have experimented with different organic materials, and settled on tetra-methyl-penta-decane (TMPD), a light oil.

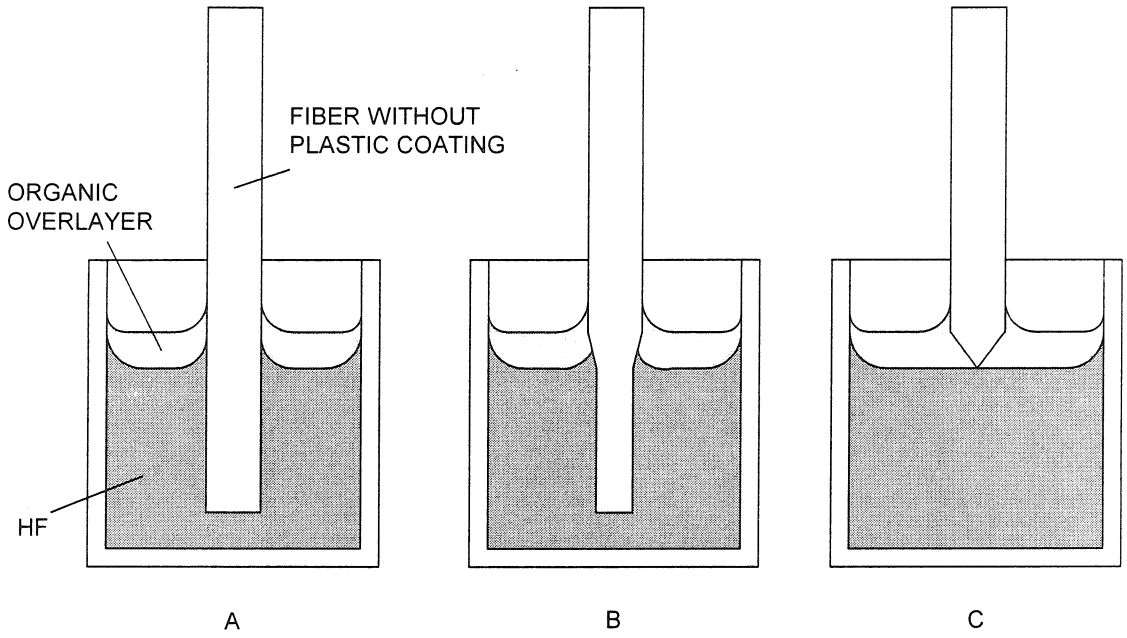

Figure A.1. Two phase etching of glass fibers: (a) fiber is placed in the etching bath, the meniscus is formed; (b) intermediate shape of the fiber, meniscus travels down towards organic/HF interface; (c) about 50 minutes later the process stops by itself, and the tapered fiber is preserved unetched in the organic layer. The fiber is mounted on Z translator in order to be able to adjust the length of the probe protracting from the tuning fork.

After the fiber is placed in the bath, a meniscus is formed at the interface between the fiber, HF and TMPD. The etching process in the bulk of the HF phase starts immediately. Closer to the interface, however, the diffusion is limited, so the etching rate is slower.

With time the meniscus travels down towards the HF/TMPD interface. In about one hour the process stops by itself. The lower part of the fiber is completely dissolved, while a smooth taper is formed in the protected zone.

The tapers are very short compared to those obtained by heating/pulling of the fiber. This is very favorable for NSOM because decreased taper length translates into increased light transmission. In fact, etched glass fibers have ~1,000-fold increase in transmission compared to pulled fibers with the same size aperture[3]. We have demonstrated a similar effect for IR-transparent chalcogenide fibers[4], described in detail in Chapter 2.

Different organic substances can be used for protective overlayer. The wetting angle at the fiber/HF/organic meniscus depends on the properties of the organic fluid. The cone angle of the taper is, in turn, determined by the wetting angle. So, by varying protective layers one can achieve different cone angles of the taper.

Finally, in a recent publication by Stockle and co-workers[5] it was demonstrated that an even simpler method works – a fiber can be immersed into the HF phase without removing the plastic coating. The tip is formed inside the coating, which is unaffected by HF. The coating is later removed by chemical or mechanical means. Tips produced this way have essentially the same cone angle as those made by two-phase etching, but the

new tips are smoother. The authors attribute this fact to a more stable etching environment inside the coating tube.

REFERENCES

[1] T. Pangaribuan et al., *Jpn.J.Appl.Phys. 2* **31** (1992) L1302-L1304.

[2] D.R.Turner, US Patent 4,469,554.

[3] D. Zeisel et al., *Appl.Phys.Lett.* **68** (1996) 2491-2492.

[4] M.Unger et al., *Rev.Sci.Instr.* **69** (1998) 2988-2993.

[5] R. Stockle et al., *Appl.Phys.Lett.*, **75** (1999) 160-162.

Appendix B. Shear-Force Position Feedback Using Piezoelectric Tuning Forks

SHEAR FORCE BASICS

Shear-force feedback is a method of choice for controlling the distance between fiber optic probe and the sample within several nanometers. All existing modifications of the method follow the following general scheme:

1. The probe is dithered in lateral direction in fundamental bending mode, or at a higher harmonic of such mode. The second harmonic of mechanical oscillation of a rod with one clamped end and one free end is not at twice, but at ~6.3 times the fundamental frequency[1]. This effect is commonly used to check if the observed resonance belongs to the probe or some other mechanical part of the assembly. The amplitude of oscillations is usually a few nanometers at the tip for probes with end radius of curvature 100-200 nm.
2. When the probe approaches the sample to within several nanometers, the amplitude of probe vibration is damped. The phase of the oscillations is also changed. Either of the signals can be tracked for the feedback purposes.

The method is somewhat similar to the AC mode of AFM operation. However, unlike the shear-force feedback the AFM probe is oscillating in the normal direction. So, technically, the origin of the forces acting upon the probe

is different: AFM senses the gradient of the local force in normal direction, while shear-force is more like a friction force.

Generalized scheme of shear-force feedback is shown in Figure B.1. Probe oscillation in lateral plane is excited by a piezo driving element. The oscillation is detected by another sensor, amplified and sent to demodulator in the feedback loop of the SPM controller.

Several methods have been used to sense the oscillation amplitude/phase change. Originally, Betzig implemented optical scheme[2]: separate laser was illuminating the apex of the probe from the side. The shadow formed by the tip was projected on a split photodiode positioned behind the probe. Phase and amplitude of the diode output are to those of the probe oscillation. This design was incorporated in the first commercial NSOM instrument – Aurora™ by Topometrix.

Despite common use in the NSOM community, this method proved to be tricky and sometimes controversial. The main difficulty is aligning the laser, probe and photodiode. The beam is usually reflected on the diode from the sample, which leads to unwanted signal change during approach. Also, uneven reflection from the sample makes signal less reliable. Finally, the presence of additional optical source may complicate delicate NSOM measurements. All these factors were driving the effort to develop non-optical feedback scheme.

The goal of non-optical approach is to couple some sort of mechanical vibration sensor to a probe to feel minute changes in the probe oscillations. At

first sight, the task seems not realistic provided that displacements and forces are extremely small (optical method worked because it used relatively long light path to amplify the small displacements of the probe). However, the sensitivity of piezo-based sensors and low noise levels of today's ICs proved to be capable of providing the non-optical solution.

One of the approaches was developed by Hsu[3]. The probe was mounted in a piezo tube that had two electrodes to vibrate the probe. The tube/fork system comprised one of the arms of a balanced bridge. Misbalance of the bridge reflected the changes in the electro-mechanical impedance of the system caused by damped oscillations of the probe. Although acceptable, this method is very temperature dependent, mostly because of fluctuations in bridge balancing.

Another approach was developed by Karrai[4] and consisted in utilizing high fidelity piezo resonators as vibration sensors. Such resonators are commonly called "tuning forks" because their geometry is similar tuning forks used in music. Piezo tuning forks (PTF) are miniature, high Q resonators tuned to a specific frequency in the range of 20 – 150 kHz. They are utilized now virtually everywhere as frequency standards in electronic equipment, which explains their low cost (~$0.40 ea.). In Karrai's scheme the fiber is glued to one arm of the fork. Vibration is either excited by an external piezo, or by directly driving PTF. Electrical signal proportional to PTF vibration amplitude/phase is generated on the PTF electrodes and serves as input for feedback circuitry. It should be noted that in this approach the monitored

resonance is that of the fork, not the fiber. Loading of the fork reduces its Q factor to several hundred (from several thousand before any modifications).

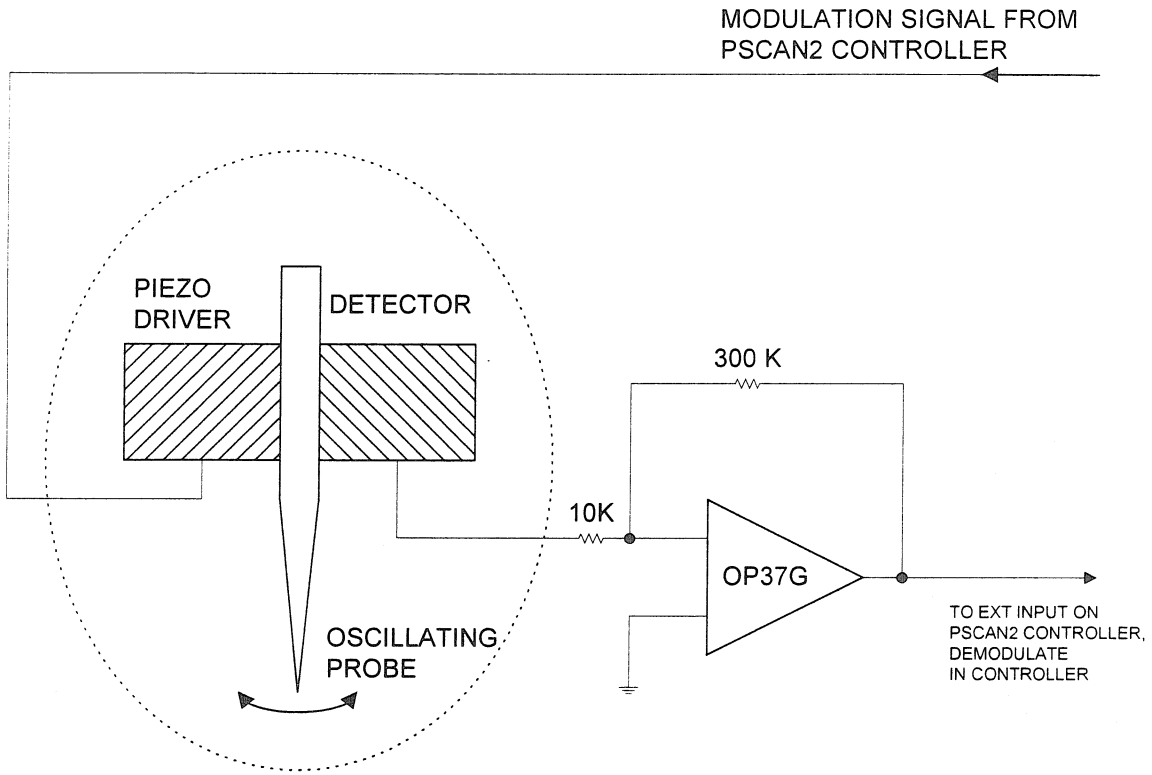

NOTES:
1. Two 9V batteries are used as power supply for pre-amplifier to minimize noise.
2. Keep wires as short as possible from detector to pre-amp.

Figure B.1. Generalized diagram of shear force feedback setup.

Simplicity, reliability and low cost of this approach led to its fast adoption in many labs soon after Karrai's publication. New NSOM instrument from Topometrix, Lumina™, is using this method for probe feedback control. This approach is also perfectly suited for vacuum applications where optical access to the probe is limited. This aspect was the reason why we have chosen this feedback for use in TOPO-MS and, subsequently, TOPOLIBS. The details of the setup and probe preparation procedures are outlined in the sections below.

It should be noted that although superior to optical feedback, PTF design is not the best in terms of robustness and ease of probe preparation. PTFs are very delicate, and it takes considerable time for probe preparation, mainly because the forks are not intended for recycling.

Since Karrai's invention, several other, less labor intensive, techniques for shear-force feedback were successfully implemented. One is so-called "sandwich" arrangement developed by Marti[5], where fiber is held in between two small piezo plates. One plate is used to excite fiber vibrations, the other one senses the vibrations. Fiber is glued into a stainless steel tube and is held in the assembly with a setscrew.

Another, even simpler, approach is developed by Tchenio[6]. In his method the two piezos are non-symmetrical: large piezo plate is used to excite the fiber vibrations. A smaller, V-shaped piezo is attached to the edge of the plate. This piezo serves as a sensor. The fiber is glued to the apex of the V-

shaped piece with a drop of cyanoacrylate glue. This arrangement is simple and robust, and allows for fast probe exchange. The geometry of this assembly is shown in Figure B.2. We have implemented this approach using a V-shaped element cut from a miniature piezo buzzer membrane, part #273-074A from RadioShack.

The latter approach has been implemented only recently. The majority of the experimental data presented in this thesis has been acquired using tuning forks as feedback sensor. Experimental details pertinent to tuning forks setup are presented below.

PREPARING A FORK

The forks can be purchased from any major electronics part supplier. We have been using Epson made oscillators purchased through DIGI-KEY (800-344-4539): vendor part number SE-3201-ND, Epson part number C-001R 32.768K-A. The forks are packaged in cylindrical cans, which should be removed prior to fiber mounting. However, the first step is to solder the fork into some holder, because if soldering is performed after opening the can, the leads are easily separated from the fork ruining the electrical contact.

Throughout the experiments we have used extensively the sockets made from breakable strips with 0.100 spacing (DIGI-KEY part number A208-ND). Any number of pins can be broken off the strip, which makes it a convenient source for miniature connectors. Tuning forks were soldered in two pin sockets that were broken off the strip. This is the first step in the process of fork preparation that is illustrated in Figure B.3.

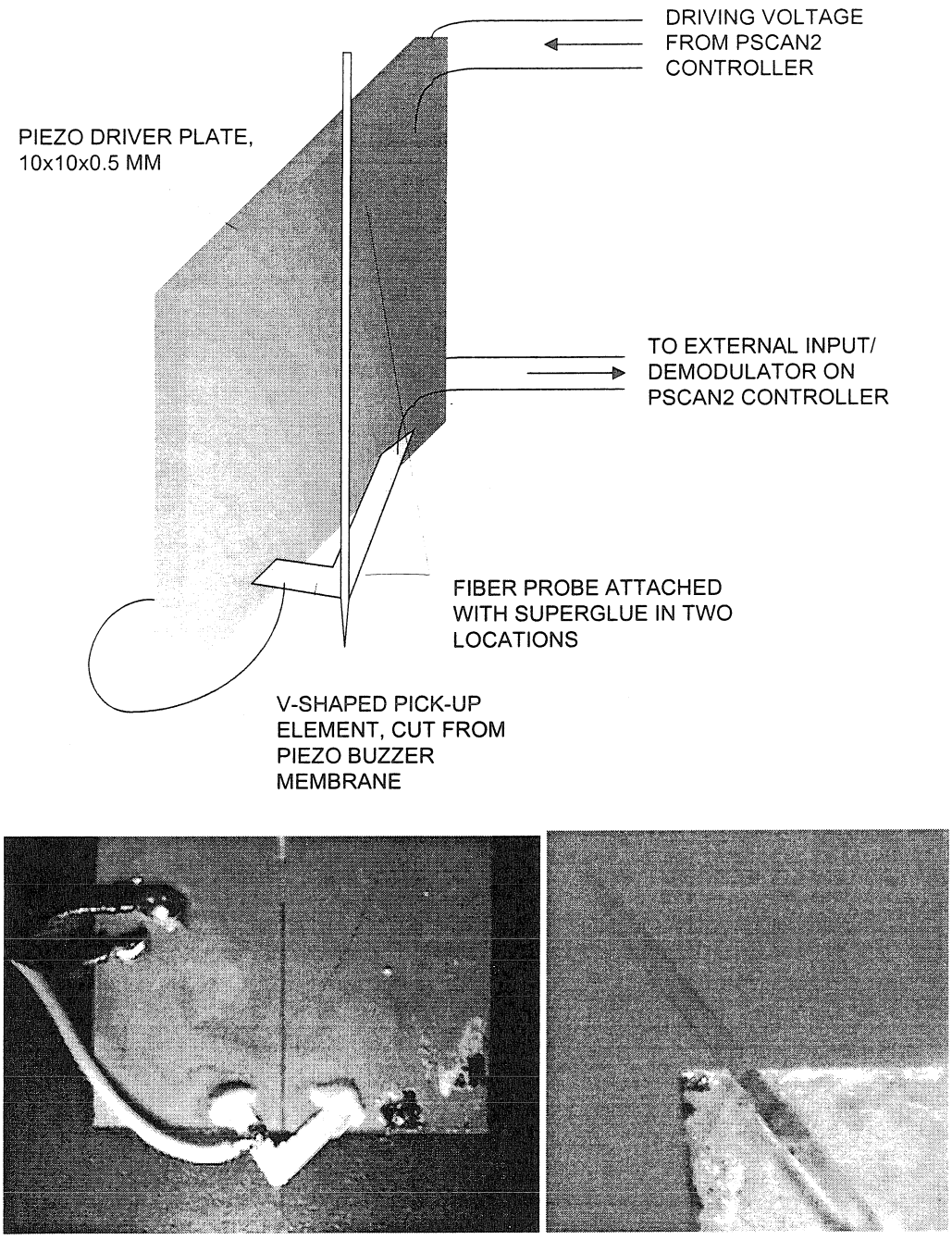

Figure B.2. Diagram and photographs of the asymmetric shear force assembly with a flexible V-shaped detector.

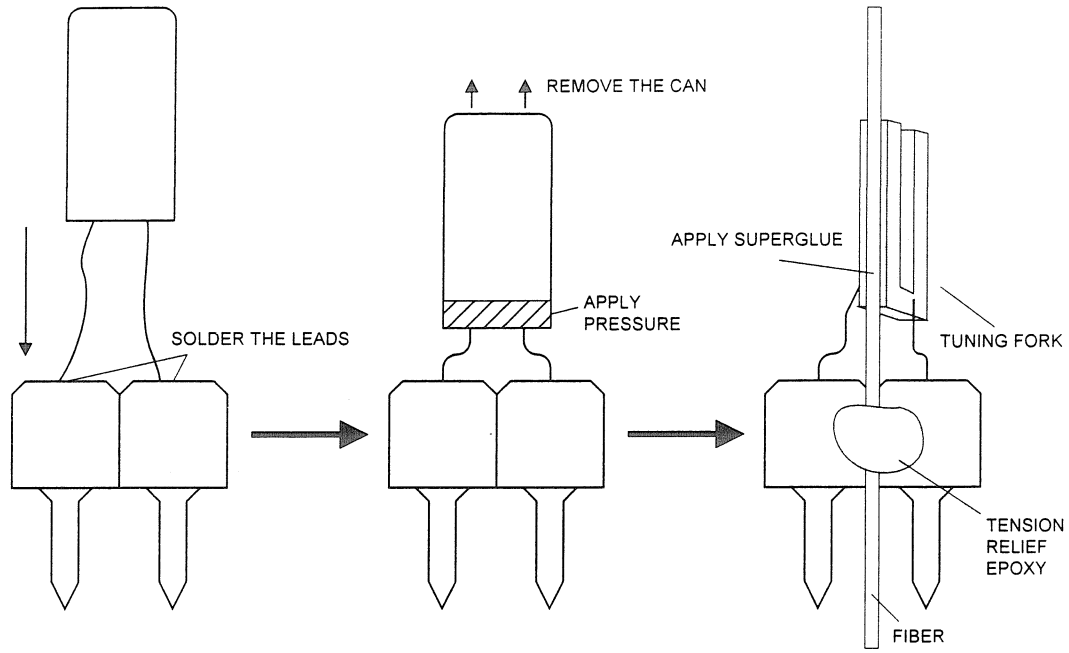

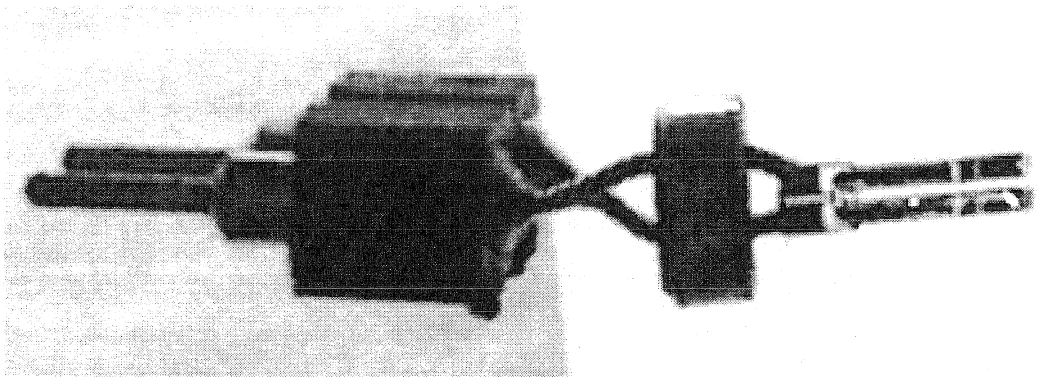

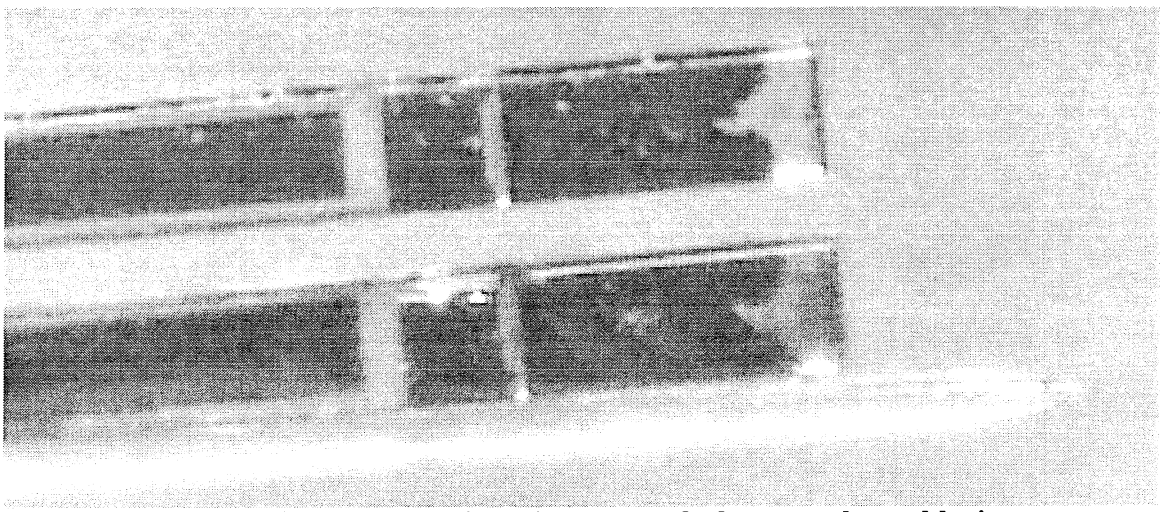

Figure B.3. Tuning fork preparation diagram and photographs: soldering, extraction from the can, gluing the fiber.

The next step is to remove the can. The can is attached to the leads with a hard epoxy. There are two ways to get rid of the can:

1. Use the can opener. Kitchen variety one would not work. A refined version, can opener for laser diodes, is sold by Thorlabs, NJ (part # WR1). This tool allows removing the can gently with minimum probability of fork damaging. The method is fast and reliable however, it has a drawback: while the fork becomes exposed, there is a metal ring with epoxy left at the bottom of the fork. This ring prevents one from mounting a long piece of fiber onto the fork. So, the can opener is useful only when short probes for "topography-only" study are to be prepared.
2. Alternatively, one can destroy the epoxy seal to remove the can. The best way to do that would be to dissolve the epoxy. Unfortunately, we were unable to find a suitable solvent. Instead, brutal force is used to mechanically crush the epoxy. The sealed region of the can is squeezed gently with needle-nose pliers all around until the epoxy gives up and becomes sand-like. *CAREFUL:* the transition is sudden, so if excessive force is applied to the pliers, tuning fork will be crushed. With some practice, this method can be used reproducibly to make naked forks.

Now the fork is ready for the fiber.

MOUNTING FIBERS ON THE FORKS

XYZ manipulators can be used for high precision mounting of the fibers. However, for all practical purposes the fibers can be mounted by hand. The fiber (with plastic jacket removed) is placed in the groove of the socket

and aligned along the fork's arm. The dimensions of the fork and the socket match nicely to allow relatively easy alignment. At least a half-inch long piece of the fiber should extend off the fork – this leaves enough length for etching.

Fiber is glued into the groove with a drop of superglue. This provides some tension relief and fixes the fiber in place. After that a tiny drop of superglue is delivered to the point of contact between the fork and fiber. The glue should wet the fiber and spread along the full area of contact. Minimum amount of glue should be used for this procedure: excessive glue will percolate down the fork and will epoxy together fork's arms killing the fork performance. If this happens, the glue (while still liquid) can be removed from the fork by gently absorbing excessive liquid from the fork with a Kimwipe.

Additional tension relief from the fiber is beneficial because the fiber-fork contact is very delicate. More epoxy can be added to fix the fiber permanently in the socket groove. Heat-shrink tubing may also be used for this purpose.

After epoxy sets, the fiber/fork assembly is transferred to the etching bath to make tapers as described in Appendix A.

HARDWARE/ELECTRICAL DESIGN

The holder for the fiber/fork assembly consists of two-pin socket and dithering piezo. The leads of the socket are soldered to a short piece of coaxial cable leading to the pre-amp.

A simple, low power pre-amp is built using single OP-37 operational amplifier. Gain of 30 is sufficient; further amplification may be done

downstream. Actually, the main purpose of the pre-amp along with signal amplification is buffering: the tuning fork acts as a good antenna picking up interference, so it's important to cut it off from the circuit. Having this in mind, it is *very* important to have a quiet power supply for the pre-amp. The standard trick is to avoid the line sources and use batteries instead. Two 9V batteries provide adequate power for OP-37.

REFERENCES

[1] W.C. Hurty and M.F. Rubinstein, Dynamics of Structures, Prentice Hall, NJ, 1964, p. 203.

[2] E. Betzig et al., *Appl.Phys.Lett.*, **60** (1992) 2484-2486.

[3] M. Lee et al., *Rev.Sci.Instr,* **67** (1996) 1468-1471.

[4] K. Karrai and R.D. Grober, *Appl.Phys.Lett.*, **66** (1995) 1842-1844.

[5] R. Brunner et al., *Rev.Sci.Instr.*, **68** (1997) 1769-1772.

[6] A. Debarre et al., *Rev.Sci.Instr.*, **68** (1997) 4120-4123.

Appendix C. Design Details of TOPO-MS II

Chapter 3 in this thesis describes the development of a novel instrument for spatially resolved chemical analysis. An uncoated probe of a near-field scanning: optical microscope (NSOM) is used to deliver laser radiation to the sample surface. Laser-desorbed species are analyzed with a time-of-flight mass spectrometer (TOF MS). Both elemental and molecular analysis can be performed with simultaneous topographical imaging of the sample. Results obtained with the prototype instrument assembled for these studies clearly demonstrated the feasibility of the technique and provided the inspiration for the construction of a second generation instrument, TOPO-MS II, which is described in this appendix. The new instrument has greatly enhanced capabilities to facilitate a wide range of studies involving spatially resolved chemical analysis at the micron and sub-micron scale.

INSTRUMENT DESIGN

Several considerations were driving the choice of platform and further modifications:

Vertical TOF to minimize space.

TOF collinear with fiber probe to improve ion collection efficiency and TOF-MS resolution.

Independent load locks for sample and probe exchange.

UHV chamber to avoid sample contamination by background gases.

To meet these objectives with minimum cost and effort, the second generation TOPO-MS instrument is being built by modifying a commercial Auger Microprobe, model JAMP-10 from JEOL. The original instrument featured a versatile UHV chamber

equipped with an electron gun column, sample manipulation stages with 5 degrees of freedom, electron energy analyzer and compact quadrupole mass spectrometer. The differentially pumped sample load lock accepts samples up to 1" diameter. The system was equipped with an ion and titanium sublimation pump for UHV pumping, and a turbomolecular pump with vibration isolation suspension for load lock pumping.

The system was extensively modified for our TOPO-MS experiment. The electron gun was removed and replaced with the TOF-MS. A low profile XY piezoscanner was added to the sample stage. The sample load lock has been modified to work with the redesigned sample stage. Finally, a custom fiber probe transfer assembly was designed and assembled for the system. The details of those modifications and suggestions for future improvements are described below. A sketch and photograph of the system are shown in Figure C.1.

One of the difficulties encountered during system modification was the abundance of peculiar flanges, seals and threads in JEOL system. All metric flanges and threads were replaced with English equivalents. The original electron column was sealed to the body of the system with a non-standard flange with a gold seal. An adapter with a standard 6" Conflat flange was mated to this seal.

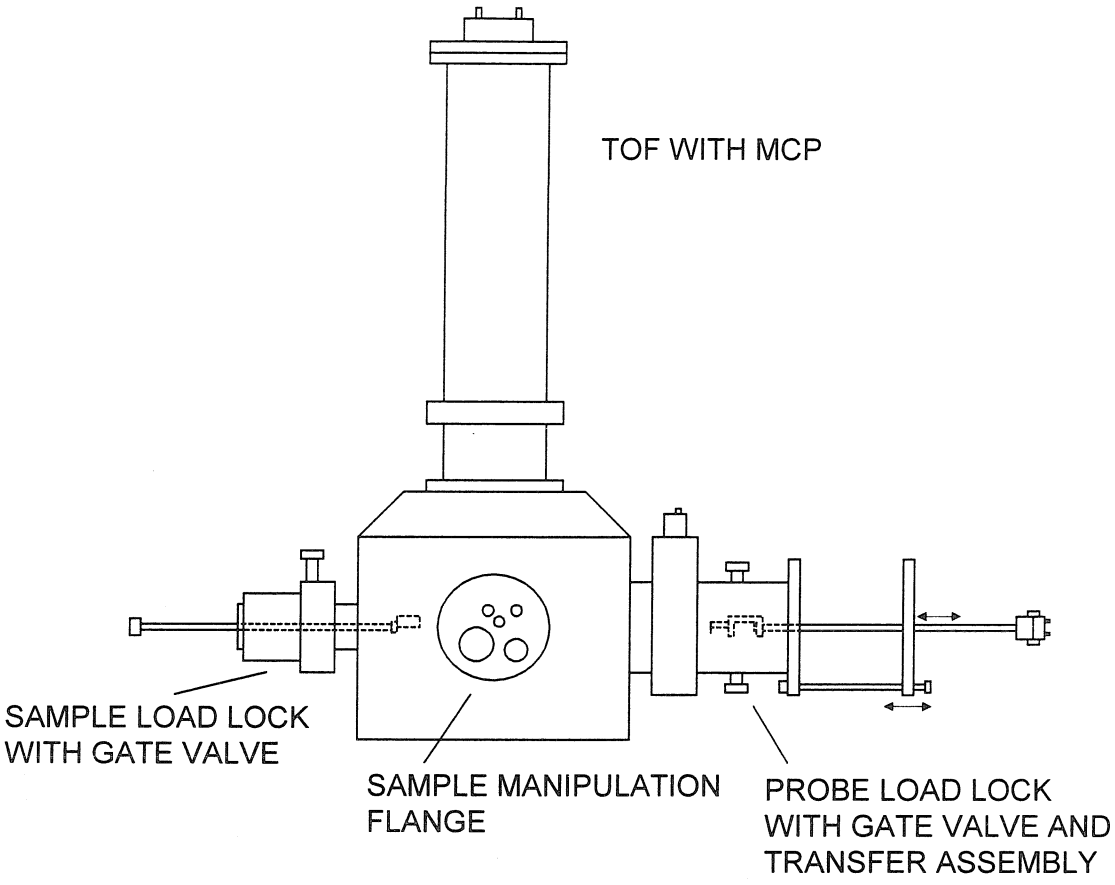

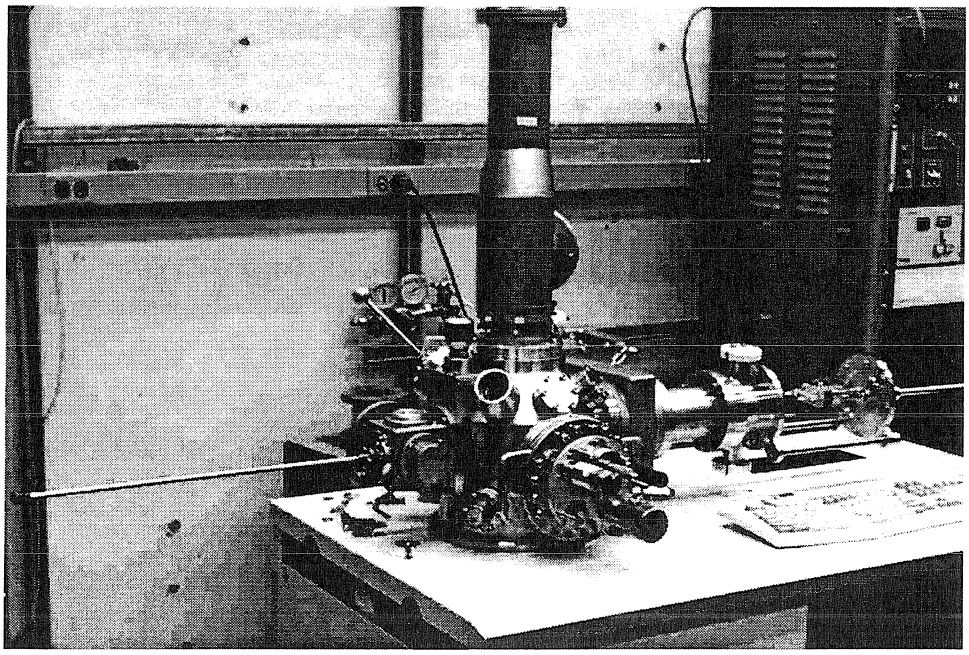

Figure C.1. Sketch and photograph of TOPO-MS II system. Drawing is not to scale.

SCANNER: CURRENT DESIGN AND CONSIDERATIONS FOR FUTURE

Currently, the scanner incorporates the following design features:

Coarse XY manipulation is done manually with micrometers on the sample manipulation stage.

Fine XY scanning of the sample is performed by a compact, low profile scanner attached to the manipulation stage.

Coarse Z approach is achieved by replacing the Z micrometer on the sample manipulation stage with a DC motorized screw.

Z piezo is separate from the scanner. It is coupled to the probe holder.

A sketch of the XY scanner is shown in Figure C.2. It is a two-axis flexure with approximately 7:1 lever arms to amplify motion of the piezos. Each axis is driven with a single stacked piezo (AE0203D16 by Tokin, Japan, also sold through Thorlabs, NJ). Nominal piezo displacement is 16 μm for 150 V. The arms are spring loaded to minimize creep.

The scanner is attached to the sample manipulation flange. A dovetail rail is bolted on top of the scanner. The matching piece of the dovetail holds the sample and can be transported in/out of the chamber with the sample transfer rod.

The Z piezo is decoupled from the XY scanner. Main consideration driving this choice was the concern of damaging the Z-piezo while changing samples since the sample exchange rod with the dovetailed holder inserts at a 90-degree angle to the Z-piezo direction. During engagement with the dovetail, considerable force is applied

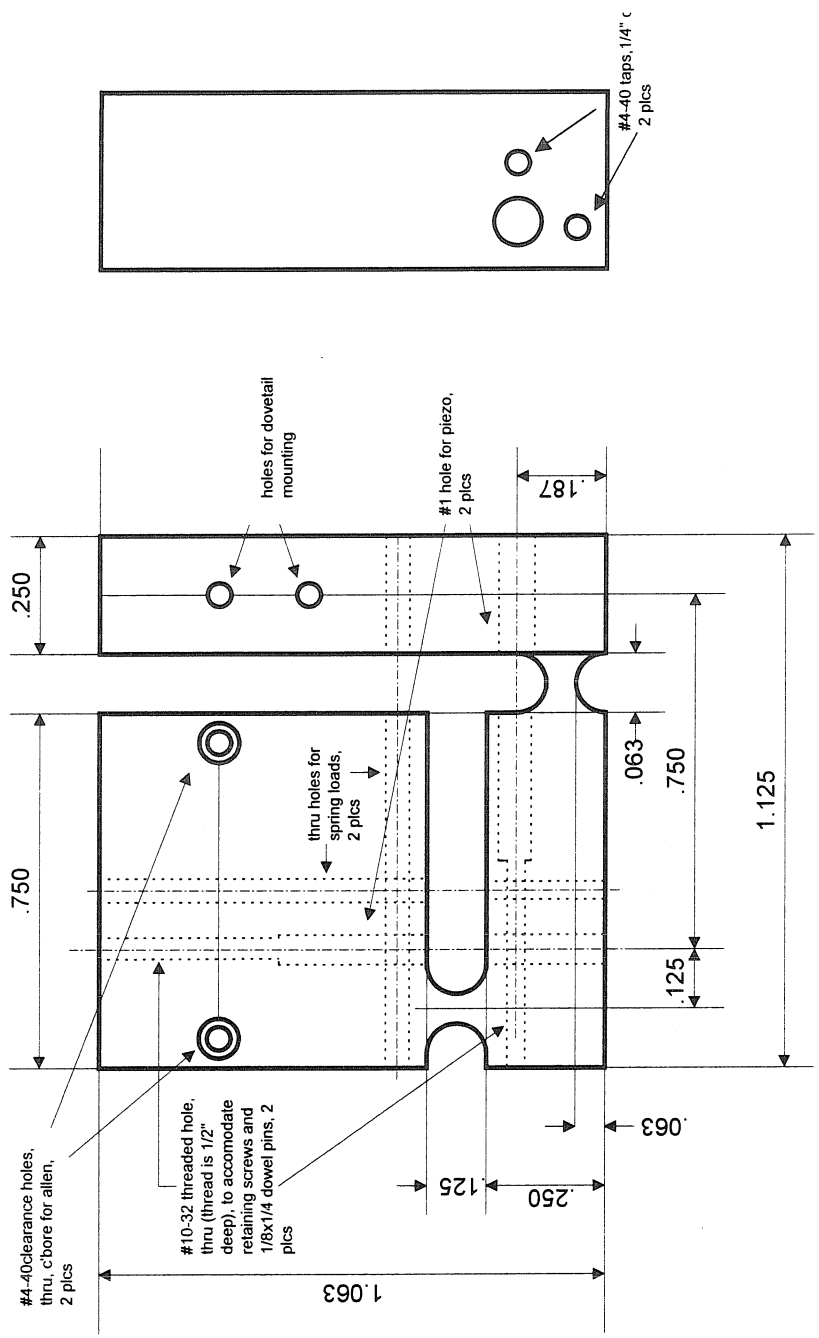

Figure C.2. XY piezo scanner. Aluminum 3/8" thick. X and Y piezos are on different elevations. Both levers are approximately 7:1. Drill all holes BEFORE milling flexures.

perpendicular to the Z-piezo which could easily break under load. With the Z-piezo mechanically decoupled from XY-piezos, it experiences no load during sample exchange.

Figure C.3 shows the details of the Z-piezo assembly. The Z-piezo is incorporated in the probe holder and is powered through wires connected to the electrical feedthroughs on the probe transfer rod (see below).

In the future it may be desirable to bring all piezo actuators outside the chamber. This would simplify operation and maintenance. One possible means to accomplish this would be to put piezo actuators between the corresponding micrometer screws and push rods on the sample manipulation flange. Alternatively, integrated micrometer/piezo translators can be implemented. Such translators are available from a number of optomechanics equipment manufacturers. The trade-off of this approach is increased load on XYZ piezos: instead of driving light scanner and probe loads, they would have to move the full spring loaded sample manipulation stage. This may limit the speed of scanning. Such considerations should be taken into account when choosing actuators for this scheme.

PROBE ASSEMBLY

The probe assembly was custom designed and machined in house. It is coupled to the probe transfer mechanism and incorporates the following components:

Probe socket with dither piezo

Z actuator

Shear-force feedback pre-amplifier

Miniature video camera for probe observation

The frame of the probe assembly also serves as the first electrode in the TOF electrostatic lens system. The assembly is electrically insulated from the transfer rod, so its potential can be adjusted relative to the sample. The assembly is shown in Figure C.3. The detailed drawings are in Figure C.6.

PROBE TRANSFER

A custom transfer system was designed and manufactured by McAllister Technical Services (Coeur d'Alene, ID). The drawing of the assembly is shown in Figure C.4. It features a hollow rod, which can be rotated and translated. The rod is held by vacuum tight bearings in a 6" OD flange with rubber O-ring. The flange itself can be translated along two rails welded to the matching flange.

The atmosphere end of the rod has a Kwik flange equipped with two BNC connectors, two 5-pin connectors, and 1/8" NPT threaded feedthrough for optical fiber.

The assembly has two 2 ¾" Conflat flanges for differential pumping and venting hook-ups. The assembly is ported to a gate valve, which isolates it from the main chamber.

TOF MASS SPECTROMETER

A linear TOF mass spectrometer has been custom designed and built for TOPO-MS II. Electrostatic ion optics were developed to accommodate a fiber probe collinear with the TOF axis. The ions are brought around the probe and then focused on the detector. Ion simulations for this arrangement are shown in Figure C.6.

The details of the TOF are shown in Figure C.5. Parts from a commercial TOF mass spectrometer (retired from Caltech's Biology Division) were used for this setup, mainly the TOF housing, high voltage feedthroughs and MCP detector assembly.

A floated ion flight tube is supported inside the TOF housing on a Teflon holder. Three electrostatic lenses are attached to the lower end of the tube. All lenses and tubes are 1" O.D., ½" long lenses are made from Kimball Physics (Wilton, NH) "eV Parts." All three lenses are ½" wide separated by ~0.1". Main flight tube is stainless steel, 75 cm long. Note that the clearance between the last lens and the probe transfer assembly is small. Caution has to be exercised when pushing the probe rod in.

Ion trajectory simulations were performed with Simion and are presented in Figure C.6. Typical lens voltages used for these simulations are indicated in Figure C.5. Ions are 10 and 1,000 amu starting with initial energy of 3 eV and having different starting direction 10-90 degrees relative to the axis of symmetry. Angular variation introduces ~1.6% spread in the arrival times for the ions of the same mass and initial kinetic energy. This is a significant improvement relative to our initial TOPO-MS I prototype. The first generation system was not collinear. Instead, the TOF tube was perpendicular to the fiber probe. Simulations of ion trajectories for this geometry showed that arrival time spread due to variation in initial ion direction was 10-15%.

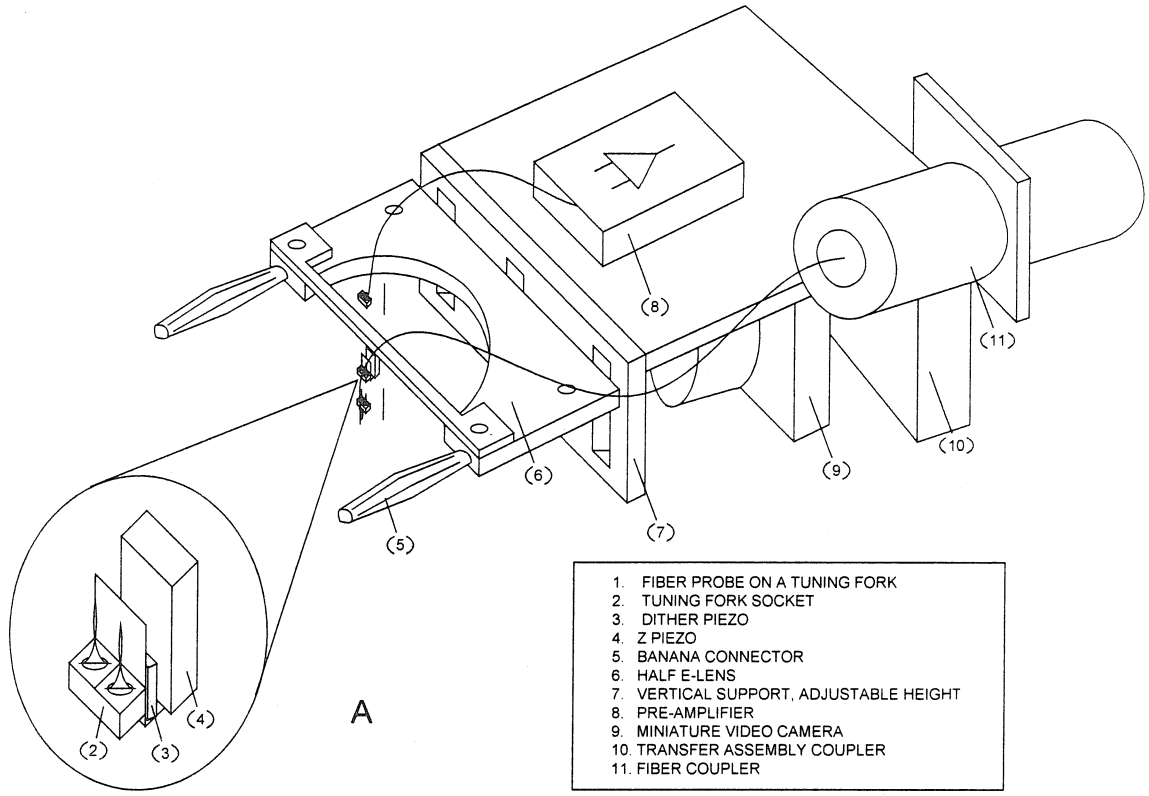

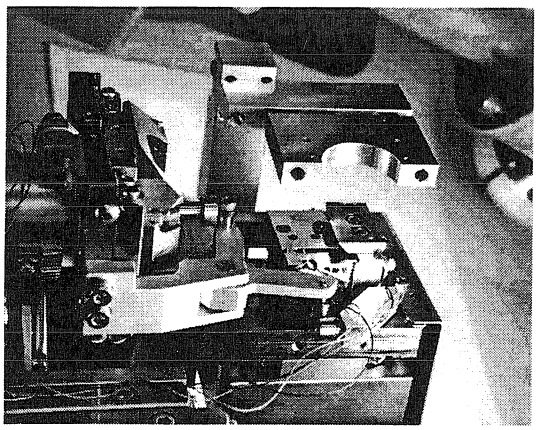

B

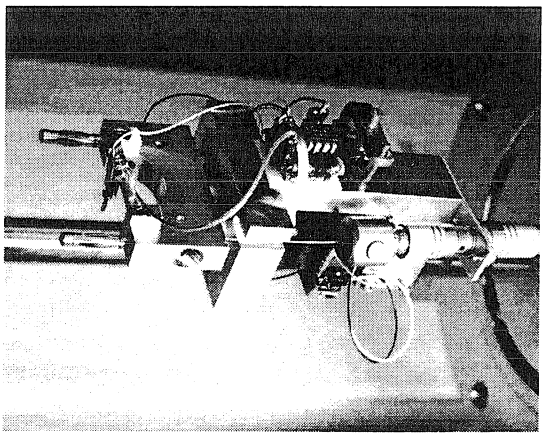

C

Figure C.3. Probe assembly. (a) Drawing of the holder assembly. (b) Photograph of the stationary part, bolted to the sample manipulation flange. Also seen is flat scanner with dovetail for sample holder mounting. (c) Mobile part of the holder assembly mounted on the transfer rod. Also seen are tuning fork, pre-amplifier circuit, fiber connectors and miniature video camera.

The sample and probe are grounded. This is a weak spot of the simulation because the probe is essentially dielectric (at least the very end of the fiber). Simion can not take into account dielectric surfaces which may be charging in the presence of ions. However, these simulations create a first approximation for a lens geometry that can be used to defocus the beam, bring it around the probe, and then focus it again behind the probe on the detector.

The simulation showed high sensitivity of the trajectories to the voltage on the first extraction lens.

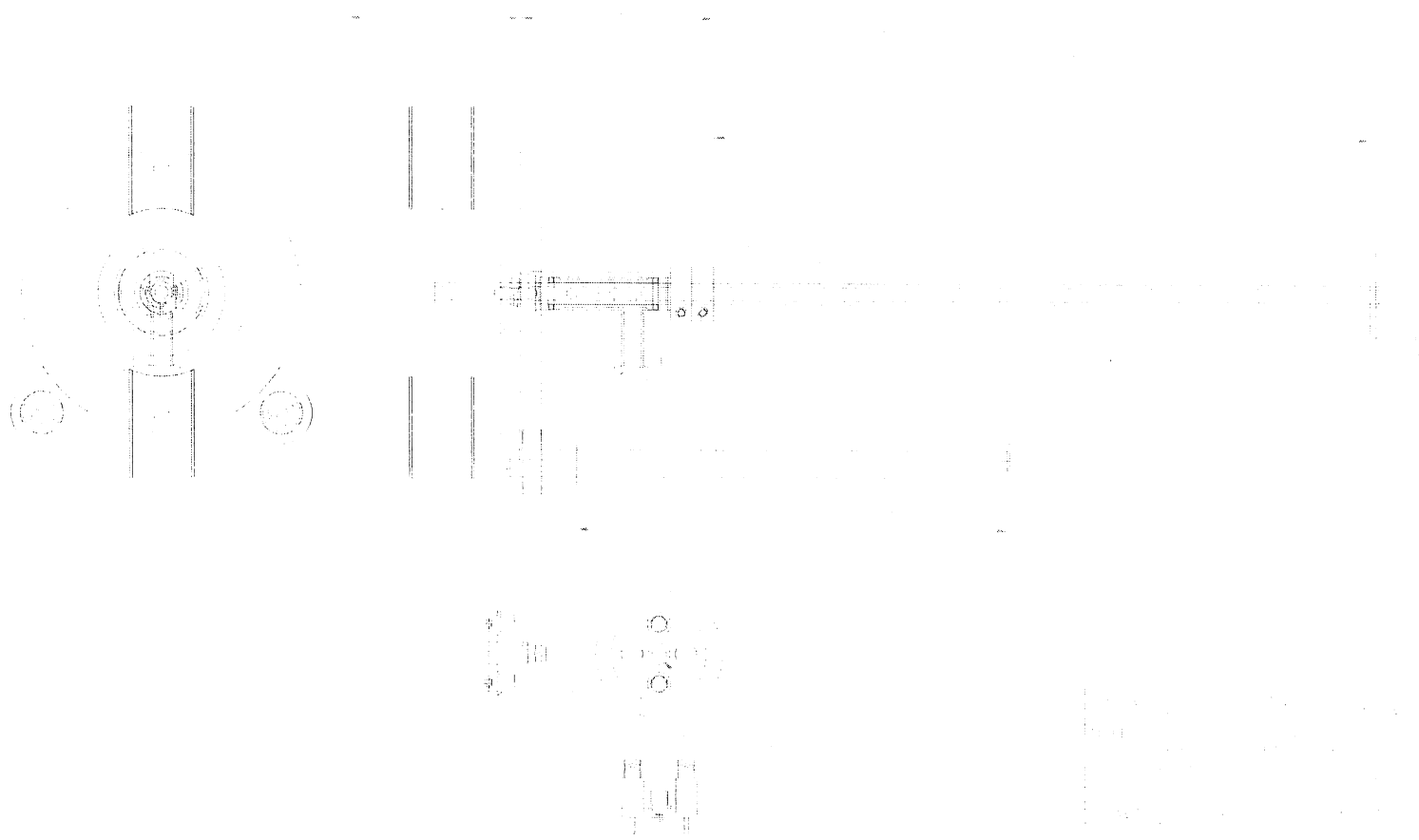

Figure C.4. Custom transfer assembly manufactured by McAllister Technical Services.

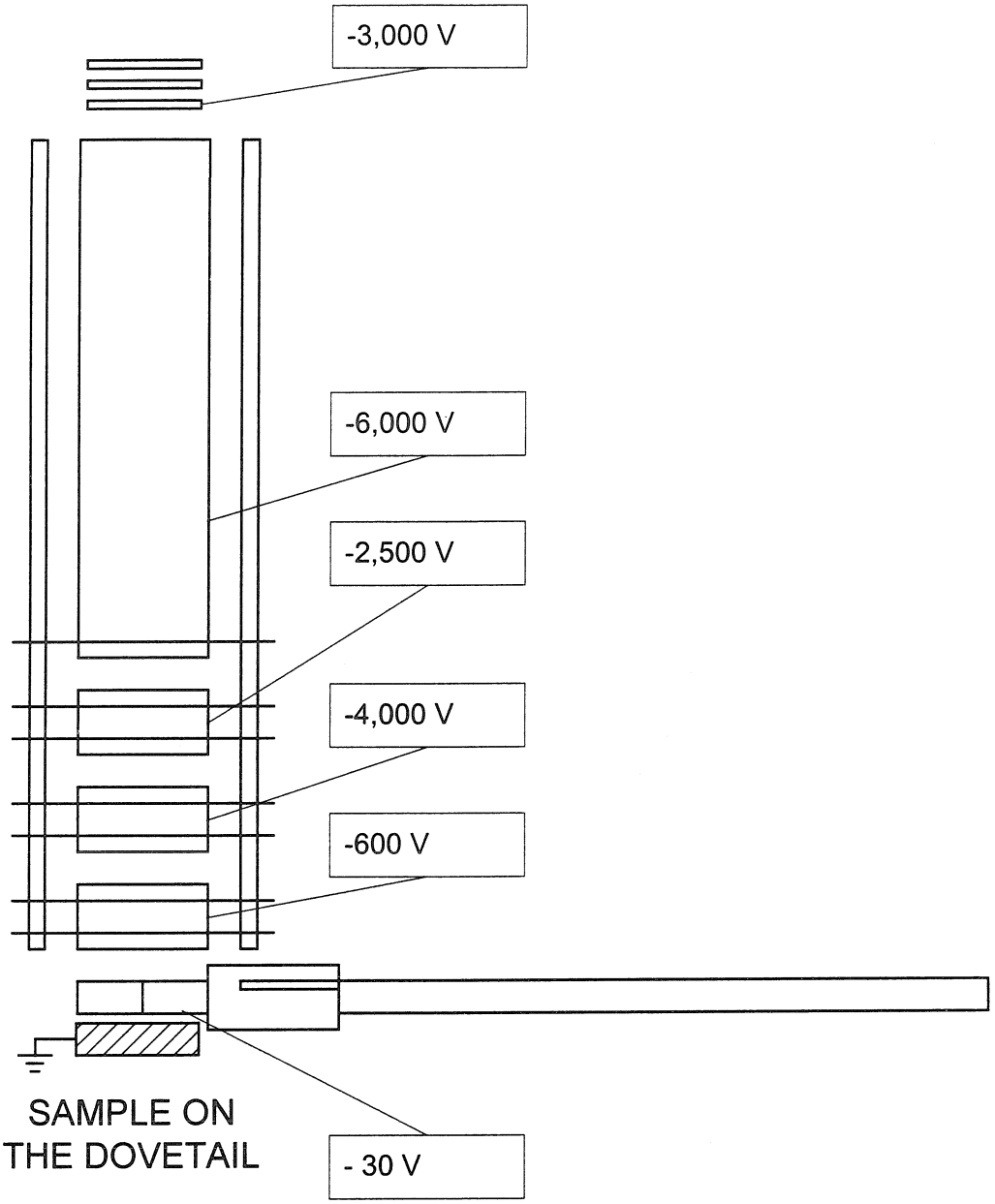

Figure C.5. TOF design. Shown are: main flight tube, three beam turnaround lenses and first lens mounted on the probe transfer assembly. Typical lens voltage used in the SIMION simulations (shown in the next Figure) are indicated. All lenses and tubes are 1" O.D. ½" long lenses are made from Kimball Physics "eV Parts." All three lenses are ½" wide separated by ~0.1". Main flight tube is stainless steel, 75 cm long. Note that the clearance between the last lens and the probe transfer assembly is small. Caution has to be exercised when pushing the probe rod in.

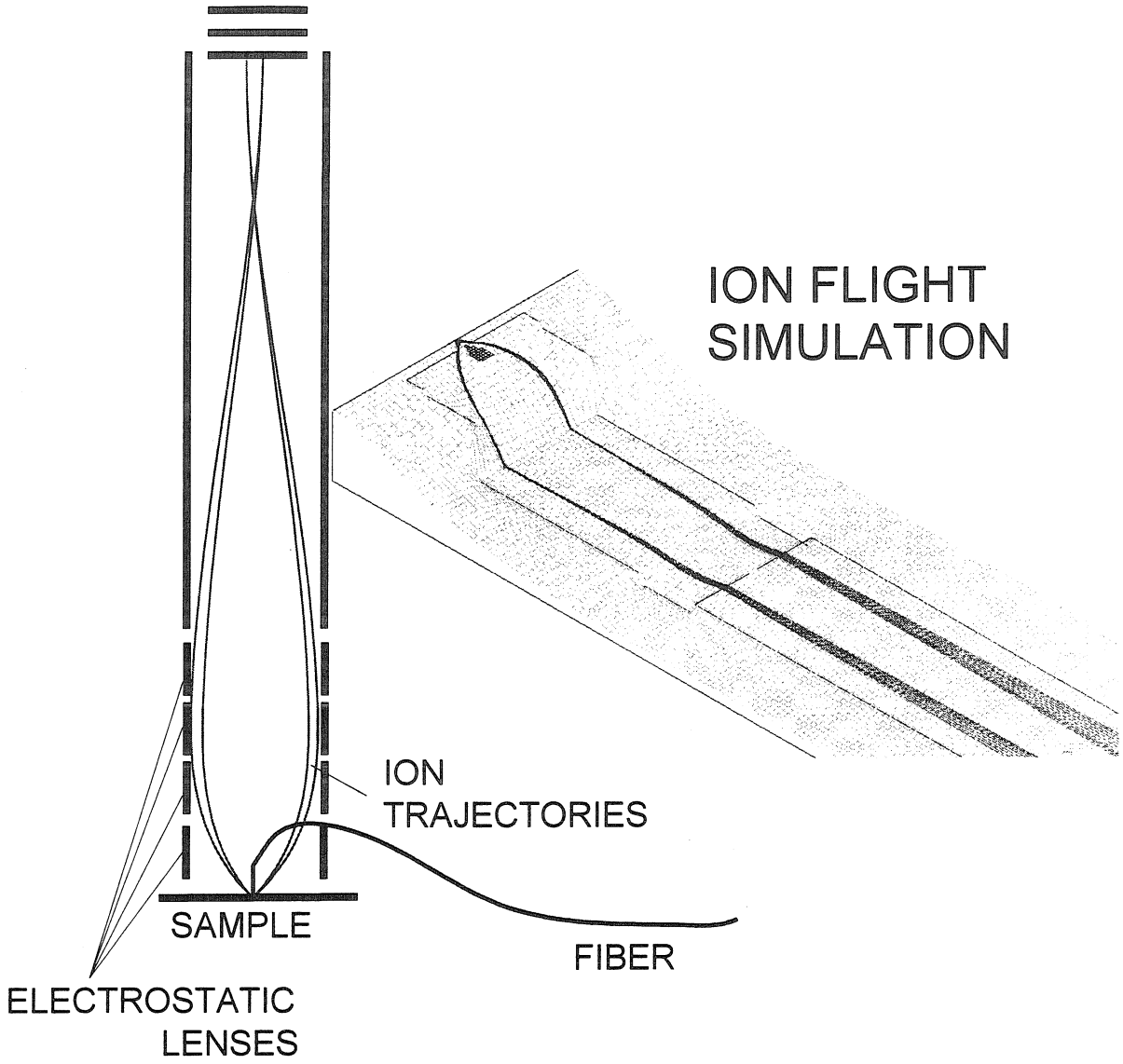

Figure C.6. A sketch of ion trajectories in TOF tube and ion trajectories on the potential surface in the Simion calculation using lens geometry and voltages shown in Figure C.5. The sample and probe are grounded. Ions are 10 and 1,000 amu starting with initial energy of 3 eV and having different starting direction 10-90 degrees relative to the axis of symmetry. Angular variation introduces ~1.6% spread in the arrival times for the ions of the same mass and initial kinetic energy.

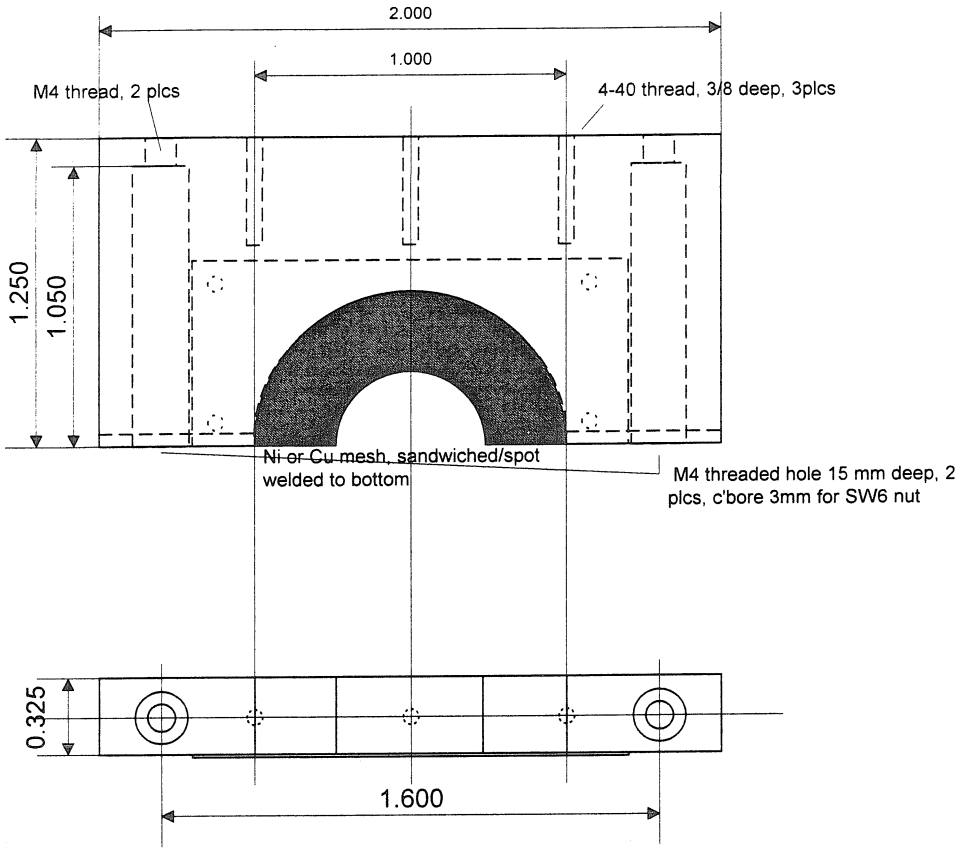

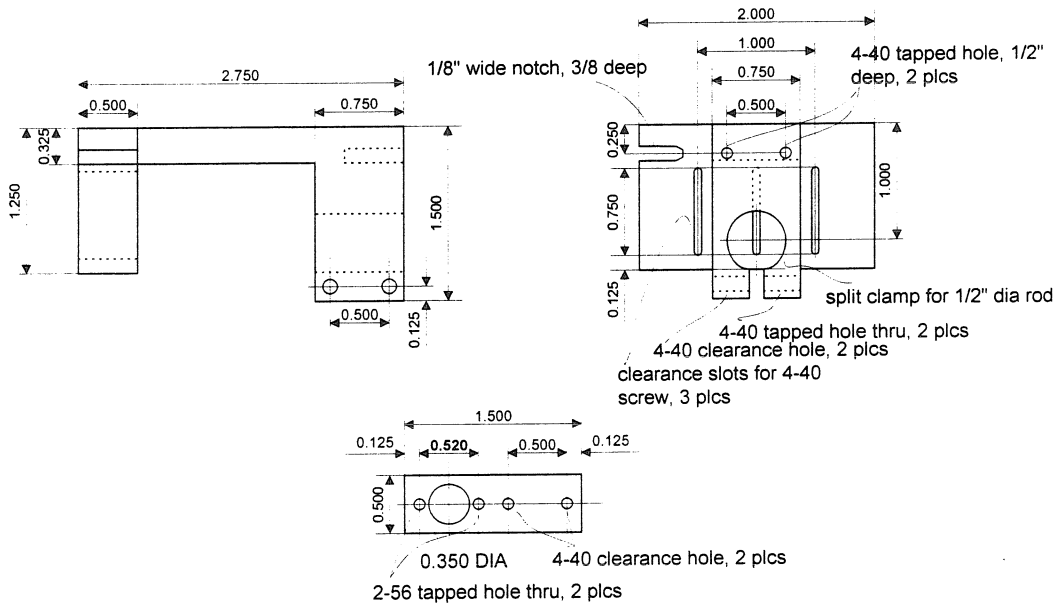

Figure C.7. Drawing of (a) the first lens/fiber holder and (b) fiber support assembly.